Bacterial Approaches to the Recovery of Scarce Metals

A dissertation presented
by
William Daley Bonificio
to
The School of Engineering and Applied Sciences

in partial fulfillment of the requirements
for the degree of
Doctor of Philosophy
in the subject of
Applied Physics

Harvard University
Cambridge, Massachusetts
April 2015

Dissertation Advisor: Professor David. R. Clarke William Daley Bonificio

Bacterial Approaches to the Recovery of Scarce Metals

Abstract

Many of the scarcest metals are critical to future energy technologies. However, these metals often have limited supplies, and their current production and recycling methods are complicated and use toxic chemicals. In order to ensure the availability of these metals alternative methods for their recovery need to be explored. This thesis describes biological methods for the recovery of some of these metals, specifically the lanthanides and tellurium. It is one of the first investigations for the biogenic recovery of either of these metals, making it unique in the field.

The lanthanides are critical elements in the high performance magnets used in wind turbines, electric vehicles, and other 'green' technologies, but they are difficult to separate from one another because of their chemical similarity. We demonstrate a biogenic method based on lanthanide adsorption to the bacteria *Roseobacter* sp. AzwK-3b, followed by subsequent desorption as a function of pK_a using a semi-continuous flow process. The desorption behavior suggests that the basicity of the individual lanthanides is important in determining their biosorption and desorption behavior. Similar selectivity was also found using phosphatidic acid liposomes. It is possible to concentrate a solution of equal concentrations of each lanthanide to nearly 50% of the two heaviest lanthanides in only two stages of enrichment, surpassing existing industrial practice. This suggests that there is an opportunity to harness the diversity of bacterial surface chemistry and liposome chemistries to fine tune the separation

and recovery of these technologically important metals, and to do so in an environmentally benign manner.

Tellurium is used in photovoltaic (PV) modules and thermoelectric generators, however it is not abundant in the earth's crust and is difficult to produce. We show that the hydrothermal vent microbe *Pseudoalteromonas* sp. strain EPR3 can convert tellurium from a wide variety of compounds, industrial sources, and devices into metallic tellurium and a gaseous tellurium species. These include metallic tellurium, tellurite, copper autoclave slime, tellurium dioxide, tellurium-based PV material (cadmium telluride), and tellurium-based thermoelectric material (bismuth telluride). Despite the fact that many of these tellurium compounds are considered insoluble in aqueous solution, they can nonetheless be transformed by EPR3, suggesting the existence of a steady state soluble tellurium concentration during tellurium transformation. Insights from these experiments on the mechanisms of tellurium precipitation and volatilization by bacteria, and their implications on tellurium production and recycling are discussed.

Contents

List of figures

To my Uncle Bill, who had a greater impact on my life than he would ever know

Acknowledgments

First and foremost I need to thank my wife, Amanda. She has sacrificed so much in her life to allow me to pursue my degree, and I am eternally grateful to her.

Next, I need to thank my advisor, Professor David Clarke. He took a chance in welcoming me to his group, and his support for me ever since has been fundamental to my success. In addition, by allowing me great freedom during the pursuit of my Ph.D., along with the challenges that bears, he has shaped my approach to problem solving, which is the most important thing I will take from my degree.

Also, I would like to thank the other members of my Ph.D. committee, Evelyn Hu and Pete Girguis. I would especially like to thank Pete for helping me during the earliest, most critical stages of my Ph.D.

There are a myriad of other people I need to thank, far too numerous to name individually. These include all the members of the Clarke group who have helped me along the way, in addition to the friends I have made during these last six years who have provided me amazing entertainment and helped make this time fly by. In particular, I need to thank Roger Diebold. He gave me confidence in myself, and guided me during my most overwhelming struggles.

Finally, I need to thank my family, especially my parents, for all of their love. They have never en-

cumbered my journey through life, and without their enduring support I would have never completed this degree.

1

Introduction

Future energy technologies will rely on the availability of scarce metals that are in limited supply and have low production yields. As an added challenge, very little is known about these metals' production, resources, and reserves. Indeed, only recently has this issue gained attention in the scientific community. Most scientific studies on metal resources have been published in the last 15 years[1], and they predict that metal production will need to increase almost tenfold to meet the growing demands, especially from developing countries[1]. This demand can be alleviated for abundant metals, such as

iron or aluminum, by increasing mining production and/or recycling efforts for which there already exists a stable infrastructure, but for metals essential to green energy technologies, such as the lanthanides, tellurium, indium, and platinum, there is no clear solution. All of these but the lanthanides are produced as byproducts from the mining of a more abundant ore, thus the already limited supply is also volatile. One approach to increase the availability of these critical metals is to improve methods for their recovery. This dissertation describes research using biologically inspired methods for the recovery and production of some of these scarce metals - specifically the lanthanides and tellurium.

Biologically inspired methods, particularly methods utilizing bacteria, may confer many advantages over traditional approaches to scarce metal recovery. For example, bacteria are known to undergo highly specific interactions with their targets, e.g. the protein transferrin specifically binds Fe(III)[2]. In addition, bacteria are usually non-toxic and can replicate, ensuring a near endless biomass for more benign processing. Furthermore, systems that utilize bacteria for continuous flow or batch systems have already been developed for industrial use in breweries, wastewater treatment plants, and cell based chemical manufacturing, amongst other applications. To date, bacterial approaches to scarce metal recovery remain unexplored. This dissertation represents the first research on bacterial processing and recovery of the lanthanides and tellurium, and presents promising results that will serve as the foundation for future research in this field.

1.1 Current microbial methods for metal recovery

Bacteria have an important role in metal geochemistry, and are known to be lynchpins in the cycling of various earth abundant metals, such as iron, manganese, calcium, and magnesium[3,4]. They are also crucial in the cycling of heavy metals, such as arsenic, lead, and mercury[3,5]. Bacteria have evolved mechanisms for interacting with these metals because the metals have forms that are soluble and available to bacteria in their natural habitats, for instance in the ocean and in streams. They interact with the

metals for their benefit, as in the case of iron redox for ATP generation, or for their detoxification, as in the case of mercury reduction to Hg°. The elements discussed in this thesis are not generally bioavailable or considered to be bioactive, and the role bacteria play in their cycling is either unknown or negligible. Nevertheless, bacteria do interact with these metals, and can be used for their recovery from solution.

The most common ways bacteria extract metals from their sources are by bioleaching and biosorption. One example of bioleaching is the practice of adding iron oxidizing bacteria to heap metal ores to enhance metal solubilization[6]. Biosorption is the practice of using biomass to adsorb metal ions from dilute solutions[7].

1.1.1 Bioleaching

Bioleaching has been used industrially to extract copper from copper sulfides, and has been demonstrated on iron, cobalt, nickel, zinc, and uranium[8]. A typical bioleaching process that liberates iron from pyrite is as follows[9]:

Fe^{3+} is added to a pyrite (FeS_2) ore in the presence of water. The pyrite is oxidized by the Fe^{3+} (creating Fe^{2+}) transforming it to a soluble sulfur species ($S_2O_3^{2-}$) and an iron ion which also goes into solution (Fe^{2+}). Chemoautotrophic bacteria (i.e. bacteria that obtain energy through oxidizing inorganic molecules) then oxidize the sulfur to form sulfuric acid and oxidize the Fe^{2+} to form Fe^{3+} (replenishing the original oxidizing agent). The excess iron ions (Fe^{2+}), now separated from the ore, go into solution and can be recovered from the heap using typical extractive metallurgical techniques, such as electrowinning.

Bioleaching has been used in the extraction of copper at an industrial scale since at least 1980, and in several instances since[6]. These processes often utilize iron oxidizing bacteria such as *Thiobacillus ferrooxidans*, although consortia of bacteria are now being developed to improve overall copper yields[6]. Today, bioleaching processes over 150 tonnes of copper ore per day[6] (compared to 50,000

tonnes produced globally per day[10]), and has been estimated to save around 50 cents per pound of copper compared to traditional methods[6].

1.1.2 Biosorption

Bacteria can be inexpensive, have rapid generation times, can tolerate a range of conditions, and have the intrinsic capacity to biosorb metals from dilute streams. For these reasons, they are used in some water remediation strategies, mainly as biosorbents for heavy metals[11,12]. In these cases the bacterial surfaces immobilize metal ions from solution, through a combination of physical, chemical, and electrostatic binding. The bacteria have a high surface area consisting of polysaccharides, lipids, and proteins which provide numerous complexation sites for metals to bind to. Biosorption alters cation mobility by indirect means and therefore is not typically selective for individual metals.

There are a number of examples in which biosorption has been used to remediate mining effluent. At the Homestake lead refinery in Missouri, USA, for instance, metal-rich waste is passed through beds of cyanobacteria, algae, and plant material. This biomass is reported to remove greater than 99% of all metals, including lead, copper, and zinc[13], which can then be safely disposed of. In addition, a pilot scale mercury remediation system has been installed at a chloralkali plant in Germany. The plant removed 99% of mercury from waste effluent through biosorption to various strains of *Pseudomonas*[14].

1.2 Goals and objectives

The overall goal of this thesis is to investigate the possibility of bacterial recovery of the lanthanides and tellurium from a variety of sources, such as solutions, compounds, devices, and mining products. We did not endeavor to merely identify and optimize a process, so the yields and purities of the recovered metals, which may be important to future applications, fall outside the scope of this thesis and were

not rigorously examined. Rather, we sought to learn and theorize about the interactions between metals and bacteria that occurred during experimentation. In the process we hoped to understand the science that governed the phenomena that were observed, and establish a framework for the bacterial recovery of scarce metals.

1.3 Content of thesis

The first two chapters present the motivation and background for the experiments that were performed. Chapter 2 discusses the lanthanides' and tellurium's supply risk, as well as their applications and current methods for their extraction and recovery from mines. Chapter 3 discusses the bacteria used during the investigation, along with the reasons each was selected.

As has been discovered in this thesis, the lanthanides biosorb to bacterial surfaces and can subsequently be selectively desorbed by washing with elutants of different pH. Their biosorption is descriped in Chapter 4 and their desorption in Chapter 5. A simple surface site binding model for the bacteria is proposed that describes the biosorption and desorption behavior of the individual lanthanides in terms of the pK_A of different surface sites. The model is tested by replacing the bacteria with a liposome having exposed phosphate groups, thought to be the principle binding site on the bacteria. The performance of the liposomes is similar to the bacteria and, furthermore, both exhibit very similar separations of the heavy lanthanides. In Chapter 6 we show that these separations can be controlled to concentrate various lanthanides from an equally mixed lanthanide solution. This biosorption - based process surpasses some of the lanthanide separations that are currently performed in industry.

Tellurium, on the other hand, is found to interact with bacteria very differently, as some bacteria have the ability to transform tellurium between its various chemical compounds. Following a summary of known tellurium microbiology in Chapter 7, Chapter 8 describes the reaction between a deep-sea vent bacteria, chosen for its high tolerance for tellurium, and several tellurium compounds.

Despite the differences between many of these compounds, it is found that the bacteria nonetheless interact with them in a similar manner. Based on the results obtained, a consistent model for the bacterial transformation of tellurium is presented.

The biological recovery of metals is nascent, but growing in importance. This dissertation concludes with a summary of the work presented, and an outlook for future researchers who explore this field.

2

Tellurium and lanthanide extraction, recovery, and supply risk

To place this research in perspective the current concern about metals' availability will be described, specifically as it pertains to the lanthanides and tellurium.

Current methods for lanthanide and tellurium extraction, separation, and purification are complex, multistage, use toxic chemicals, and have poor yields. Additionally, these elements have low

abundances and geopolitical considerations affecting their availability. Taken together, these these metals' supplies can be at risk to a number of disruptions and threats, and new methods for their production and recycling are needed. This is especially important to these metals because it is likely that their demand will increase significantly as green technologies are implemented world wide. This chapter summarizes tellurium's and the lanthanides' supply risk, as well as the current means by which these metals are extracted.

2.1 Supply risk

A metal's supply risk can be defined as the vulnerability of that metal's supply chain, or, in other words, the probability that metal becomes unavailable. A metal's overall supply risk is composed of many risk factors, and the two that are most relavent to this thesis are the resource supply risk, which is the risk associated with the overall abundance of a metal, and the geopolitical supply risk, which is the risk associated with governments controlling the production or reserves of a metal. As will be described below, tellurium's major supply risk is a resource risk, whereas the lanthanides' supply risk is a geopolitical risk.

2.1.1 Resource supply risk

Metals can be grouped into three major categories of abundance: the abundant metals, the semi-scarce metals, and the scarcest metals.(Figure 2.1) The abundant metals consist of the rock-forming elements such as iron, aluminum, sodium, and magnesium that occur at least at one atom per thousand silicon atoms (silicon being the most abundant metal). They are widespread throughout the world and occur at high concentrations in their ores. Unsurprisingly, these same elements have higher production and more applications than less abundant metals, and have been used in tools and devices throughout history. They are also the primary products of many mines, from which other metals are recovered as

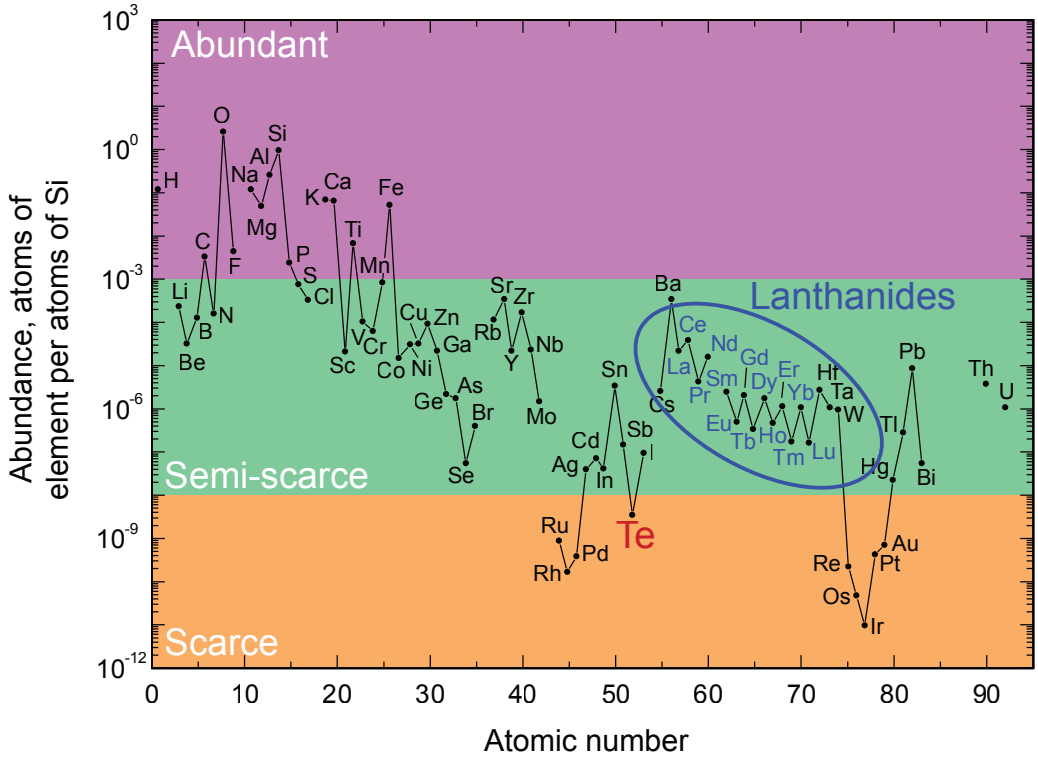

Figure 2.1: Abundance of the elements as a function of atomic number. Tellurium is a scarce element, with an approximate concentration of 1 ppb compared to silicon, and the lanthanides are semi-scarce elements, with concentrations ranging between approximately 10 ppm and 100 ppt. (This figure is adapted from one published by the United States Geological Survey.) [15]

byproducts.

In contrast, the semi-scarce metals consist of metals that occur at lower concentrations, between 10 ppt and 100 ppm relative to silicon. Examples of these metals are cobalt, nickel, molybdenum, lead, and the lanthanides. These metals have many applications, but they are not used in the same volume as the abundant metals. Many of the semi-scarce metals can be mined as primary products or produced as byproducts from mining other metals.

Finally, the scarce metals are metals that are present in the earth's crust at concentrations less than

10 ppt relative to silicon, and include metals such as rhodium, iridium, platinum, and tellurium. Due to their high costs, these metals are not widely used and are often substituted with other metals where feasible. They are nearly always produced as the byproducts from mining other metals. The scarce metals present a supply risk because they are not abundant enough to ensure their availability, and their supply is inelastic with their demand, because it is tied directly to the mining of the primary ore from which it is produced.

An element's supply risk is also a function of the existence of widespread mineable ores. Even if an element is abundant, if its ores are limited to specific regions of the world then geopolitical factors become important. A well-known example of this is oil, where proven reserves and production are largely concentrated to the Middle East, Russia, and South America. A method of quantifying diversity in a marketplace is the Herfindahl-Hirschman Index (HHI)[16]. Although the HHI was created to determine business competition in assessing monopolies for antitrust cases, it has been recently used by T. Graedel to assess the elements and their geopolitical risk[17]. The HHI represents the concentration of market share that countries have over metal production, and can be applied to both production of materials (i.e. the countries that produce the materials), or the proven reserves of materials (i.e. the countries where these materials exist). It is calculated for each element with the following equation, where N is the total number of countries involved, and s_i is the percent market share of country i in the world production or reserves of a given element.

$$HHI = \sum_i^N s_i^2$$

As a part of this thesis work, the HHI's for most elements were calculated based on USGS data from 2011, and they are shown in Table 2.1[18]. A high HHI is associated with a concentrated market, and as a rule of thumb in businesses an HHI over 2500 is considered 'highly concentrated'[16]. Examples of metals with high HHI's are the lanthanides, since production is currently confined to China, the

platinum group elements, where, although production occurs in many countries, proven reserves are highly concentrated in South Africa, and niobium, where both reserves and production are principally in Brazil.

The periodic table in Figure 2.2 (also produced as part of this thesis) shows the elements that have supply risks either due to concentrated production or reserves as measured by HHI, or lack of abundance. Any element shaded red in one of the three sections should be considered at a supply risk. Some of these metals which are deemed to have supply risk are also important to future energy technologies. For example, neodymium, praseodymium, and dysprosium are used in permanent magnets in electric motors and generators, and tellurium is used in solar cells. The results of the HHI and abundance analyses are supported by a different methodology used by the U.S. Department of Energy to compare each elements' supply risk to its criticality in future energy technologies[19].(Figure 2.3) The results show many of the lanthanides and tellurium are among the scarcest and most critical elements. New methods are needed for the recovery and recycling of these elements, to ensure that that their scarcity does not prohibit their use in new energy conversion devices.

2.2 Tellurium applications and production

2.2.1 Applications

Since its discovery in 1782[20], tellurium has rarely been recovered or produced from mining operations because of its minimal usage and limited applications[21]. In the last decade though, the optical, electronic, and processing properties of tellurium have been exploited to create among the cheapest solar cells per power output[22] and among the highest efficiency thermoelectrics[23].

The largest application of tellurium is in cadmium telluride (CdTe) solar cells. CdTe has a band gap of 1.45 eV at 300 K, making it almost perfectly matched to the peak of the solar spectrum[24]. Current CdTe solar cells can reach efficiencies above 20%, making them amongst the best-in-class pho-

Table 2.1: Calculated Herfandahl-Hirschman indices for each elements' production and reserves [18]. Starred values show a high degree of uncertainty. The lanthanides are shaded in gray.

Element	$HHI_{production}$	$HHI_{reserves}$	Element	$HHI_{production}$	$HHI_{reserves}$
He	3200	3900	Ru	3200*	8000*
Li	2900	4200	Rh	3200*	8000*
Be	8000	4000*	Pd	3200	8000*
B	2900	2000	Ag	1200	1400
C	500*	500*	Cd	1700	1300
N	1300	500*	In	3300	2000*
O	500*	500*	Sn	2600	1600
F	1500*	1500*	Sb	7900	3400
Na	1100	500*	Te	2900	4900
Mg	5300	500*	I	4900	4800
Al	1600	1000*	Cs	6000*	6000*
Si	4700	1000*	Ba	3000	2300
P	2000	5100	La	9500	3100
S	700	1000*	Ce	9500	3100
Cl	1500*	1500*	Pr	9500	3100
K	1700	7200	Nd	9500	3100
Ca	3900	1500*	Pm	9500	3100
Sc	5500*	4500*	Sm	9500	3100
Ti	1100	1600	Eu	9500	3100
V	3300	3400	Gd	9500	3100
Cr	3100	4100	Tb	9500	3100
Mn	1600	1800	Dy	9500	3100
Fe	2400	1400	Ho	9500	3100
Co	3100	2700	Er	9500	3100
Ni	1000	1500	Tm	9500	3100
Cu	1600	1500	Yb	9500	3100
Zn	1600	1900	Lu	9500	3100
Ga	5500*	1900*	Hf	3400*	2600*
Ge	5300	1900*	Ta	2300	4800
As	3300	4000*	W	7000	4300
Se	2200	1900	Re	3300	3300
Br	3300	6900	Os	5500*	9100*
Rb	6000*	6000*	Ir	5500*	9100*
Sr	4200	3000*	Pt	5500	9100*
Y	9800	2600	Au	1100	1000
Zr	3400	2600	Hg	5500	3100
Nb	8500	8800	Tl	6500*	6500*
Mo	2400	5300	Pb	2700	1800
			Bi	5300	6000

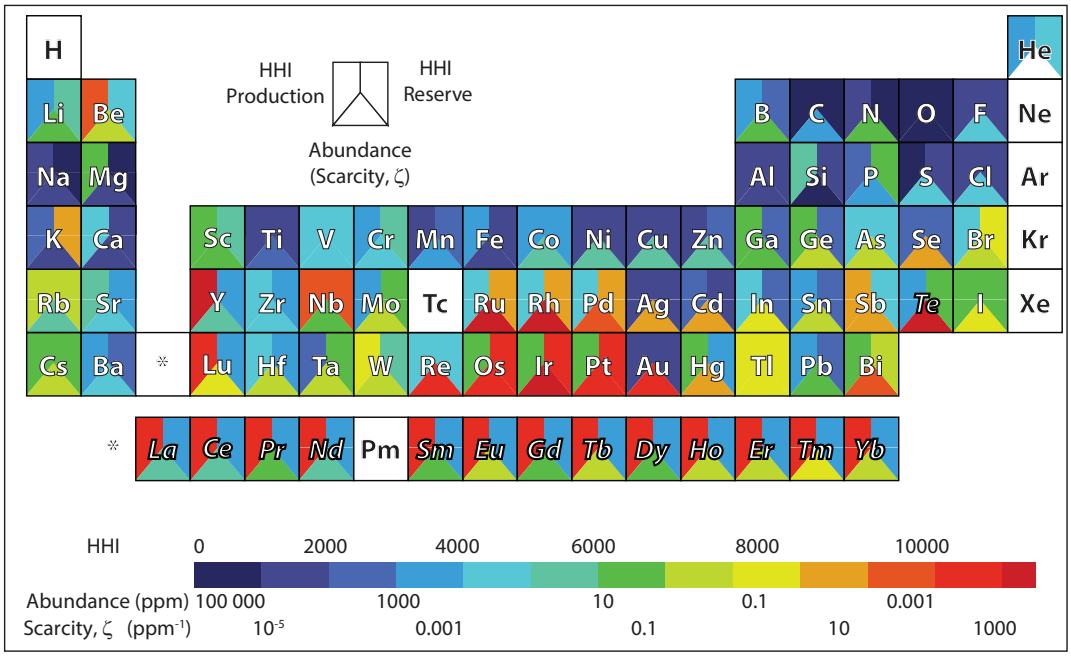

Figure 2.2: Periodic table with each elements' HHI production, HHI reserves, and abundance shaded. The magnitude of each of these parameters is shaded from blue to red in order of increasing HHI and scarcity. Elements with red sections are considered to have supply risk. Used with permission [18].

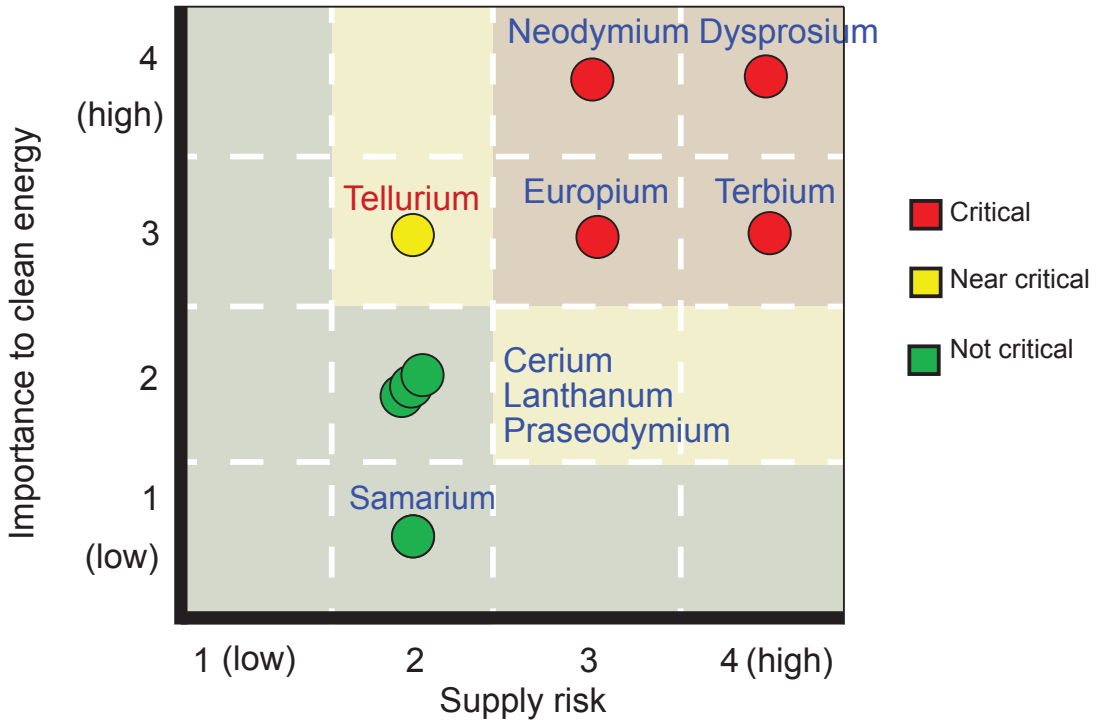

Figure 2.3: Plot of elements' importance to clean energy as a function of supply risk. Tellurium and some lanthanides are deemed critical and near critical elements. (Figure reproduced from one published by the U.S. Department of Energy.)[19].

tovoltaics (PVs)[25]. They also have relatively simple architectures consisting of only 6 layers: glass, transparent conductor (SnO_2), window (CdS), alloy layer (CdS_xTe_{1-x}), absorber (CdTe), and metal contact[26]. These factors contribute to making CdTe solar cells the cheapest commercial solar cells based on cost per watt. In 2008, more thin-film solar cells, dominated by CdTe PV modules, were produced in the U.S. than any other kind[27]. A brief analysis of the impact of tellurium's low abundance on the solar cell industry is presented in Appendix F.

Another application for tellurium is in Peltier coolers and thermoelectric generators, which primarily utilize bismuth telluride to convert between heat and electricity[28,23,29]. The scarcity of tellurium, however, has driven research towards other compositions that are less efficient than bismuth telluride[28,23]. More effective recovery of tellurium could expand the use of bismuth telluride thermoelectrics.

2.2.2 Production

Tellurium is produced as a byproduct of copper mining, and an abridged process for its recovery used in the United States is outlined below.(Figure 2.4) In copper ore it exists primarily as tellurides (e.g., Cu_2Te, AgTe), with an abundance of ~0.1 ppm[30,31,32]. Like copper's other 'daughter elements' (e.g. gold, silver, selenium, and platinum group metals (PGMs)), tellurium first undergoes copper's recovery circuit. It is mined, milled, floated, smelted, casted and finally electrolyzed where it is freed from copper and collects, along with other impurities, as anode slime (shown schematically in Figure 2.5)[32,33]. Each of these processes are intended to purify copper, not tellurium, and much tellurium is lost (particularly during smelting)[34,32]. Nonetheless, the anode slime contains ~1% tellurium, enriched 10^5 times from copper ore[34,32].

Purification from the anode slime varies between refineries, but the chemical steps for a typical process are shown below. First, the anode slime is acid leached in an autoclave (150 °C, 2 atm) for 1 week to convert tellurium to tellurous acid (H_2TeO_3)[32]. This solution is filtered through copper powder

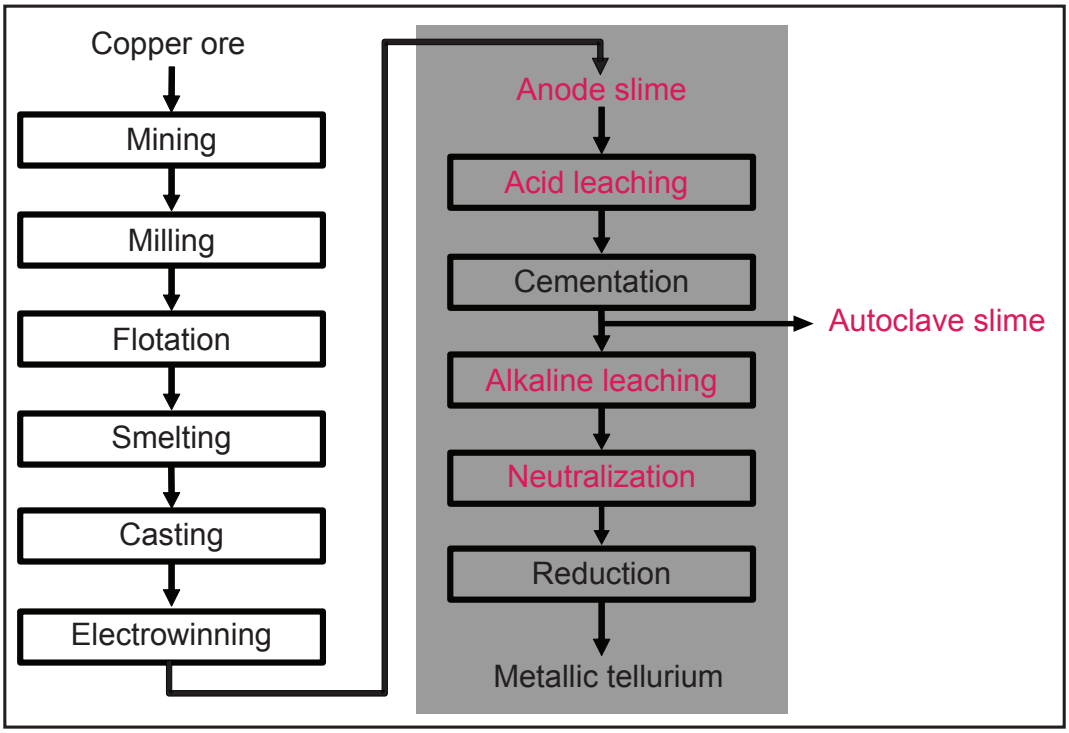

Figure 2.4: Abridged tellurium production flow chart used in the United States[35,32]. Gray shaded region shows where tellurium production begins. Red text shows possible tellurium sources for bacterial recovery. Also, the electrowinning step is described in detail in Figure 2.5.

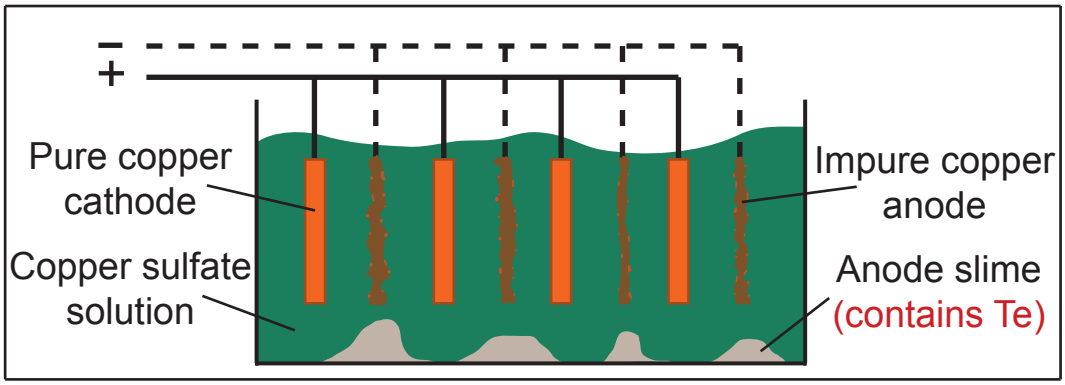

Figure 2.5: Copper is electrolytically purified from an impure copper anode to a pure copper cathode. The impurities from the copper anode settle at the bottom of the chamber as 'anode slime'. This anode slime contains high levels of tellurium ($\%_{textTe}$=1%) and is currently used as the primary source for tellurium.

where the tellurium 'cements' (i.e., reacts) to form copper telluride (CuTe) (i)[32,33]. Then, sodium carbonate (Na_2CO_3) oxidizes telluride to sodium tellurite (Na_2TeO_3) (ii)[35,32]. Next, the sodium tellurite is neutralized to pH 5, forming tellurium dioxide (TeO_2)(iii)[35,32]. Finally, sulfur dioxide (SO_2) reduces tellurium dioxide to metallic tellurium (Te°) (iv)[35,32]. Tellurium's recovery from anode slime has efficiencies between 20-80%[36,37]. The effluent of the autoclave step in the process, called autoclave slime, contains tellurium and is a potential source for bacterial tellurium recovery[35,32].

Tellurium production from anode slime:

(i) $$4Cu + H_2TeO_3 + 2H_2SO_4 \rightarrow Cu_2Te + 2CuSO_4 + 3H_2O$$

(ii) $$Cu_2Te + Na_2CO_3 + O_2 \rightarrow 2CuO + Na_2TeO_3 + CO_2$$

(iii) $$Na_2TeO_3 + H_2SO_4 \rightarrow TeO_2 + Na_2SO_4 + H_2O$$

(iv) $$TeO_2 + 2SO_2 + 2H_2O \rightarrow Te^{\circ} + 2H_2SO_4$$

We note that there are alternate processes to purify tellurium from its various mining sources (e.g., tellurium bearing soda slags, and acid-plant sludges and muds)[35,32].

2.3 Lanthanide applications and production

2.3.1 Applications

The largest use of the lanthanides by volume is probably in glasses and ceramics, where they are used as additives to colorize these materials or absorb ultraviolet light, and to polish their surfaces[38]. Another important application is hydrocarbon cracking, where lanthanide oxides (primarily lanthanum oxide) are used to break down long-chained hydrocarbons into short-chained ones[38]. In addition, the lanthanides are used in many 'green' energy technologies, such as phosphors in advanced lighting, intermetallics in fuel cells and batteries, and permanent magnets in wind turbines and electric vehicles.

High performance electric motors and generators rely on lanthanides, where they are used in high energy product permanent magnets for converting between mechanical and electrical energy[39]. Among the materials with the highest magnetic energy and highest coercivity are neodymium iron boron magnets ($Nd_2Fe_{14}B$), and so they are used in the gear boxes of wind turbines and electric car motors[40]. These magnets sometimes have samarium, dysprosium, or terbium added in order to increase their coercivity and high temperature performance. A brief case study on the impact of neodymium's availability on the electric car market is presented in Appendix F.

Lanthanide based phosphors are used to convert incident light into important wavelengths in the visible spectrum. Many of them were originally developed for use in cathode ray tubes, and are now used in fluorescent and LED lighting. $Eu^{2+}:Sr_4Al_4O_{25}$, for example, after excitation with ultraviolet

light, irradiates blue light at 425 nm[38]. Terbium and lanthanum can be combined in Tb^{3+}:$LaPO_4$ phosphors to create green light at 535 nm[38]. These and other lanthanide based phosphors are necessary to create so-called 'natural' lighting that appears to match incandescent lamps' spectra.

Lanthanide intermetallics can store large amounts of hydrogen per unit volume. One application is hydrogen storage, where alloys such as $LaNi_5$ adsorb hydrogen to form $LaNi_5H_6$[38]. It is commercially used in fuel cell vehicles because the adsorption and desorption of hydrogen is fully reversible over a large number of cycles by changing the temperature or pressure. Another major use is in nickel metal hydride batteries, where protons are stored in the lanthanide-based anode (for example $La(Ni_{3.6}Mn_{0.4}Al_{0.3}Co_{0.7}))$[38]. During recharging they desorb and combine with an electron at the cathode. Nickel metal hydride batteries are used in a variety of electronics and electric vehicles.

Additionally, an important magnetostrictive material (i.e. a material that undergoes a strain under a magnetic field) is Terfenol-d, which is an iron - dysprosium - terbium alloy ($Tb_{0.3}Dy_{0.7}Fe_{1.92}$)[38]. Terfenol d is a high powered actuator that is used in valve controls and large sonar systems.

Many of these applications have only been developed in the last 60 years because before then the lanthanides were too difficult to separate to study individually. It was only with the advent of modern lanthanide separation techniques have the lanthanides' properties been fully characterized, and applications for lanthanides grown. In the next section these separation strategies and techniques will be discussed in depth.

2.3.2 Production

The lanthanides are difficult to recover because they are chemically similar and naturally occur together. They are found in minerals such as Bastnaesite, Monazite, and Xenotime, where they occupy the same cationic lattice sites because of their identical valency (3+), and similar size. This means the lanthanides cannot easily be separated using typical and uncomplicated mineral purification methods that take advantage of differences in elemental size, density, reduction/oxidation potential, and/or

melting/boiling points.

The overall approach to recovering the lanthanides is generally the same world-wide. Lanthanide ore is mined from the ground and crushed to a particle size of 100 μm. This powder passes through a series of flotations that separate out the flotation tails (i.e., waste) from the lanthanide mineral. The lanthanide mineral is then chemically processed to remove impurities (e.g., Sr, Th, U, and Ca). Finally, the pure lanthanide concentrate is dissolved into a chloride solution that is the input for separation into individual lanthanides as described below.

The lanthanide chlorides ($LnCl_3$) are typically separated through a series of liquid-liquid extractions. During the liquid-liquid separation process an aqueous mixture of lanthanide chlorides is combined with an immiscible organic liquid[38]. Individual lanthanides partition differently between the organic and aqueous phases based on the small differences in their basicities which, in turn, change their relative solubilities in each of the liquid phases[38]. Then, the two liquid phases are isolated and the lanthanides scrubbed (i.e. recovered) from each phase. The scrubbed solutions are continuously fed through numerous solvent extraction stages to further improve the purity of the recovered elements[38]. Typically, the lanthanides are separated into groups of lanthanides based on their masses(e.g. 'lights' and 'heavies'), and then subsequently separated into individual lanthanides if necessary for a given application.

The organic phase is usually a phosphate material dissolved in kerosene. Industrially, these include di-2-ethyl-hexyl-phosphoric acid (HDEHP), and 2-ethyl-hexyl-2-ethyl-hexyl phosphonic acid (EHEHPA). The aqueous phase is normally at low pH in a common inorganic acid, for example 0.1 M HCl, or 1 M HNO_3. Besides the scrubbing solutions, other variables also affect the separation; the concentration of solutes and lanthanides, pH of the solution, and temperature all play a role. For example, solubility of Gd^{3+} in EHEHPA increases with pH and EHEHPA concentration[41].

The effectiveness of lanthanide separation can be quantified using the following calculations. The measure of an individual lanthanide's affinity to a particular phase (aqueous or organic) is known as

the distribution coefficient, and is the ratio of the lanthanide between the two phases. A figure of merit, called the separation factor, quantifies the degree of separation between lanthanides; it is defined as the ratio of distribution factors of two lanthanides. The further the separation factor is from unity the better the separation is; in industry, the separation factors for neighboring lanthanides is as low ~1.12[38].

Distribution coefficient: $$D_{Ln} = \frac{[Ln_{organic}]}{[Ln_{Aqueous}]}$$

Separation factor (Yb from Lu): $$\alpha_{Lu}^{Yb} = \frac{D_{Yb}}{D_{Lu}}$$

Other methods for separating lanthanides that have been demonstrated include selective oxidation/reduction, fractional crystallization/precipitation, and ion exchange. The lanthanides typically exist in nature as trivalent cations, nevertheless Ce, Pr, and Tb exhibit tetravalency, and Sm, Eu, and Yb exhibit divalency, so these elements can be oxidized and reduced from a mixture if in large enough quantities. In industry this is commonly performed with Ce, which is removed during lanthanide processing by oxidation to Ce^{4+}. Fractional crystallization/precipitation separates the lanthanides based on slight differences in crystallization or precipitation as a function of temperature or solubility, respectively. Ion exchange is a chromatographic technique in which a mixture of lanthanides is passed through a charged column, and the lanthanides separate out based on their affinity to the column over long distances and times. This method achieves ultra-high purities at the expense of low throughputs and limited species separation. The majority of lanthanide separation is performed by solvent extraction[38], requiring multiple stages and the use of toxic chemicals.

2.4 Summary

Advanced lighting devices, hydrogen based batteries, electric motors and generators, photovoltaic cells, and thermoelectric generators are all important future energy technologies that rely on the availability of the lanthanides or tellurium. In many cases these elements have unique properties and are difficult to substitute with other elements, making their ongoing availability critical to the implementation of these devices. Unfortunately, they each have supply risks and their production and recycling are challenging. The next chapter describes the various bacteria which will be used to help recover and separate these elements.

3

Bacteria used for lanthanide and tellurium recovery

The purpose of this short chapter is to describe the choice of the various bacteria used in this thesis and the basis for choosing them. Because the field of research explored in this thesis is at an embryonic stage and without any prior literature regarding lanthanides and tellurium, there is little guidance in the literature for selecting particularly promising bacteria. Furthermore, as neither tellurium nor the

lanthanides are earth abundant metals, and neither are environmentally available to any great extent, it is also difficult to obtain bacterial strains that are exposed to them in the natural environment. For this reason, bacteria from various environmental niches were selected, with a focus on extremophilic bacteria.

3.1 Hydrothermal vent bacteria

Hydrothermal vents are geological structures that form at separating tectonic plates in the depths of the ocean. These vents eject a superheated water solution known as hydrothermal vent fluid into the ocean. The vent fluid forms when seawater seeps into the crust surrounding the vents. It is heated and acidified as it flows through the crust. It also becomes anaerobic and leaches a suite of metal ions from the crust, resulting in a unique chemistry like no other on earth. As the hot fluid flows out of the vent it serves as the energy source for an entire ecosystem of prokaryotes, eukaryotes, archaea, and higher level organisms. The energy is mainly derived from sulfur oxidizing bacteria that convert hydrogen sulfide to sulfate. This rich diversity of life exists at high temperature (~350°C), high pressure (~25 bar), and low pH (~3.5)[42].

Based on several studies of the vent chimneys, it is known that the vent fluid is particularly rich in the lanthanides and tellurium. As the acidic water travels through the crust it dissolves and accumulates these metals. The vent fluid from the East Pacific Rise, a vent field west of Chile, contains lanthanides in concentrations that can be two to three orders of magnitude higher than is common in seawater[43,44].(Table 3.1) Tellurium is also 50 times more concentrated in vent fluid compared to the surrounding seawater[45]. Interestingly, vent walls have the highest reported concentrations of tellurium on the earth. Tellurium substitutes for sulfur in the walls and has been measured at concentrations of 45 ppm[46].(Table 3.2)

Extremophiles from hydrothermal vents have evolved unique mechanisms to survive in the pres-

Table 3.1: Lanthanide concentration in the East Pacific Rise vent fluid(pM)[44,43]

Lanthanide	Seawater	East Pacific Rise
Lanthanum	29	7770
Cerium	5.5	14837
Praseodymium	4.4	2045
Neodymium	21.4	7969
Samarium	4.1	1477
Europium	1.1	3977
Gadolinium	6.3	1624
Terbium	0.92	201
Dysprosium	6.4	1058
Holmium	1.7	171
Erbium	5.5	397
Thulium	5.4	285
Ytterbium	0.88	39
Lutetium	170	9336

Table 3.2: Tellurium content in the east pacific rise vent fluid and vent walls[46,45]

	Seawater	Vent fluid	Vent wall
Tellurium	13 ppq	461 ppb	45 ppm

ence of high metal concentrations in and around vents. They tend to produce higher levels of extracellular polymeric substances (EPS), and this EPS is higher in functional groups for metal binding[47]. They also produce higher levels of efflux pumps to keep metals outside their walls. Many also undergo both assimilatory and dissimilatory reactions with wide range of metals beyond just iron, like cobalt, tungsten, and chromium[48]. Some can even respire atypical metals like vanadium, and selenium[49]. Bacteria from vents were chosen for this thesis because they are resilient in extreme environments and have evolved unique mechanisms that enable them to thrive in the presence of concentrated metals.

Three strains of bacteria from the East Pacific Rise vent field were collected for this study from C. Vetriani of Rutgers University: *Pseudoaltermonas* sp. EPR3, *Alcanivorax* sp. EPR7, and *Acinetobacter* sp. EPR 174. Each strain was initially cultured to study mercury resistance[50]. Their innate ability to detoxify mercury makes them good candidates for studies on other trace elements. The three strains come from genera with other unique properties that make them attractive for this project. Strains from the genus *Pseudoalteromonas* are unusually resistant to tellurium, and have shown the ability to reduce tellurium for metabolism in anaerobic conditions[49,51,52,53]. Strains from *Alcanivorax* produce EPS that is rich in a unique class of glycolipids that are hydrophobic and allow it to exist in high metal concentrations[54]. Finally, strains from *Acinetobacter* have been shown to produce an extracellular substance capable of breaking down a wide range of metal compounds, and show a high resistance to many metals[55,56].

3.2 Other bacteria used in this thesis

The strain *Roseobacter* sp. AzwK-3b was selected because it has the ability to rapidly oxidize Mn(II) to Mn(IV)[57], which was attributed to extracellular superoxide generation[58]. It was obtained from C. Hansel of the Woods Hole Oceanographic Institute who had cultured this strain from the Elkhorn Slough, which is a coastal estuary near Monteray Bay in California. The *Roseobacter* phylum is well

known to be able to transform a number of sulfur species to dimethyl sulfide and other organosulfur compounds[59] and to have high surface to volume ratios, making them capable of high metal uptake[60].

Shewanella Oneidensis MR-1 was purchased from the American Type Culture Collection (ATCC) and is an iron-reducing bacterium that was first isolated in Oneida Lake, USA. It has a high metabolic diversity (i.e. capable of obtaining energy from many sources) and has become a model organism to study metal-microbe interactions. It has the ability to reduce many metals for metabolism, including manganese and iron, and for this reason it is commonly used in microbial fuel cells[61]. In addition, recent research has shown that it can produce extracellular bacterial nanowires that are capable of transporting charges between individual cells[62]. *Escherichia coli* P8 was also purchased from the ATCC. It was chosen because it is the only bacteria identified that had been previously studied in relation to the lanthanides *and* tellurium. In addition, *E. coli* is an archetypal bacteria used in microbiology, so it has already been studied extensively.

Bacteria from the genera *Pseudoalteromonas*, *Sphingobacterium*, and *Halomonas* were acquired from R. Dutton of Harvard University, who isolated them from cheese rinds. These genetically diverse strains present various interesting features to study. The *Pseudoalteromonas* obtained from the cheese rinds is likely a different strain from *Pseudoaltermonas* sp. EPR3 and thus it should have many of the same tellurium resistant properties as noted above. *Sphingobacterium* is a genus that produces high levels of sphingophospholipids, and bacteria from this genus have been considered for cadmium remediation because of their biosorptive capacity[63]. *Halomonas* is a halophilic genus of bacteria. These bacteria are known to be highly tolerant to a wide range of metals[56] and have been suggested for Sr remediation because of their ability to remove strontium from solution[64]. One particular species of *Halomonas*, *Halomonas Maura*, produces a unique EPS polymer that is efficient at removing metal ions from solution[65].

3.3 Summary

The bacterial strains used for experimentation were selected because of their different attributes that promised to be effective in bacterial processes with the lanthanides and tellurium. Specifically, *Pseudoalteromonas* sp. EPR3 was highly resistant to tellurium and was able to transform it in unique ways, so that strain is the primary focus of Chapter 8. *Roseobacter* sp. AzwK-3b, on the other hand, was effective in separating the lanthanides, and this strain underwent most of the experimentation in Chapters 4, 5 and 6. In the next chapter the background on biological interactions with the lanthanides is described, along with experimentation on the lanthanides and the strains discussed above.

4

Lanthanide biosorption

In contrast to many other common metals, the lanthanides are not considered bioactive. For instance, studies on mice show that they slightly accumulate in the liver and bones, but are otherwise excreted [66]. Overall, they have low toxicities (median lethal dose = 100 mg/kg), which have allowed for their approval in various therapeutics [67]. Two of the approved therapies take advantage of lanthanide compounds' ability to bind phosphates. One of these is the use of lanthanum carbonate in treating hyperphosphatemia, which is an elevated level of phosphate in the blood. The other is the use of cerium

nitrate in treating burn victims. The cerium nitrate binds phosphates in the wound, which allows for a calcium rich scab to form. The scab is harder and impermeable to bacteria, and decreases the likelihood of infection. In addition, the characteristic luminescence of the lanthanides in certain hosts makes them useful in biological imaging, where they are often chelated into larger molecules to sensitize the luminescence effect [68]. Various applications in cells such as phosphate identification, pH levels, and enzyme kinetics have all been probed using lanthanide luminescence. Another notable characteristic of the lanthanides is that some have similar ionic radii to calcium, so many lanthanides can be substituted for calcium in the calmodulin protein. This has been utilized to investigate the structure and function of this protein by various fluorometric assays [69].

These biological applications of the lanthanides are rather specialized, because, as previously mentioned, the lanthanides are not considered bioactive. Instead, the primary interaction between the lanthanides and organisms, especially microorganisms, is biosorption. In this chapter we will investigate lanthanide biosorption to bacteria and discover that these elements, while chemically similar, biosorb differently.

4.1 Lanthanide biosorption background

Biosorption has been considered for harvesting valuable metals from solution, and so previous studies, many of which are very recent and are contemporary with the studies performed as part of this thesis research, have explored bacterial biosorption in order to recover the lanthanides. These studies were usually relatively simple explorations of lanthanide biosorption, and consisted of batch experiments in which first, known masses of lanthanide cations were combined with biomass in an aqueous medium, then the system was allowed to equilibrate, and finally the amounts of lanthanides removed from solution (i.e. biosorbed to the biomass) were measured. The variables tested in these studies include: lanthanide atomic number, type of biomass, hydration of biomass, viability of biomass, contact time

between lanthanides and biomass, pH of working solution, and temperature. From these studies it appears that the viability of the biomass (i.e. live vs. dead biomass) does not affect biosorption[70,71]. It also appears that the aqueous media in which the cells are grown does influence biosorption[72], although the hydration of the biomass prior to biosorption, wet or dry, does not[73,74,75,76]. Additional studies have shown the kinetics of lanthanide biosorption are extremely rapid[77,72,70,78,79,80,81,76] with studies showing over 99% biosorption within 5 min[82,71]. Also, the pH of the solution at which biosorption occurs is important. At lower pH levels biosorption occurs to a lesser extent than at higher pH levels[77,82,78,71,81,83,76]. This holds true below circumneutral pH levels, above which the lanthanide ions precipitate as hydroxides[84]. The temperature of the solution appears to have a small influence on biosorption, with the highest biosorption occurring between 30°C and 50°C[85].

Many types of biomass have been tested for their lanthanide biosorption capacity, and each varies in its ability to bind the lanthanides. These biomasses include a range of Gram-positive[86], Gram-negative[82,71], and acid-fast (i.e. resistant to staining) bacteria[70,74], spent rootlets[77], leaf powder[87], fungi[88], seaweed[79], and microbial mats[81]. There are a limited number of studies that focus specifically on differences between biomass. One has shown that *Bacillus subtilis*, a gram-positive bacterium, and *Escherichia coli*, a gram-negative bacterium, biosorb the lanthanides similarly. Others have shown that different binding models are better suited to fitting biosorption data to different bacteria[72]. These studies go along with other non-lanthanide ion studies that show biosorption does not vary to a large degree among different types of biomass, and that many of its properties are common to all biomass[89,90].

Very few studies have focused on differences between the individual lanthanides, and those that have concluded that when compared to other ions they behave similarly[70,80]. Some differences between the lanthanides do exist, though. For example, in batch reactions with individual lanthanides the light lanthandies and heavy lanthanides tend to biosorb more than those with intermediate atomic mass[74,76]. However, when the lanthanides are combined in competition, the heavy lanthanides tend

to biosorb more than the light lanthanides[82,81,83]. Also, there is one study, published during the course of writing this thesis, that shows that at low pH the heavy lanthanides biosorb more than the light lanthanides[91].

Some lanthanide biosorption experiments using both spectroscopic techniques and surface modifications have characterized the actual surface sites that are likely to be involved in lanthanide biosorption. While these sites are not known in detail, and different bacteria may behave differently, the lanthanides are generally believed to biosorb to complex arrangements of carboxyl and phosphate groups[82,78,86,71,81,83,75]. The carboxyl and phosphate groups have published pK_a values that range from 1-6, and this range is supported by multiple potentiometric studies using individual lanthanides[78,86,75]. The carboxyl groups have a single-bonded oxygen with a $pK_a \sim 4$, whereas the phosphate groups' binding site varies depending on if the phosphate has a monoester or diester bond: the phosphoester group has a $pK_a \sim 6$[92] and the phosphodiester group with a much lower $pK_a \sim 2$[92]. Studies by Ngenwya et al. (2009) and Takahashi et al. (2010) have utilized x-ray absorption spectroscopy (XAS) to conclude that carboxyl, and particularly phosphate surface groups, are generally responsible for lanthanide biosorption.

Gram-negative bacteria are known to have a complex outer membrane on which biosorption can occur. The membranes include proteins, phospholipids, and lipopolysaccharides[93]. These molecules can present amine, hydroxyl, carboxyl, and phosphate groups to varying degrees, but only the carboxyl and phosphate groups are normally associated with metal binding[94]. The role of extracellular polymeric substances (EPS) are generally not considered in biosorption studies, but recent evidence suggests their contribution may, in fact, be important[95,96,97]. EPS can consist of up to 80% of nucleic acids, making it a large source of phosphate groups for binding[98].

Many of the lanthanide biosorption experiments presented in this chapter are distinct from those described above. As described in chapter 3, the biomass included strains of bacteria that had never before been tested for their biosorption ability. Also, in some experiments biosorption during bacterial

growth was studied rather than in the stationary phase. Additionally, the majority of experiments used a mixture of all the lanthanides for biosorption rather than single lanthanides, and in others the lanthanides were first chelated with organic acids. In addition, only a few of the experiments were carried out in batches, as is usually performed. Instead, as will be discussed in Chapter 5, a semi-continuous biosorption process was developed that allowed for the study of lanthanide desorption, in addition to biosorption.

4.2 Batch biosorption studies

In this section batch studies performed to measure differences in lanthanide binding between bacterial strains and individual lanthanides are described. The full details of the experiments are in Appendix A. Cultures of the following strains were incubated with a mixture of all 14 lanthanides: *Sphingobacterium* sp., *S. oneidensis*, *Halomonas* sp., EPR3, EPR7, EPR174. The amounts of lanthanides biosorbed to each strain were measured by sampling the media before and after biosorption occurred and the lanthanide content in these samples was measured using inductively coupled plasma - mass spectrometry (ICP-MS). The differences in the lanthanides' mass were assumed to be biosorbed. This amount was divided by the initial mass of the lanthanides in the solution in order calculate the biosorbed mass fraction of each lanthanide. Two biosorption experiments were performed with different growth conditions. In the first, the lanthanides were added to cultures in stationary phase.(Figure 4.1) In the second the bacteria were inoculated into a solution that contained the lanthanides, and grown in the presence of the lanthanides.(Figure 4.2)

In the experiments with lanthanides added to strains in stationary phase, there was consistent lanthanide biosorption between strains and individual lanthanides.(Figure 4.2) Between 80-99% of the lanthanides biosorbed to each strain, with the three hydrothermal vent strains (EPR3, EPR7, EPR174) biosorbing less than the others. In all cases there was very little difference between the individual lan-

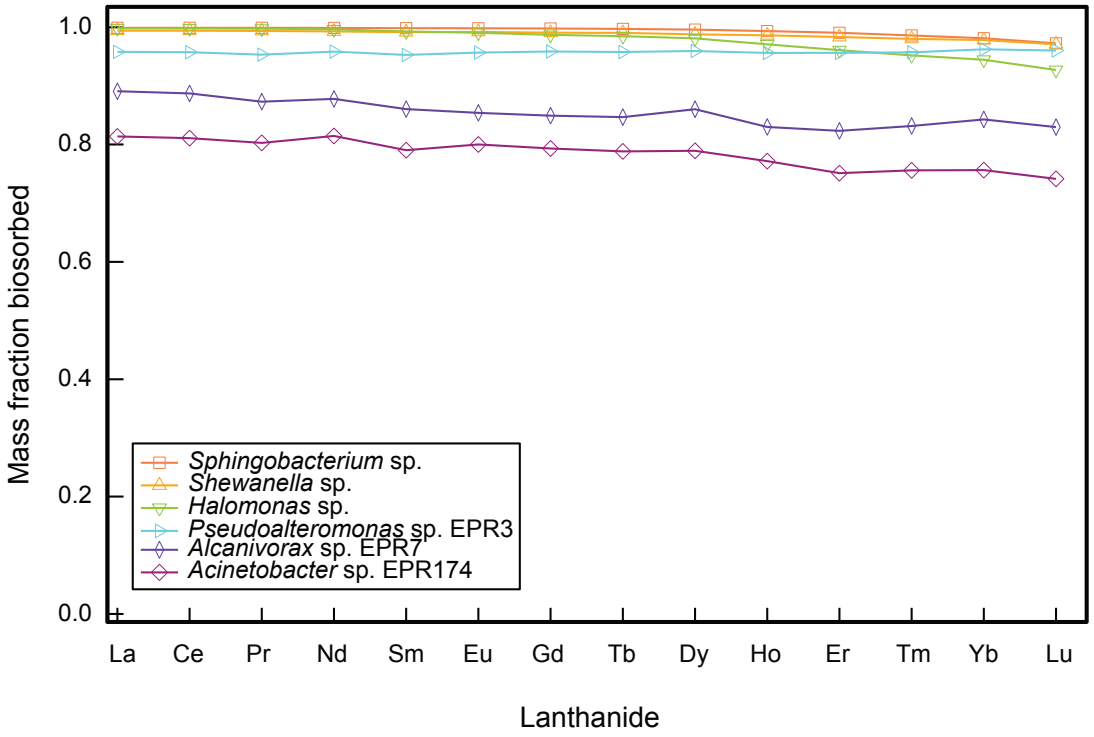

Figure 4.1: Biosorption of each lanthanide after a mixture of all the lanthanides are added to stationary phase cultures of various bacterial strains and allowed to incubate for 1 day. The three hydrothermal vent strains biosorb the least amount of lanthanides, however each strain biosorbs at least 75% of all the lanthanides. There is a slight decrease in biosorption with atomic number.

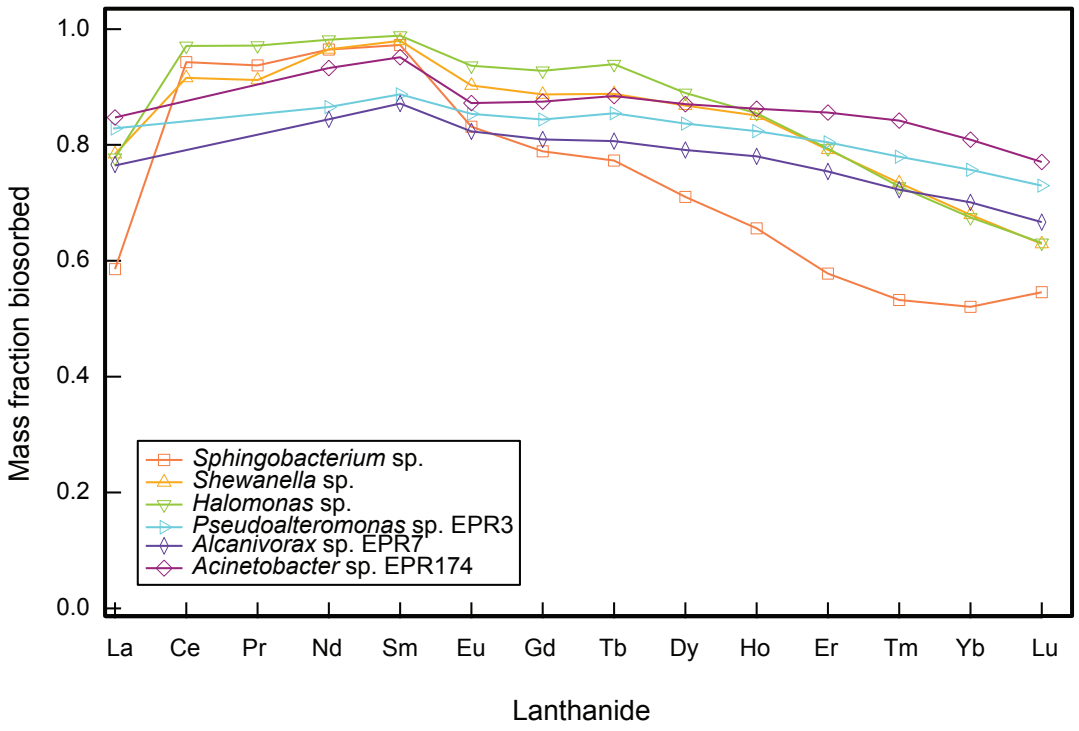

Figure 4.2: Biosorption of each lanthanide after various bacterial strains are grown in the presence of a mixture of all the lanthanides for 11 days. In each strain lanthanum biosorbs considerably less than cerium, and there is an overall decrease in biosorption with atomic number for all lanthanides above samarium.

thanides, with some showing a slight decrease in biosorption with lanthanide atomic number. This decrease was always minor, and never more than 5% of the total mass biosorbed. In contrast, the strains that were grown in the presence of the lanthanides had a lower total biosorption, and marked differences between the biosorption of individual lanthanides. Nearly all the strains saw a decrease in total biosorption by as much as 10%. In these strains lanthanum consistently had lower biosorption than cerium, and there was a general decrease in biosorption with increasing atomic number for all lanthanides after samarium. This decrease could be substantial, and in some cases there was a decrease of 5% biosorption between neighboring lanthanides.

As stated, each strain biosorbed a different amount of the lanthanides, and nearly every strain biosorbed less lanthanides during growth than when in stationary phase. These differences can be understood by differences in total biomass between strains and between growth phases. The total biomass was not measured and we would expect less biomass (e.g. during growth) to decrease biosorption because of the lesser surface area and number of surface groups[7].

There are a number of reasons that biosorption decreased with lanthanide atomic number. Regardless of growth phase, at circumneutral pH levels Gram-negative bacteria bind higher levels of the light lanthanides than heavier ones[71]. The drastic decrease in heavy lanthanide biosorption in bacteria grown with the lanthanides, though, may be attributed to differences in the production of EPS and peptidoglycan. Bacteria that are dividing produce less EPS than those in stationary phase[95], and EPS is rich in phosphate groups which are thought to primarily bind the heavier lanthanides[83]. In addition, it has been shown using *E. coli* that dividing bacteria produce lesser amounts of peptidoglycan than those that are in stationary phase[99]. Peptidoglycan is rich with carboxyl groups which has also been attributed to heavy lanthanide binding[83].

4.3 Biosorption of chelated lanthanides

The lanthanides are sometimes chelated in industry to aid in their separation, so neodymium and praseodymium, two adjoining lanthanides in the lanthanide series, were chelated with dipicolinic acid in order to determine its effect on biosorption. A sample of the bare neodymium and praseodymium cations along with a sample of chelated neodymium and praseodymium dipicolinate were incubated with EPR3 for 1 day. As with our previous studies, the samples were spun down and the biosorbed lanthanide masses were measured using ICP-MS. EPR3 biosorbed the bare cations in solution almost identically, with 76% biosorption. When the lanthanides were chelated though, the EPR3 biosorbed slightly more praseodymium, and substantially more neodymium, at levels of 78% and 86% respectively.(Figure 4.3)

While the chelation led to a difference in biosorption between these two lanthanides, the mechanism for this is unclear. The chelation should influence steric interactions between bacterial surface sites and the ligated lanthanides, and may also affect coordination of the ions. It has been shown that decreased binding coordination leads to higher biosorption[91], so it is possible the chelation changed the size difference between neodymium and praseodymium enough so that the praseodymium became lesser coordinated than the neodymium, and thus biosorbed less.

4.4 Reversibility of biosorption

Metal adsorption and desorption to bacteria has been shown to be reversible, including with the lanthanides[100,71], and is fundamental to the biosorption mechanism. In order to demonstrate reversibility, lutetium was combined with *Roseobacter* AzwK-3b in a batch system. The pH of the batch was incrementally decreased and then incrementally increased and the amount of lutetium in the batch was measured after each step as a function of pH.(Figure 4.4) These measurements showed that the amount of lutetium that biosorbed to the biomass was similar during both the pH descent (lutetium

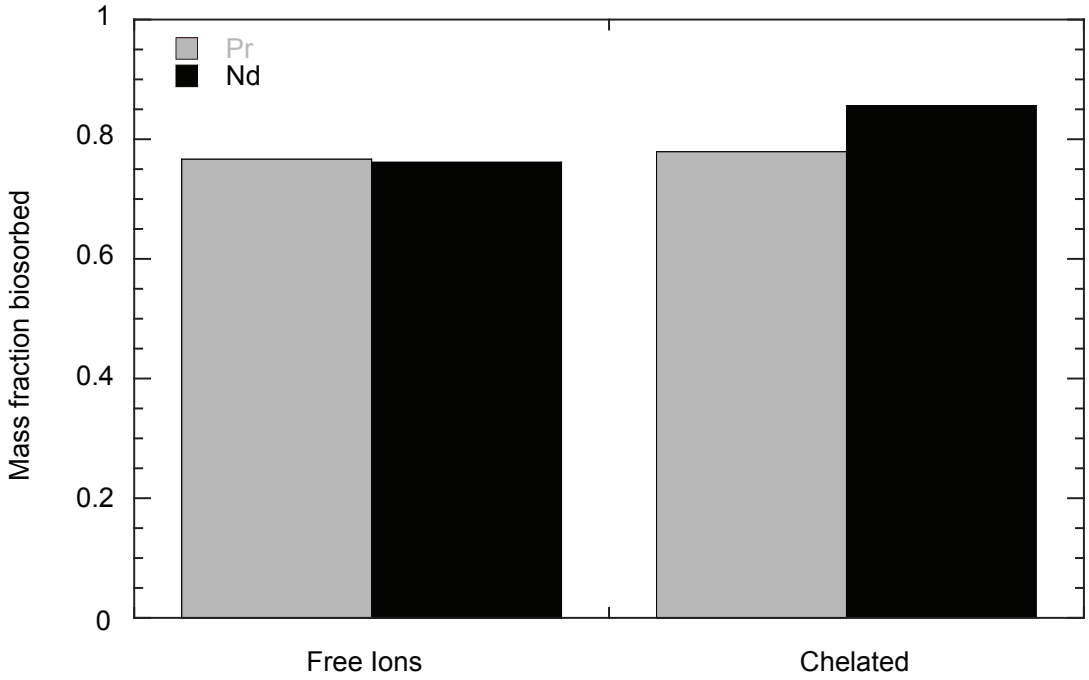

Figure 4.3: Biosorption of cationic (free ions) and chelated (coordinated to dipicolinic acid) praseodymium and neodymium. The free ions of each lanthanide biosorb similarly, but the chelated ions show a marked difference, with higher levels of neodymium biosorption.

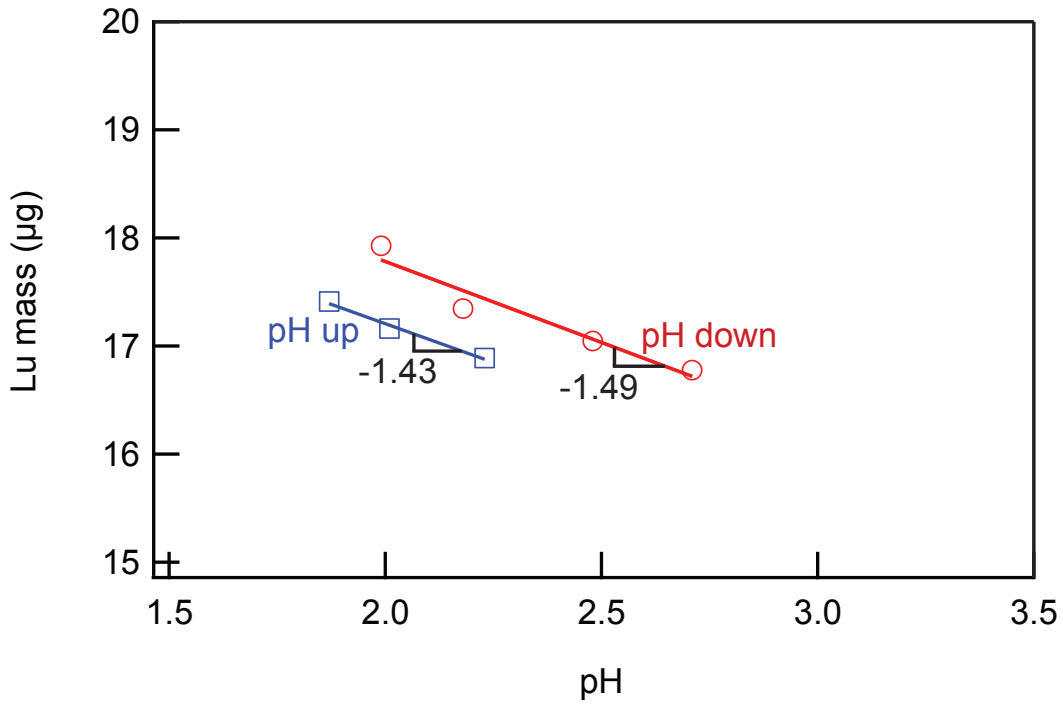

Figure 4.4: Plot of Lu mass in the media of a batch culture of *Roseobacter* sp. AzwK-3b as a function of the pH of the media being stepped down and then back up. As the pH is stepped down the mass of Lu in the media increases as it is desorbed from the surface of the *Roseobacter* sp. AzwK-3b. As the pH is stepped up the Lu in the media decreases as it re-biosorbs to the bacteria. The levels of Lu in the media, and the slopes of the Lu mass vs. pH are similar during both the step down and the step up, even though the media settled at slightly different pH levels. This demonstrates that Lu was bound, then desorbed, then rebound to the bacteria and shows that the process is reversible.

desorption) and pH ascent (lutetium adsorption), showing reversible biosorption/desorption. The pH levels at which the system equilibrated varied slightly when decreasing and increasing the pH, showing some error in the experiment which cannot be easily explained, but the slope of the sorption vs. pH is similar for both cases.

4.5 Summary

The lanthanides were shown to biosorb to each of the bacteria tested. This was demonstrated through batch studies in which lanthanides were removed from solution after incubation with the bacteria, and through the reversibility experiment that showed the total amount of lanthanide in solution was inversely proportional to the pH of the solution. There were some differences in biosorption between the lanthanides tested and the bacteria tested; the heavy lanthanides biosorbed less than the others, and the vent bacteria biosorbed less than the others. In addition, there were differences in biosorption dependant on the growth phase of the bacteria, as growing bacteria appeared to biosorb less, but with more diffrentiation between the lanthanides. Finally, changing the size of the lanthanides by chelation did have an effect on biosorption, and among the lanthanides tested the smaller chelated lanthanides exhibited greater overall biosorption. These experiments provide little insight into the sites the lanthanides are bound to on the surface of the bacteria, and if the different lanthanides bind to different sites. The next chapter will explore this possibility by investigating lanthanide desorption from the sites to which they are bound.

5

Lanthanide desorption

The batch experiments in Chapter 4, especially showed that the individual lanthanides did not biosorb uniformly across the lanthanide series. We hypothesized that these differences, however slight in the batch studies, arose from differences in the actual bacterial sites to which the lanthanides were bound, and that certain surface sites preferentially bound certain lanthanides. Based on the batch studies new experiments were designed in an attempt to isolate the lanthanides based on the surface site to which they were bound, so as to study these sites individually. This resulted in the development of a semi-

continuous filtration assay, which was used in the majority of the lanthanide experiments reported herein.

In this chapter we will discuss the development of this assay and its use in determining specific bacterial binding sites, which appear to bind the lanthanides based on their pK_a. Evidence for this pK_a dependent binding is reinforced through lanthanide adsorption experimentation on individual lanthanides and through the use of liposomes, rather than bacteria.

5.1 Development of the lanthanide desorption assay

In order to study bacterial surface sites an assay was developed that exposed bacteria to various pH washes, and then isolated the bacteria from those washes. Initially this isolation was accomplished using centrifugation. In this scheme the bacteria were exposed to lanthanides for biosorption, and then spun down to a cell pellet. The supernatant was removed and the cell pellet washed and vortexed with a low pH solution. The process of centrifugation, removal of supernatant, and exposure to a wash solution was repeated until the cell pellet had been exposed to a series of sequentially lower pH wash solutions. The lanthanide content of each solution was measured by ICP-MS to determine which lanthanides desorbed from the bacteria with each pH wash. This process was time consuming and some cells from the pellet would be lost after each wash, causing errors. For these reasons, subsequent experiments were performed by a semi-continuous filtration assay.

The filtration assay, which allows for the biosorption of the lanthanides followed by their desorption with sequentially lower pH washes, was advantageous because it was more easily controlled and elliminated many of the errors that ocurred in the centrifugation assay. The main components of the assay are a syringe, syringe filter, and syringe pump, and they function by using the syringe pump to repeatedly pass solutions from the syringe past the syringe filter. First, pH 7 water is pumped past the filter in order to wet it. Then an adsorbant, normally bacteria, is pumped past the filter, and the adsor-

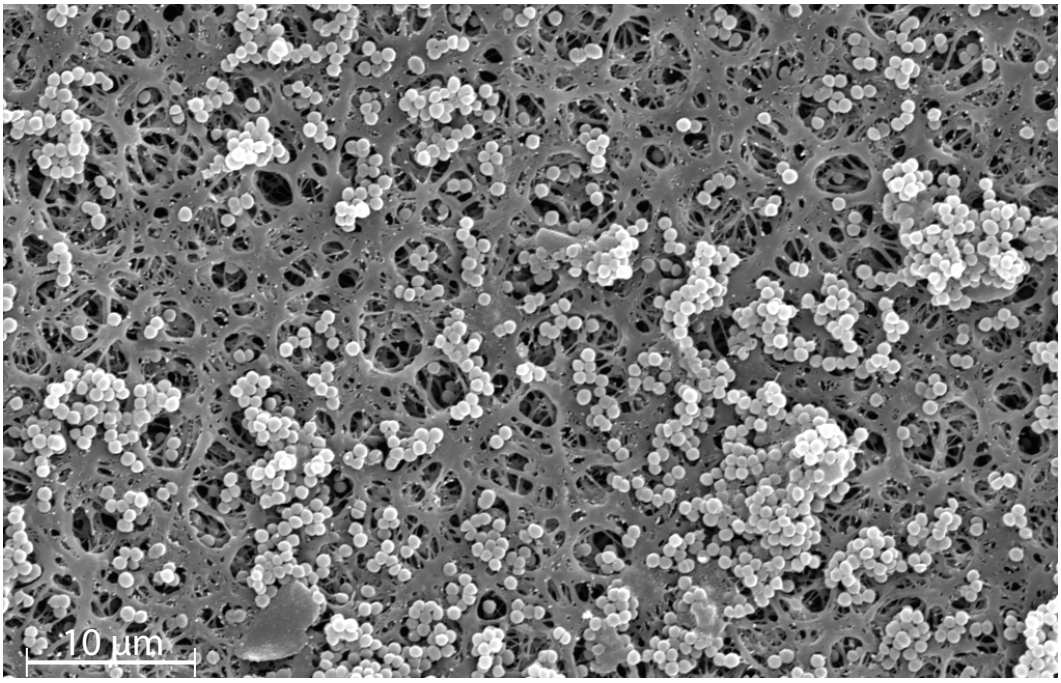

Figure 5.1: Scanning electron microscope image of *Roseobacter* sp. AzwK-3b on a Pall Acrodisc GHP filter. The bacteria are the lighter colored spheres, and the filter is the darker mesh behind them.

bant is retained by the filter.(Figure 5.1) Then, a 2 µg mixture of all the lanthanides is pumped past the filter allowing for adsorption to the adsorbant to occur. Finally, ten solutions (5 mL each) from pH 6 to pH 1.5 in increments of 0.5 pH units are pumped past the filter in order of decreasing pH, desorbing many of the bound lanthanides in the process. The lanthanide concentration of each solution exiting from the filter was measaured by ICP-MS. The full experimental details of this procedure and those based on it are described in detail in Appendix A.

Various control experiments, as will now be described, were performed to validate the filtration assay and to tune certain parameters. A Pall Acrodisc GHP filter with 0.2 µm pores was used for the filter because it retained the bacteria and did not adsorb the lanthanides. This was shown in tests of the assay without any adsorbant that showed minimal lanthanide binding.(Figure 5.2) 5 mL of the wash

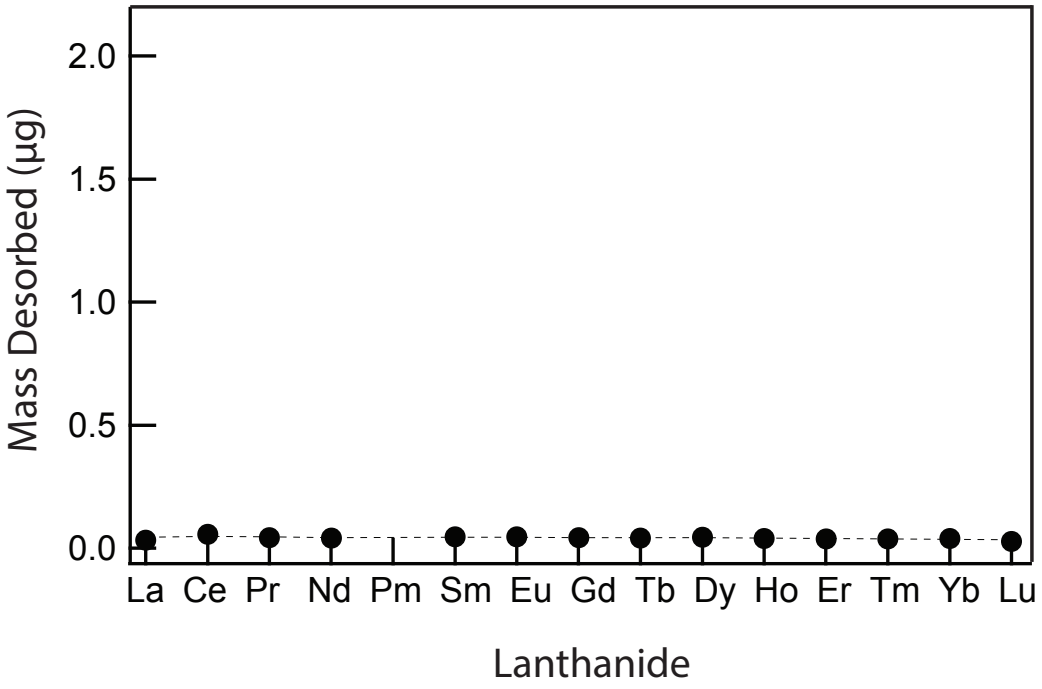

Figure 5.2: The masses of each lanthanide desorbed as a function of pH wash from a bare Pall Acrodisc GHP filter. The filtration assay was performed using this filter without any adsorbent, and minimal lanthanide adsorption to the filter occurred.

solutions and a pumping rate of 2.5 mL/min was used because it passed enough liquid at a reasonable speed over the adsorbants to fully desorb the lanthanides. This was shown by performing a filtration assay where drops of the solution were recovered. At 2.5 mL/min, 5 mL of the various wash solutions had completely desorbed the lanthanides.(Figure 5.3)

5.2 Lanthanide desorption from the bacterial strains

The filtration assay results for mixed lanthanide solutions over various bacteria are presented in this section, and are shown graphically as bar charts depicting the amount of each lanthanide desorbed as a function of each pH wash. All of the lanthanides were assayed together as a mixture in each run,

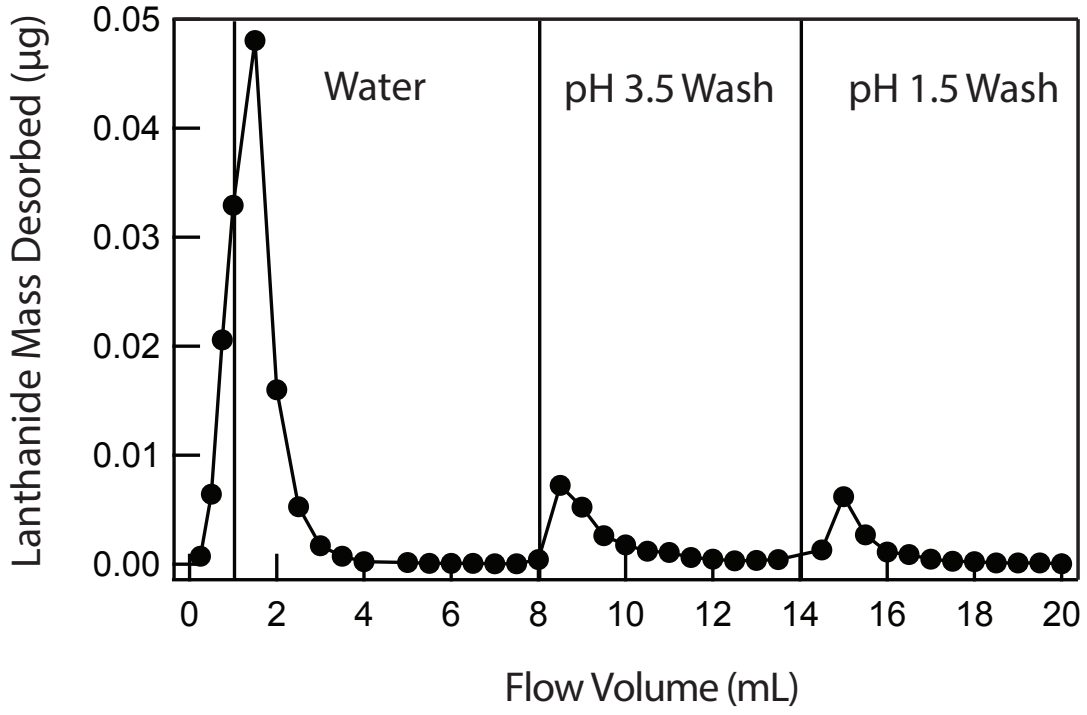

Figure 5.3: Filtration assay showing the cumulative mass of all the lanthanides desorbed as a function of volume of wash passed through the filter. Initially, 1 mL of a 2 µg/mL lanthanide mixture was passed over a filter coated in *Roseobacter* sp. AzwK-3b. This was then followed, in sequence, by 7 mL of water, then 6 mL of pH 3.5 wash, and finally 6 mL of pH 1.5 wash. At flow intervals of approximately 500 µL, an individual drop (approximately 35 µL) was recovered from the filter and analyzed by ICP-MS. These results indicate that the lanthanides are completely desorbed after approximately 5 mL of wash are passed over the bacteria at a rate of 2.5 mL/min. Based on these results, 5 mL was selected as the volume of acid washes used in all the filtration desorption experiments.

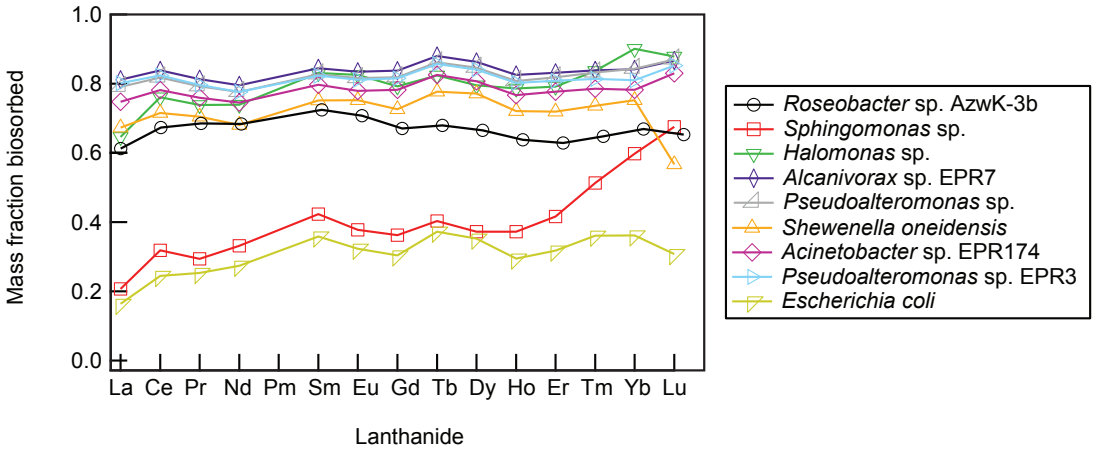

Figure 5.4: Mass fraction of individual lanthanides biosorbed to various strains of bacteria from an equal mass mixture of all the lanthanides during the filtration assay. Biosorption to the bacteria was mostly independent of the lanthanide atomic number although there is a slight preference for the heavier lanthanides.

but graphically they are presented as separate bar charts, each with the same scale. The local maxima in lanthanide mass are shown as gray bars.

The lanthanide biosorption to nine different strains was studied using the filtration assay. As shown in Figure 5.4 the total amount of each lanthanide that biosorbed varied little between the lanthanides, in agreement with the batch data presented earlier.(Figure 4.1) In the semi-continuous filtration process, though, lanthanum tended to systematically biosorb slightly less than the other lanthanides. Again, the total biomasses were not controlled, but it is worth noting that two strains, *Sphingomonas* sp. and *E. Coli*, biosorbed markedly lower masses of lanthanides than the other strains.

E. coli, *Pseudoaltermonas* sp., and each of the hydrothermal vent strains, EPR3, EPR7, and EPR174, exhibited similar lantahnide desorptions, with the desorption primarily occurring over the pH range between the pH 4 and 6 washes. In addition, the overall desorption was very similar between all lanthanides, with lanthanum having the lowest desorption at these high pH levels. *E. coli*'s desorption differed slightly in that the lanthanides also desorbed at lower pH washes, between pH 2 and pH 4.

The mass for each lanthanide desorbed at each pH is shown for EPR3 and *E. coli* in Figure 5.5 and Figure 5.6, respectively. Plots for the desorption of the *Pseudoalteromonas* sp., EPR7 and EPR174 are similar, so they are shown in Appendix B.

The other strains, *Spingomonas* sp., *Shewanella oneidensis*, *Halomonas* sp., and *Roseobacter* sp. AzwK-3b showed more inter-lanthanide variability in lanthanide desorption. Each of these strains had multiple pH washes in which a different lanthanide was predominantly desorbed. In addition, at low pH washes, between pH 1.5 and 2.5, these strains desorbed high levels of the heaviest lanthanides and low levels of the others. Bar charts that illustrate this desorption for *Roseobacter* sp. AzwK-3b (Figure 5.7) and *Halomonas* sp. (Figure 5.8) are shown here, and the bar charts for *Sphingomonas* sp. and *Shewanella oneidensis*, which are similar, are shown in Appendix B.

One of the major findings was that the masses of the different lanthanides desorbed differently as a function of pH wash. As the variation is with pH, the simplest explanation is that the lanthanide ions bind to, and desorb from, sites on the bacterial surface according, at least operationally, to their acid dissociation constants. Although the number of distinct binding sites on each strain is unknown, the desorption elutions suggest that there are between 1 and 2 different sites for *E. coli*, *Pseudoaltermonas* sp., EPR3, EPR7, and EPR174, and between 3 and 4 different sites for the other bacteria.

5.3 Binding model for lanthanide biosorption and desorption

Our binding model for the results described above is presented schematically in Figure 5.9, which shows a bare bacterial cell biosorbing and then desorbing the lanthanides. When the bacteria are cultivated in artifical seawater (ASW), ions in the solution media, such as Na^+ are loosely bound to the bacterial surface sites. (We show these sites initially as unbound in the figure). When the surface sites are exposed to the mixed lanthanide solution, our findings suggest that the lanthanide ions exchange with the loosely bound ions and biosorb to the bacterial surface. Then, as decreasing pH washes are

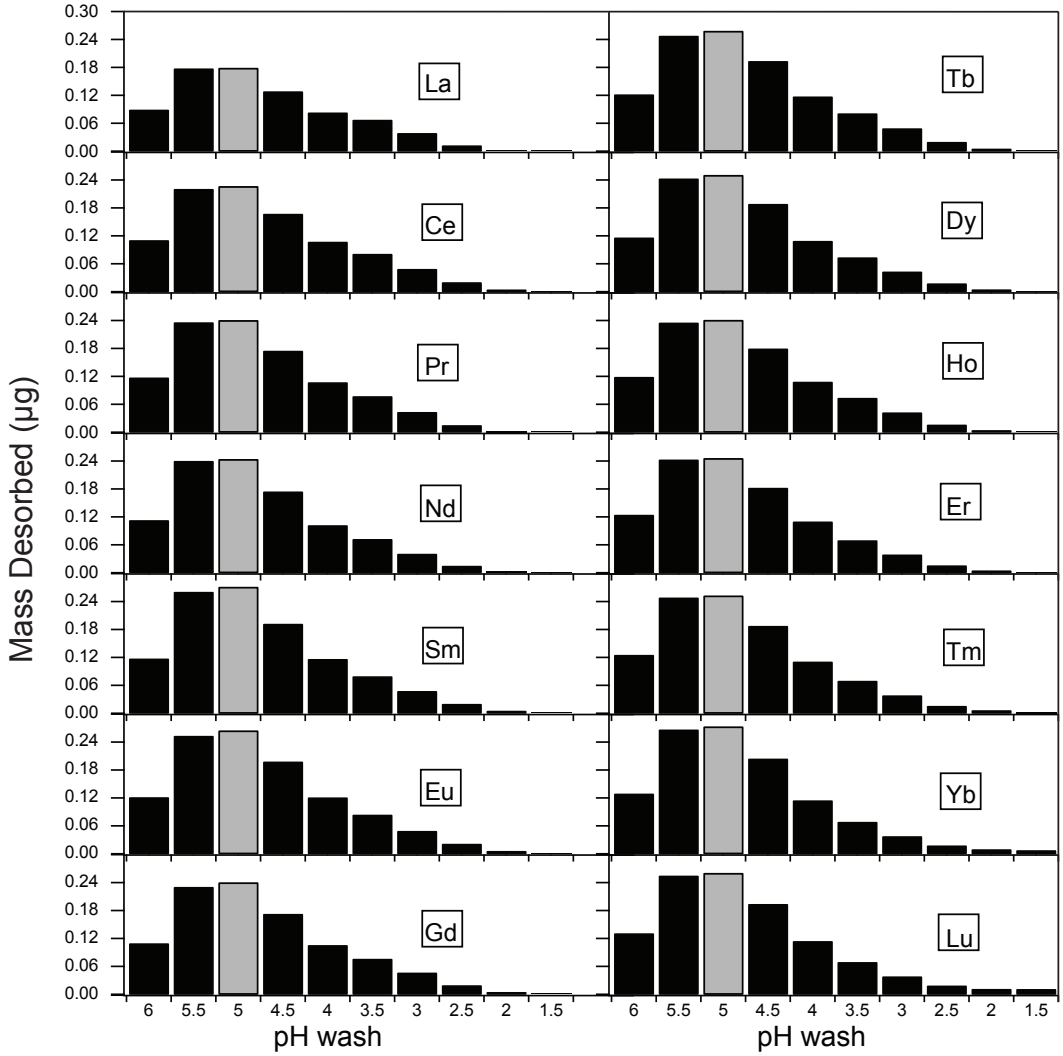

Figure 5.5: The mass of each lanthanide desorbed from *Pseudoalteromonas* sp. EPR3 at 0.5 pH intervals during the filtration assay as a function of pH wash. Each lanthanide had a similar desorption behavior, with most of their masses being desorbed during the pH 5.5 and pH 5 washes. The local maximum in the mass desorbed for each lanthanide is indicated with a gray bar, and suggests there may be just one prominent binding site with a $pK_a \sim 5$.

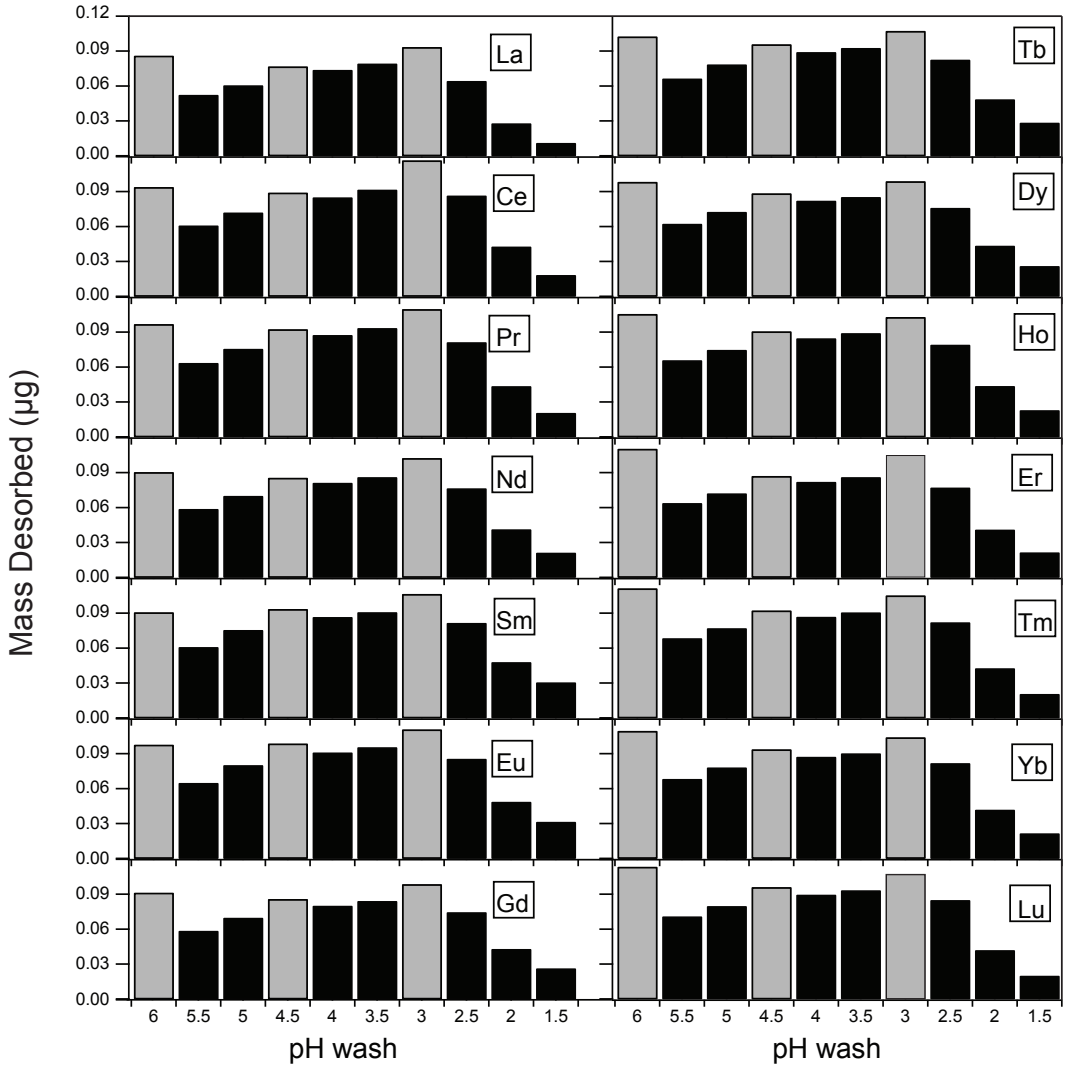

Figure 5.6: The mass of each lanthanide desorbed from *Escherichia coli* at 0.5 pH intervals during the filtration assay as a function of pH wash. Each lanthanide desorbed similarly with little differences between them. They each desorbed at many different pH levels though, with high amounts desorbing with the pH 6, 4.5, and 3 washes. These three washes are shown in gray because they are local maxima of desorption, suggesting that there are at least 3 binding sites on the bacterial surface with pK_a's that match their pH washes.

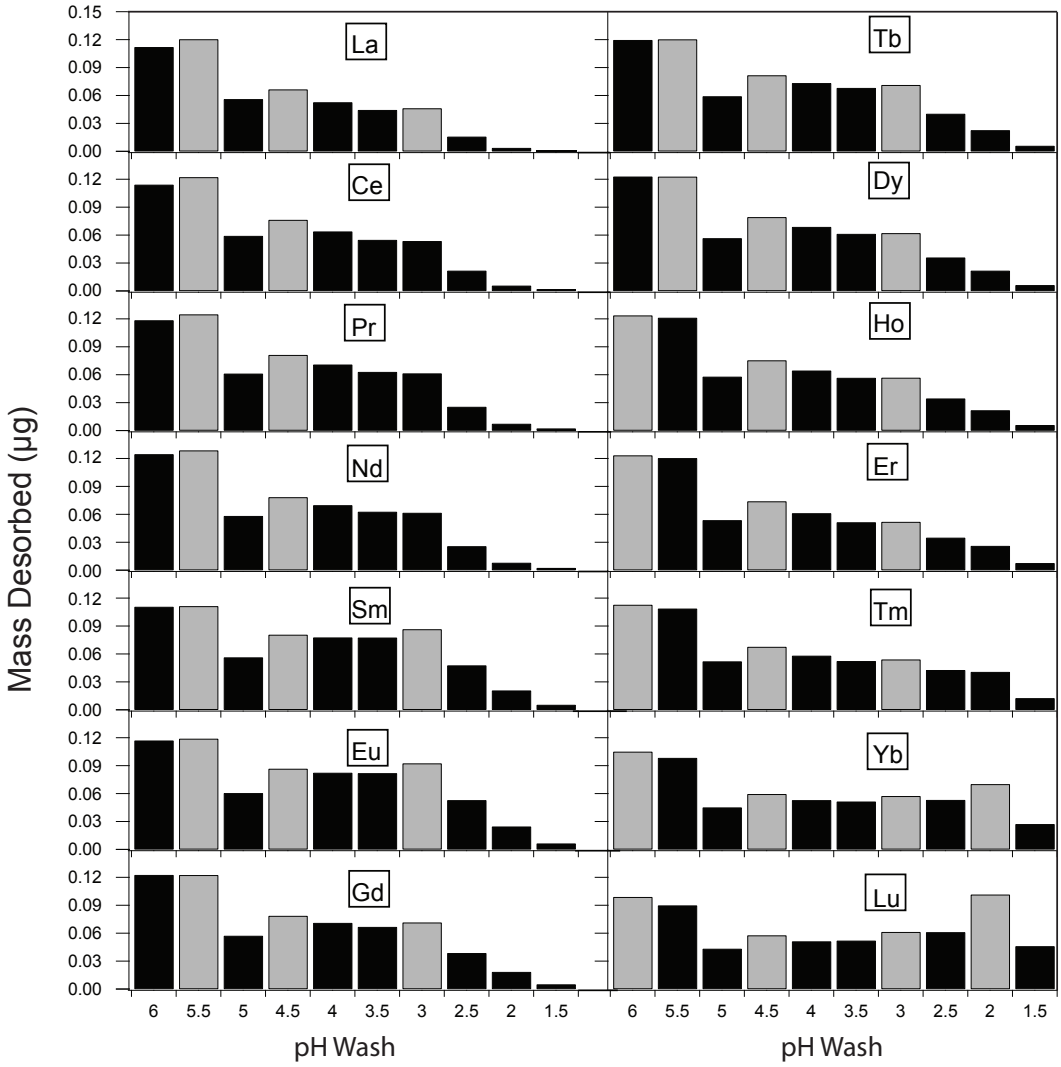

Figure 5.7: The mass of each lanthanide desorbed from *Roseobacter* sp. AzwK-3b at 0.5 pH intervals during the filtration assay as a function of pH wash. Although the masses of the lanthanides desorbed during the two highest pH washes, pH 6 and pH 5.5, was relatively insensitive to the lanthanide atomic number, lower pH washes revealed marked differences with atomic number. Furthermore, the graphs indicate more light lanthanides desorbed with higher pH washes, and more heavy lanthanides desorbed with lower pH washes. These differences in desorption facilitate separation between the heavy and light lanthanides. Local maxima in the mass desorbed with successively lower pH, indicated by the gray bars, suggest there may be as many as four distinct bacterial sites, corresponding to the four pH's of 5.5-6.0, 4.5, 3.0 and 2.5, responsible for lanthanide absorption.

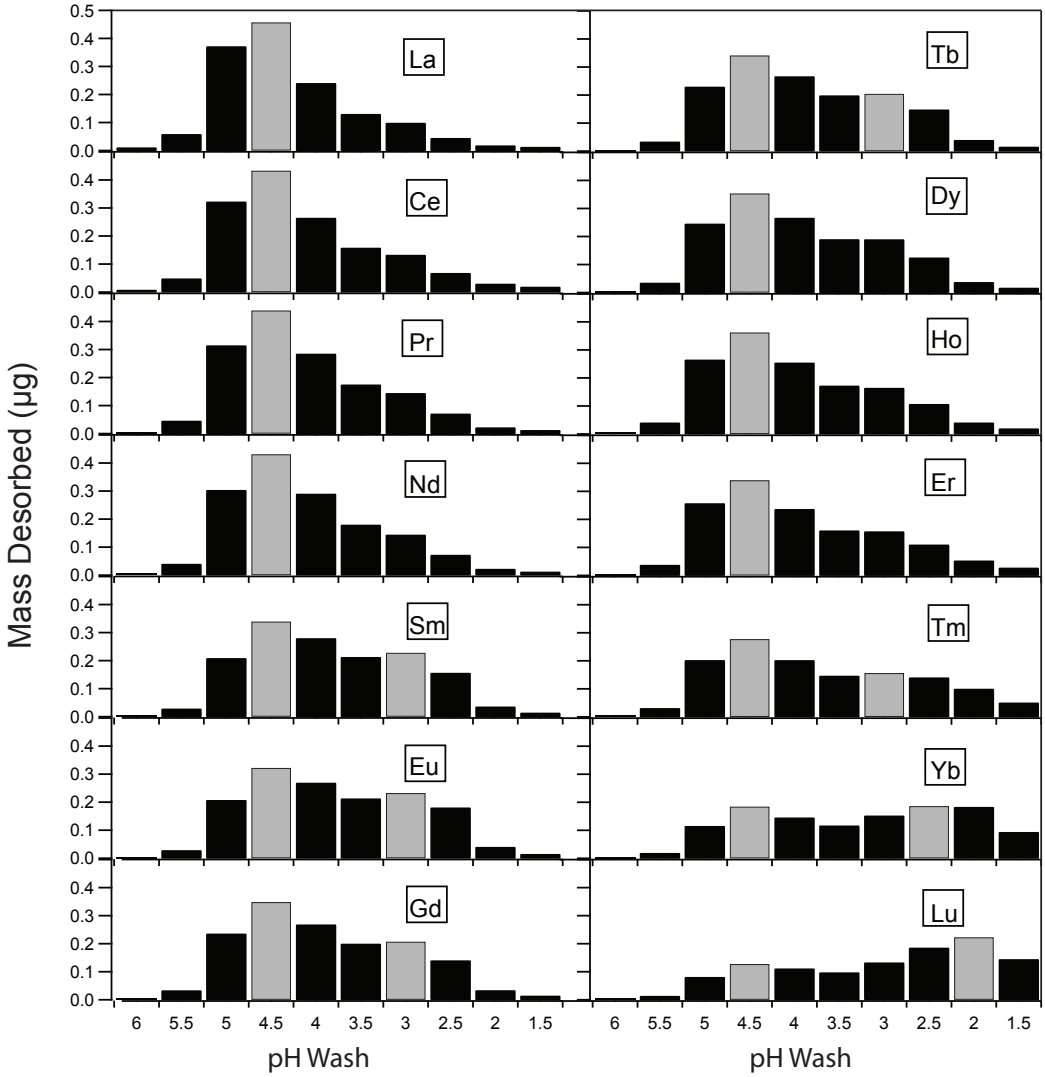

Figure 5.8: The mass of the individual lanthanides desorbed from *Halomonas* sp. at 0.5 pH intervals upon elution as a function of pH wash. As with the data obtained using *Roseobacter* sp. AzwK-3b (Figure 5.7, the higher pH washes desorb more of the lightest lanthanides whereas the lowest pH washes desorb more of the heaviest lanthanides. The significantly lower desorption in the high pH range (5.5 and 6.0) indicates that *Halomonas* sp. may lack the high pK_a absorption sites present on *Roseobacter* sp. AzwK-3b.

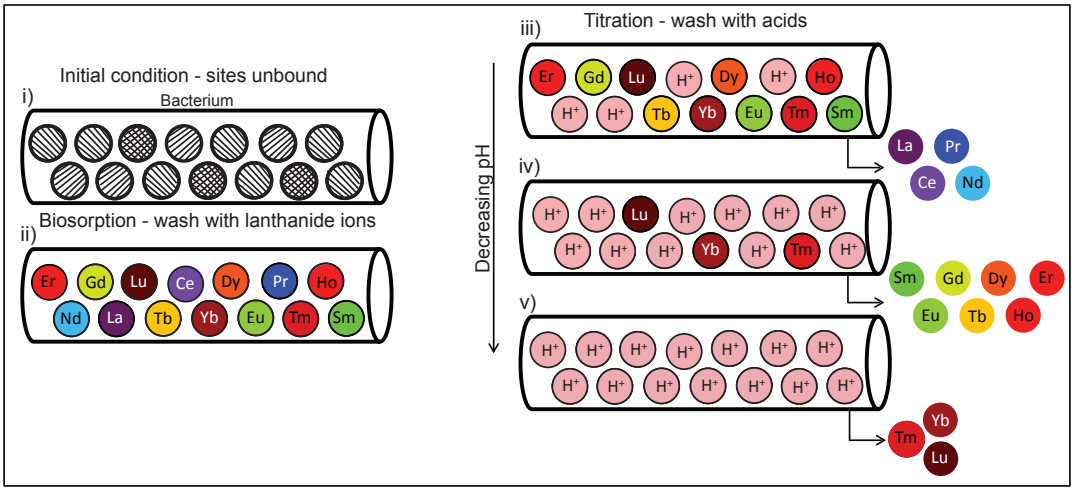

Figure 5.9: Schematic illustration of lanthanide biosorption to and desorption from bacterial surfaces. Initially, (i) individual surface sites, shown as open circles, on the bacterium are unbound or only weakly bound to Na^+ or K^+ from the ASW solution in which it is cultivated. After washing with the mixed lanthanide solution at circumneutral pH, the lanthanides absorb to all the various surface sites (step ii). Subsequently, with washing with successively lower pH solutions (steps iii-v) the lanthanides preferentially desorb according to the pK_a of the surface sites to which they are bound, exchanging with protons until only the heaviest lanthanides are finally exchanged.

passed over the bacteria, the surface sites desorb their bound lanthanides, exchanging with protons from the acid solution according to the pK_a of the sites. Specifically with *Sphingomonas* sp., *Shewanella oneidensis*, *Halomonas* sp., and *Roseobacter* AzwK-3b, the most acidic lanthanides (i.e. Yb and Lu) are only desorbed with the most acidic pH washes because these lanthanides are bound to the lowest pK_a sites.

The pH wash at which a lanthanide desorbed is the pH at which that site protonated, namely the pK_a of that surface site. (Strictly, the pK_a of a surface site is the pH of the wash at which 50% of the lanthanides desorb from a surface site and are replaced by protons.) Our results indicate that those surface sites having higher pK_a's tend to bind the lighter, more basic lanthanides, and those having lower pK_a's tend to bind the heavier, more acidic lanthanides. The preference for surface sites to

bind individual lanthanides was especially pronounced for the low pK_a sites, which almost exclusively appear to bind Yb and Lu. While the underlying reason for the variation in lanthanide desorption with pK_a is unknown, we attribute it to the variation in basicity and associated ionic size across the lanthanide series[101], the so-called lanthanide contraction[102,103]. The desorption elutions suggest that there are, possibly, many broad pK_a sites to which lanthanide ions can adsorb. The *Roseobacter* sp. AzwK-3b, for example, has 4 binding sites with pK_a's at approximately 6.0-5.5, 4.5, 3, and 2. Many of these bacteria have sites with similar pK_a's which may resemble similar binding sites. Seven of the nine strains (all but the two *pseudoaltermonas* sp. strains) appear to have binding sites with a pK_a's of approximately 3.0 and 4.5.

As mentioned earlier, the identities of the individual binding groups are not known. However, bacterial surfaces are known to consist of polysaccharides with various chemical groups exposed on their surfaces. It is generally understood that two of these, phosphate and carboxyl groups, are the most important to lanthanide binding (14, 16) and it is likely that they are also on the surface of each of the bacteria used. The carboxyl group has one singly bound oxygen atom to which lanthanide binding can occur, whereas the phosphate group can have either one oxygen ion, in the case of a diester linked phosphate, or two oxygen ions in the case of a monoester linked phosphate, though one of these oxygen atoms is likely protonated at neutral pH's and may be unavailable for binding[104]. On the surface of the bacteria, the local conformations and spacings between the groups capable of binding to a lanthanide ion, as well as steric effects, can be expected to result in a distribution in the pK_a values of the different lanthanide binding sites. The resulting local variations in pK_a may obscure the presence of other binding sites but our elution assay data suggests that there may be between 1 and 3 sites with distinct binding pK_a's for *E. coli*, *Pseudoaltermonas* sp., EPR3, EPR7, and EPR174, and as many as 4 for the others. Although not included in the binding model, it is likely that lanthanides are also absorbed to the EPS which is known to consist of polysaccharides, proteins, lipids, and DNA. Indeed, previous studies have shown the importance of EPS in biosorption[96]. DNA, with its low pK_a diester

phosphate backbone, is likely to be especially effective in biosorbing the heaviest lanthanides[91]. In our experiments, the EPS is likely to be produced by the bacteria during their cultivation, and from the nutrient-rich ASW media as it contains yeast extract.

5.4 Individual lanthanide binding

In the previous sections the lanthanide solution passed over the bacteria contained equi-mass concentrations of all 14 lanthanides, consequently, the biosorption and desorption of individual ions could be competeing with one another for the same sites. In order to examine this, solutions containing only lanthanum or lutetium were individually put through the filtration assay containing *Roseobacter* sp. AzwK-3b as the adsorbant. The results of these titrations are shown in bar graphs in Figure 5.10 where the lanthanum and lutetium masses desorbed during each pH wash are normalized to the total mass of lanthanum and lutetium that desorbed during the filtration, so as to account for variations in the total masses of lanthanum and lutetium added. (It should be noted that the masses of lanthanum and lutetium are zero for some of the higher pH washes because their masses were diluted past the point of sensitivity for the ICP-MS. These masses though, would have been sufficiently small and should not alter the results.)

When lanthanum was filtered individually nearly all the mass desorbed with the pH 2.5 and pH 3.0 washes. This result differs from the filtration of lanthanum in the lanthanide mixture, where large masses desorbed between pH 3 and pH 6 washes. Lutetium desorbed at the same pH (pH 2) individually as it did when combined with the other lanthanides in the mixture. The competition between lanthanides apparently does affect lanthanide binding, but this has yet to be investigated.

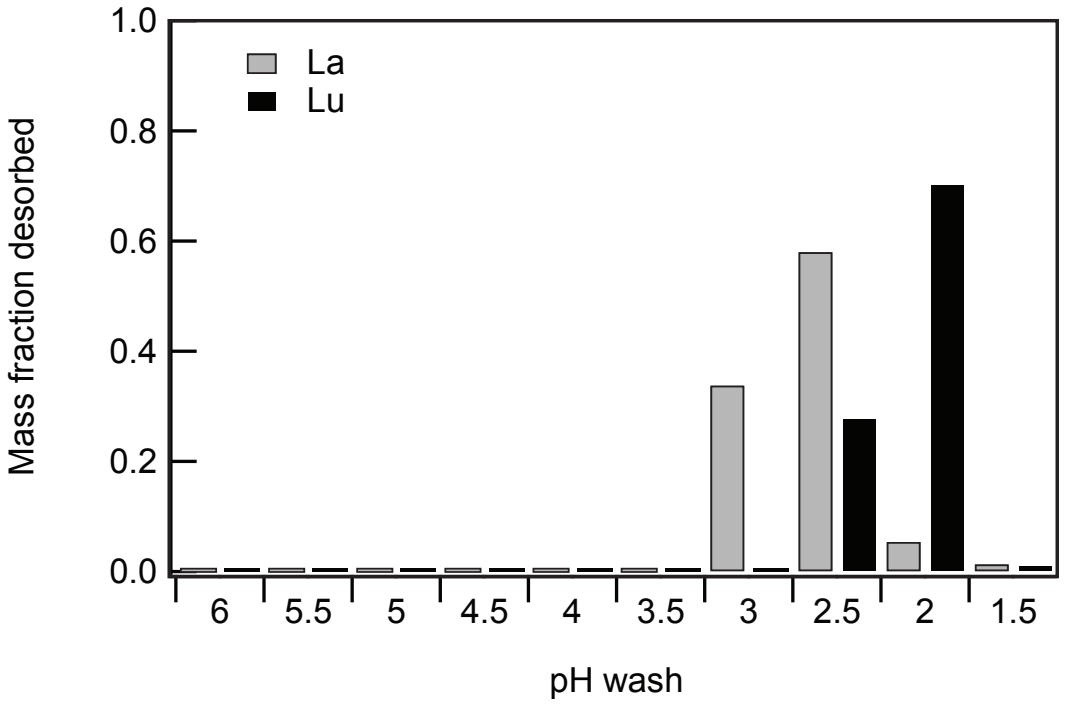

Figure 5.10: Bar graph of the desorption of La and Lu when individually biosorbed to *Roseobacter* sp. AzwK-3b during the filtration assay. The masses desorbed are normalized to the total amount of each lanthanide recovered so as to correct for differences in the masses recovered. The pH wash at which the highest mass of La desorbed was at a lower pH than in the filtration that included a mixture of all the lanthanides, decreasing from a pH wash of 5.5 to a pH wash of 2.5. The pH wash at which the highest mass of Lu desorbed was the same wash as with the filtration that included all the lanthanides (pH wash of 2.0).

5.5 Effect of pre-protonating the bacterial surface

Motivated by our simple model, the adsorption and desorption experiments were repeated with *Roseobacter* sp. AzwK-3b but after first pre-protonating the bacterial surface by washing the bacteria with a pH 2.5 wash prior to the lanthanide biosorption step. The masses desorbed are shown in the bar graphs of Figure 5.11. As can be seen by comparing with Figure 5.7, which is on the same scale, substantially less of each lanthanide desorbed from pH washes above the pre-protonation pH, whereas similar lanthanide masses were recovered using pH washes below the pre-protonation pH. Indeed, lesser masses of the lightest lanthanides and similar masses of the heaviest lanthanides desorbed from the bacteria after they were pre-protonated by the pH 2.5 wash.(Figure 5.12) The experiment was repeated using a lanthanide solution at pH 3.0 rather than the circumneutral pH lanthanide wash from before.(Figure 5.13) The desorption behavior was similar.

The pre-protonation experiments, shown schematically in Figure 5.14, provide further support for lanthanide binding to surface sites on the bacteria according to their pK_a's. By washing the bacterial surface with a highly acidic solution (pH 2.5) prior to exposing the bacteria to the lanthanide solution, protons adsorb to all the surface sites having a higher pK_a than the pre-protonation wash's pH. Then, when the surface sites are subsequently exposed to the lanthanide solution there is, as shown by our observations, very low lanthanide sorption to sites higher than this pH, and similar lanthanide sorption to sites lower than this pH. This behavior occurs because the sites having pK_a's at the pre-protonation pH and higher are bound with protons, preventing them from binding the lanthanide ions. The sites having pK_a's lower than this pH are not protonated and are consequently able to bind the heaviest lanthanides just as they do without the pre-protonation treatment. Then, during the lowest pH elution washes, only those lanthanides can be desorbed.

The circumneutral pH lanthanide solution may have been deprotonating the bacterial surface because it was at a higher pH than the pre-protonation pH. Even so, we would expect many of the sites

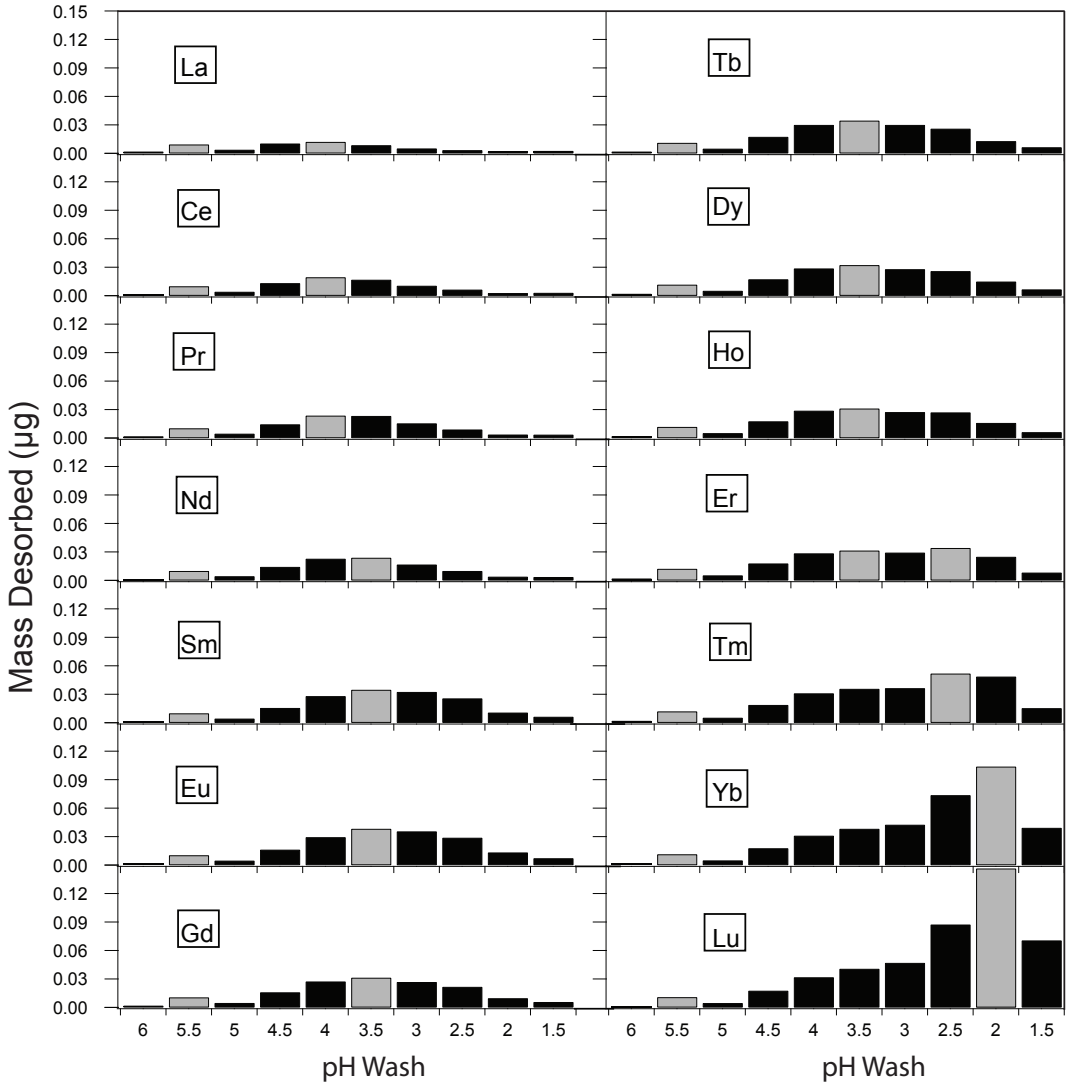

Figure 5.11: Plot showing the effect of first pre-protonating the *Roseobacter* sp. AzwK-3b with a pH 2.5 nitric acid wash on the mass of each lanthanide desorbed during a subsequent filtration assay as a function of pH wash. The lanthanide solution used was at a circumneutral pH. The bacteria desorbed lesser amounts of all the lanthanides at pH washes higher than the pre-protonation wash (pH 2.5) as compared to those in Figure 5.7. The bacteria desorbed similar masses of the lanthanides at pH washes lower than the pre-protonation wash. As shown, these were enriched in the heaviest lanthanides.

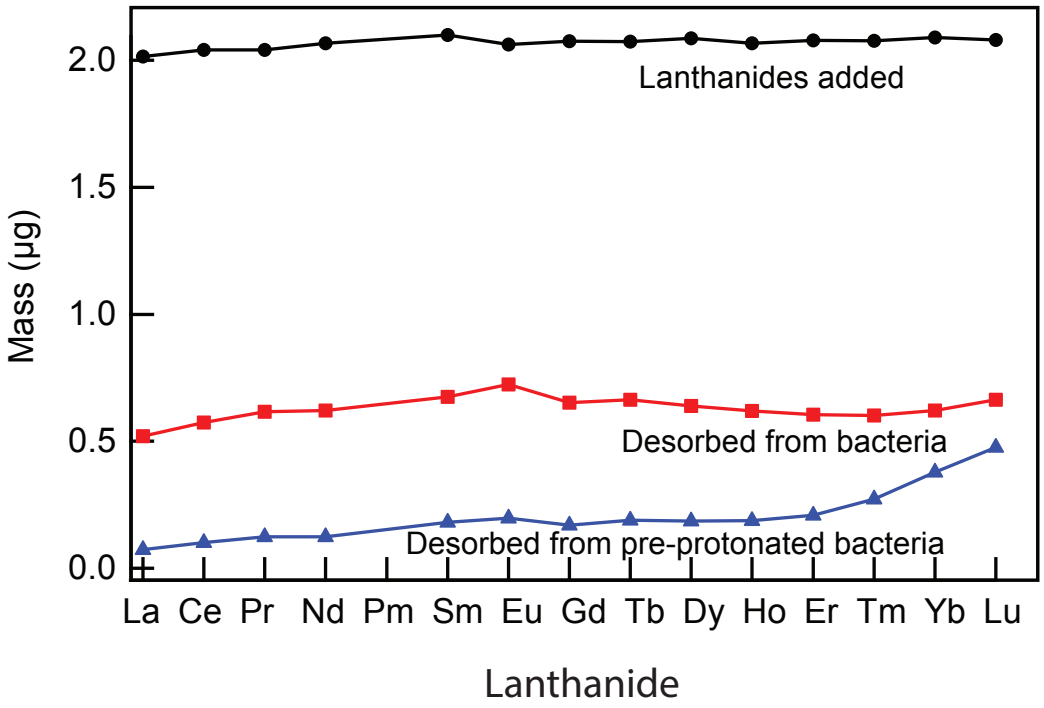

Figure 5.12: Masses of individual lanthanides desorbed from regular and pre-protonated *Roseobacter* sp. AzwK-3b during the filtration assay. Similar masses of the heavier lanthanides and lesser masses of the lighter lanthanides are desorbed from the pre-protonated bacteria as compared to the regular bacteria. This occurs because many of the light lanthanide binding sites on the pre-protonated bacteria are protonated and unable to bind the lanthanides.

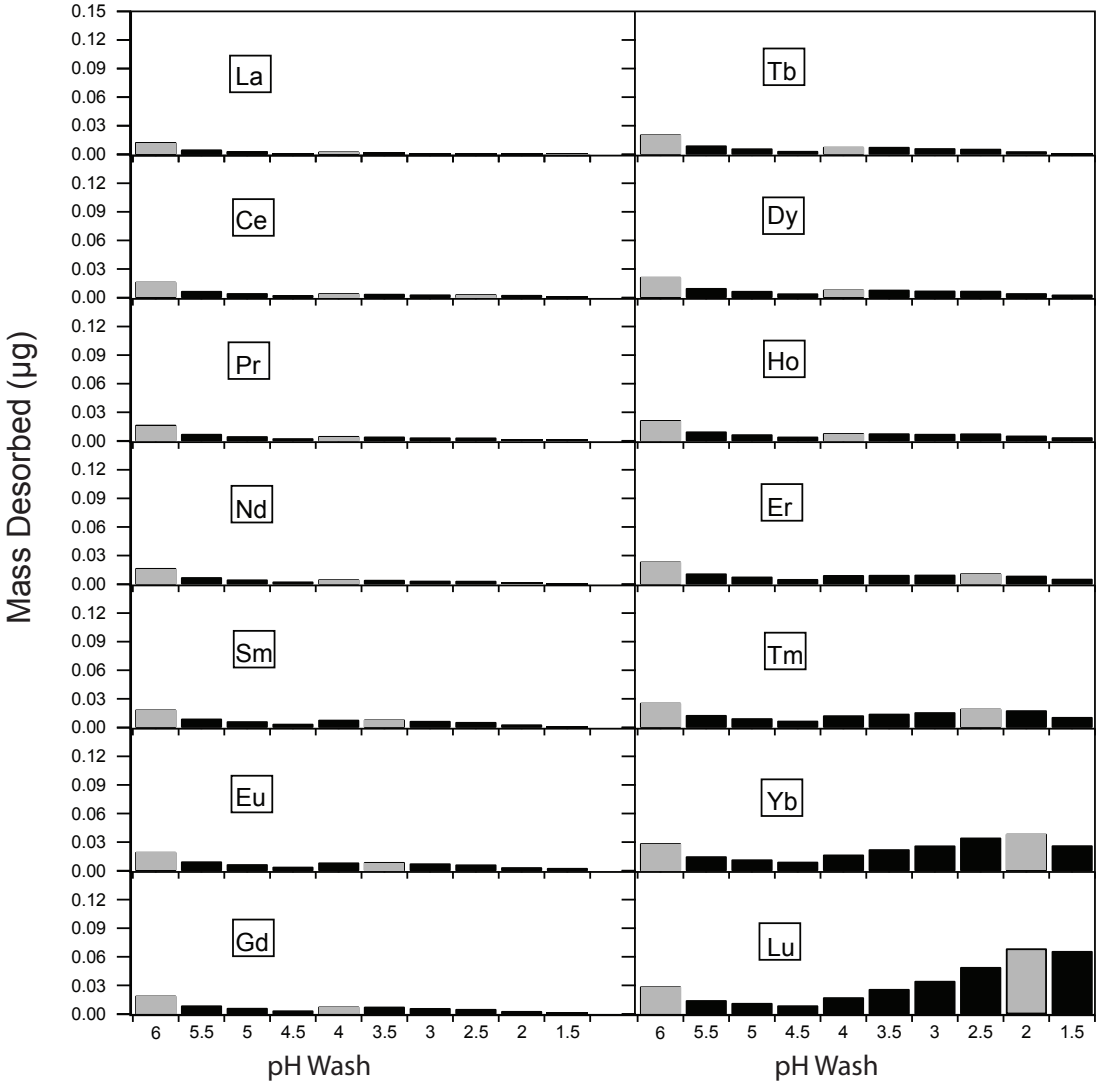

Figure 5.13: Plot showing the effect of first pre-protonating *Roseobacter* sp. EPR3 with a pH 2.5 wash prior to performing a filtration, this time using a pH 3.0 mixed lanthanide solution. There were lower masses of lanthanides desorbed for all pH's above pH 3.0 as compared to Figure 5.11, but there were also lower masses desorbed with washes below this pH.

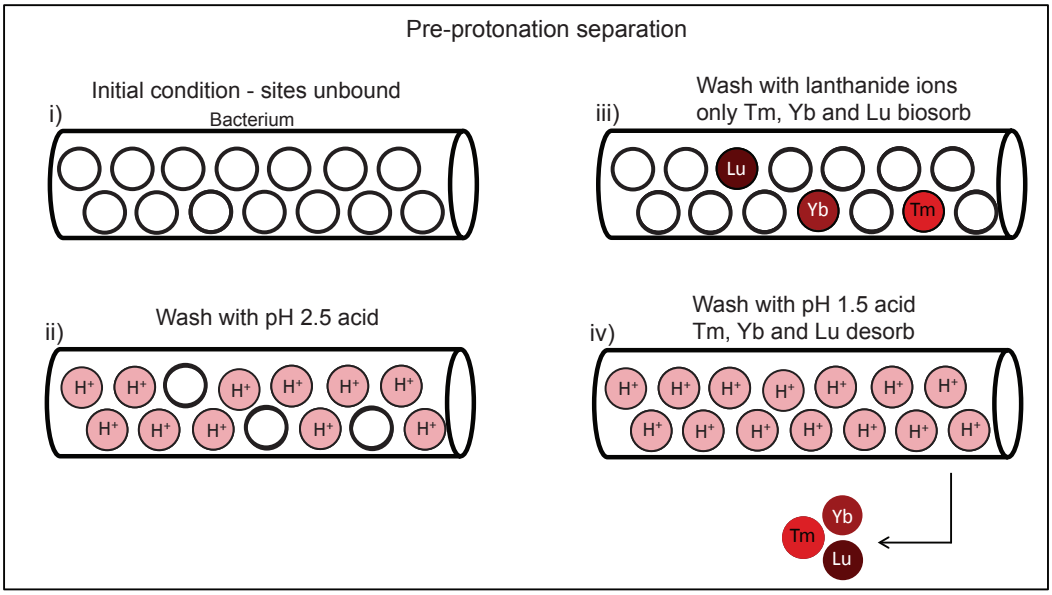

Figure 5.14: Schematic illustration of lanthanide sorption to, and desorption from, a bacterial surface that has been pre-protonated. Washing the bacterium with a low pH solution protonates those sites on the bacterium that have higher pK_a's than the pH of that wash, and leaves the lowest pK_a sites unbound. Upon washing with the mixed lanthanide solution, only the heavier lanthanide ions, such as Lu, Yb and Tm, can bind to the bacterium surface. Subsequent washing with an even lower pH solution releases these lanthanides, protonating the sites they were bound to.

to remain protonated and the mechanism to hold because the lanthanide sorption and deprotonation processes occur over a short time. This potential deprotonation was confirmed to have only a minor effect on the lanthanide desorption when similar results were obtained using the low pH lanthanide solution (pH 3.0) (Figure 5.13). Deprotonation by the circumneutral pH lanthanides may have been occurring to a small extent though, because there were higher levels of lanthanides that desorbed in the high pH washes compared with the other run. However, there was also more overall lanthanide desorption with the low pH washes, so these observations may instead be due to differences in total biomass passed across the filter. Indeed, when the masses of each lanthanide biosorbed are normalized to the total amount of lanthanides added the results show a decrease in the lanthanide binding above the pre-protonation pH and an increase above it. (Figure 5.15)

5.6 Lanthanide adsorption to liposomes

Liposomes are often used to model Gram-negative bacterial surfaces because they both consist of a lipid bilayer outer membranes[105]. Liposomes are especially useful in this capacity because they are simpler than bacterial surfaces, and their surface groups can be controlled depending on which lipids are used to create the liposomes. For those reasons phosphatidic acid (PA) liposomes, which have a single monoester phosphate group on their surfaces, were created (Figure 5.16), and were used in the filtration assay instead of bacteria. The PA liposomes were chosen because, as previously discussed, it is believed that the phosphate sites are most important to lanthanide binding. The liposomes ranged in size from 0.25 μm to 50 μm diameter, and details of the liposome creation and filtration assay can be found in Appendix A.

The PA liposomes were used as the adsorbant in the filtration assay, and had their lanthanide biosorption and desorption measured. Similar to the bacteria, it was found that the lanthanides strongly adsorbed to the PA liposomes, as shown in Figure 5.17. Unlike the bacteria, however, there was lit-

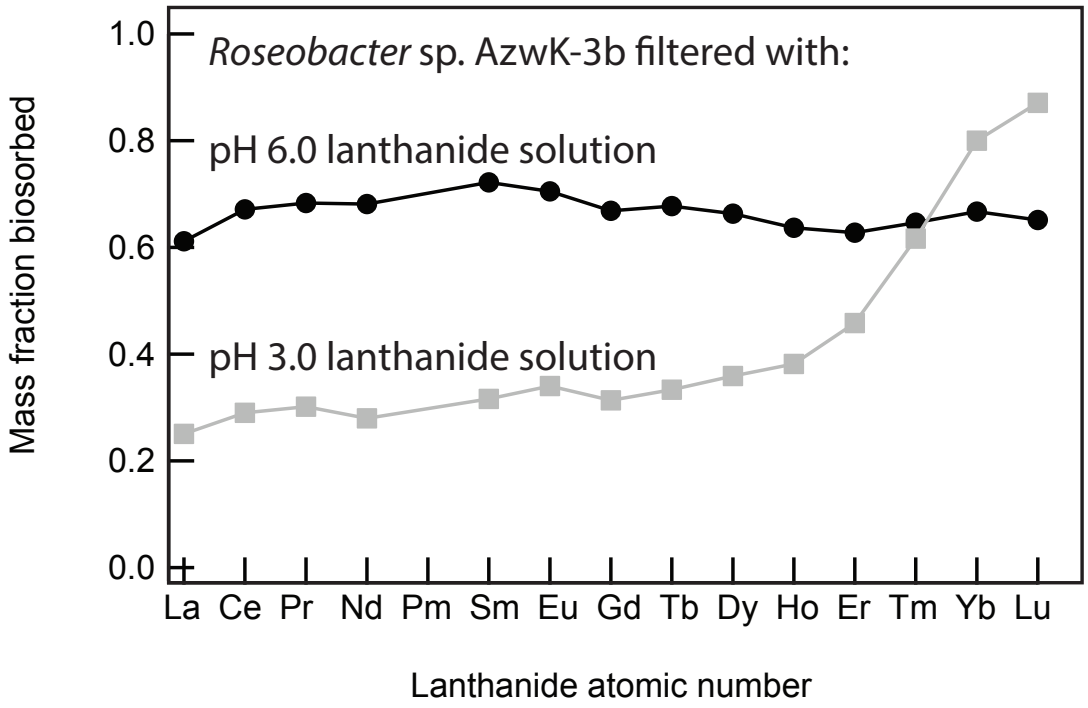

Figure 5.15: Normalized lanthanide biosorption to *Roseobacter* sp. AzwK-3b during the filtration assay. The lanthanides biosorb differently depending on the pH of the lanthanide solution. Approximately 60-70% of each lanthanide biosorbs to the bacteria from the pH 6.0 lanthanide solution whereas lesser amounts of the lighter lanthanides and greater amounts of the heavier lanthanides biosorb from the pH 3.0 lanthanide solution. This occurs because the low pH solution protonates many of the higher pK_a sites that would normally bind the lighter lanthanides.

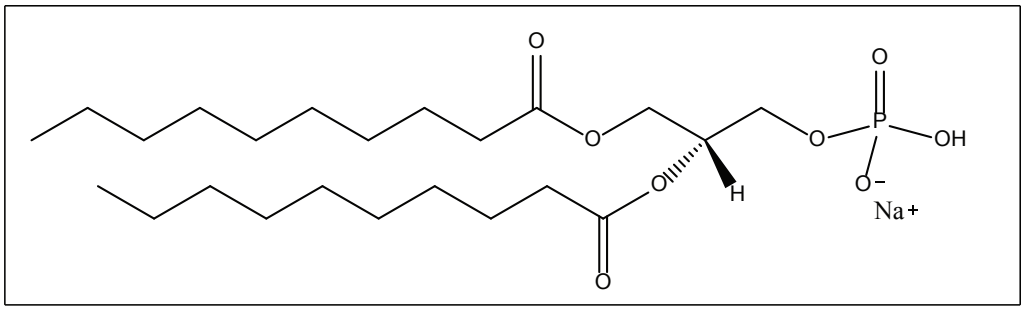

Figure 5.16: Chemical structure of phosphatidic acid lipid used in the study to make liposomes. (10:0 PA 1,2-didecanoyl-sn-glycero-3-phosphate (sodium salt)).

tle or no desorption at pH's above 3.5, though greater masses of the light lanthanides still desorbed with higher pH washes and greater masses of the heavy lanthanides still desorbed with lower pH washes.(Figure 5.18) The heavier lanthanides primarily desorbed with the pH 2.0 and pH 1.5 washes, and notably there was a factor of 18 more Lu desorbed in the pH 2.0 wash than the pH 2.5 wash. It was found that the final wash at pH of 1.5 was especially effective in separating the heaviest lanthanides, desorbing more than a factor of 15 as much Lu as La.

As the liposome was selected because it only contains monoester phosphate head groups capable of binding to the lanthanides, it was expected that the adsorption and desorption would occur at a well-defined pK_a around 3.0, according to published data[104], and in accordance with the pK_a binding model there was little or no desorption at pH's greater than 3.5.(Figure 5.18) Surprisingly though, there was significant desorption at much lower pH's below the pH we would associate with binding to the phosphate groups. One possible explanation, based on work showing that La^{3+} and Gd^{3+} induce shape changes in lipid vacuoles[106,107,108,109], is that the lanthanides induce shape changes in the liposome surfaces that, in turn, alter the steric effects of binding, leading to local variations in pK_a. One would also expect that the pK_a's of the binding sites would be further broadened by the effect of longer range surface distortions caused by adsorption of multiple lanthanide ions over the surface

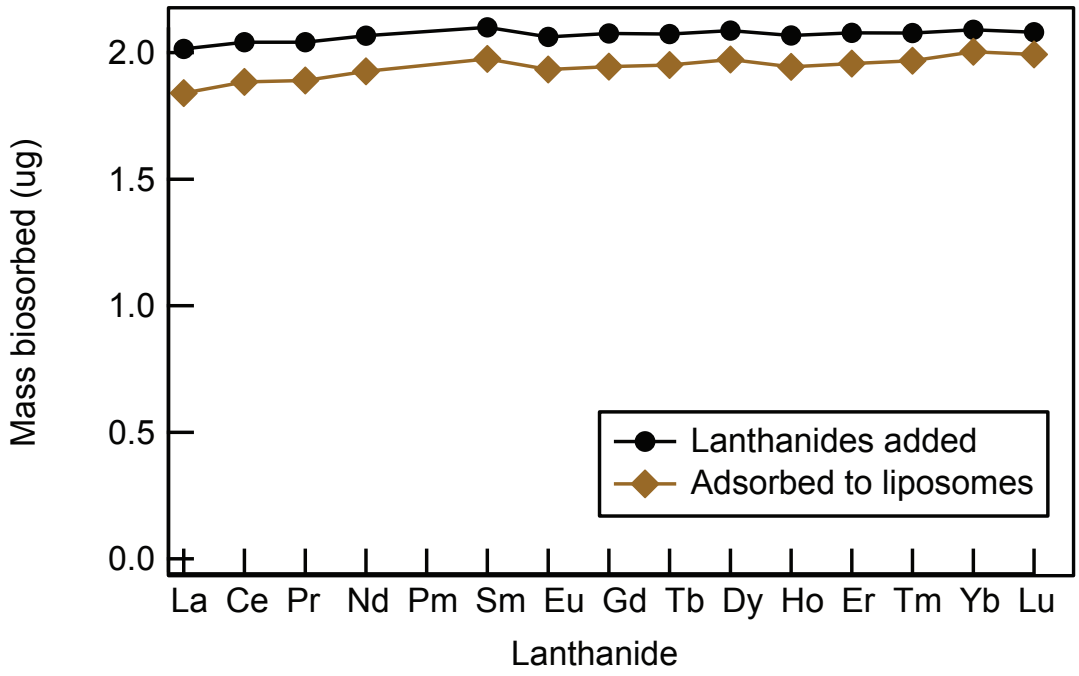

Figure 5.17: Mass of individual lanthanides adsorbed to liposomes from an equal mass mixture of all the rare-earths. The liposomes adsorbed a large fraction of the lanthanides from solution and also exhibited a slight but discernable increase in adsorption along the lanthanide series (0.05 μg/Z).

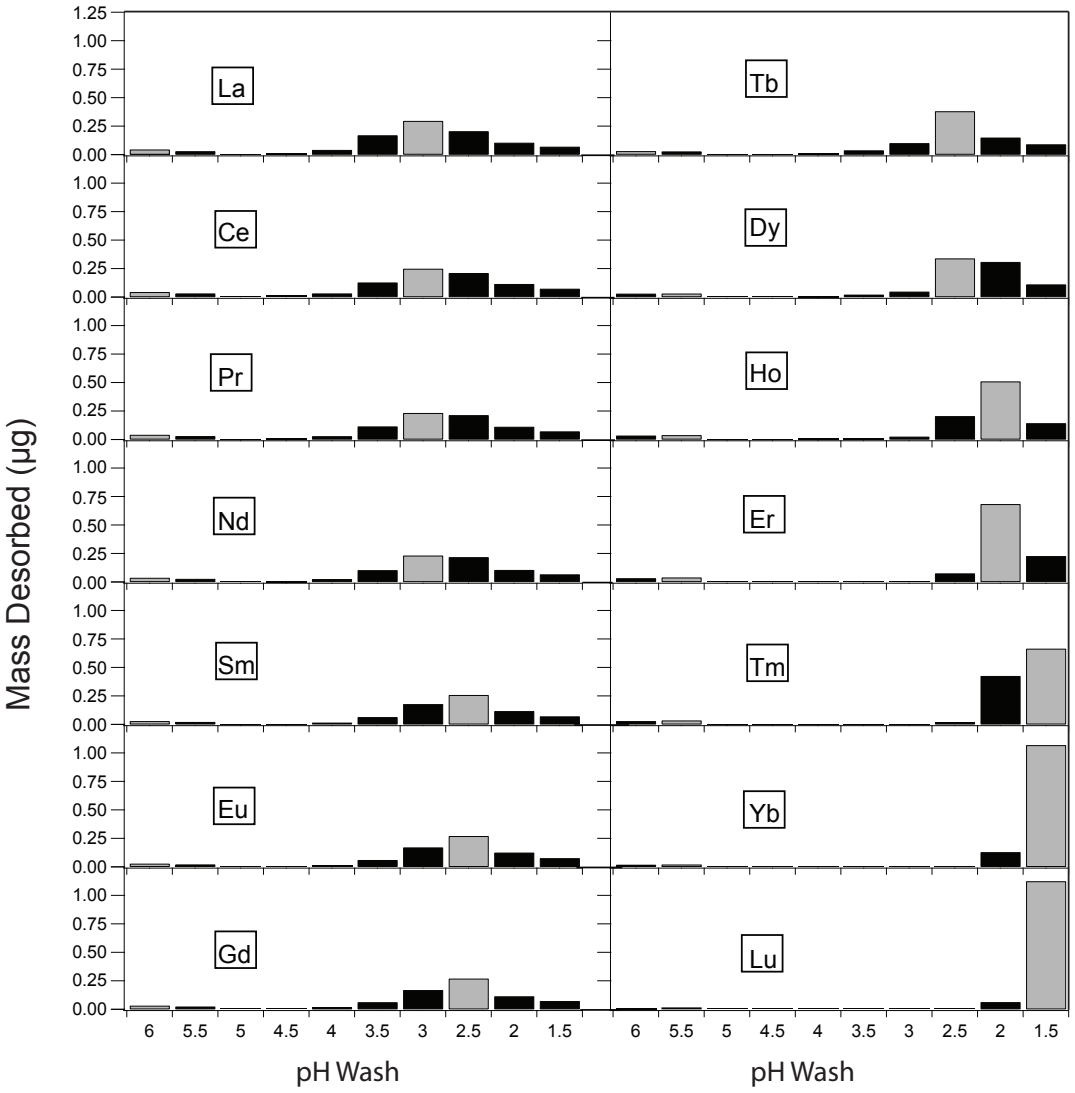

Figure 5.18: The mass of each lanthanide desorbed from the PA liposomes during the filtration assay as a function of pH wash. In marked contrast to the desorption behavior exhibited by the bacteria, almost no lanthanides desorb at higher pH washes than the pH 3.5 wash. Like the bacteria though, the lanthanides desorb in different pH washes according to their atomic number. For the lighter and intermediate lanthanides, most of the ions desorb between a pH of 3.5 and 2, whereas for the heavier lanthanides, the majority desorb between 2.5 and 1.5.

and, consequently, there would be no unique liposome surface landscape and, correspondingly, no unique pK_a.

The effect of pre-protonating the liposomes was also investigated using a pre-protonation wash at pH 2. The results are shown in Figure 5.19, and illustrate that the lanthanide desorption exhibits similar but even more marked differentiation than after pre-protonation of the bacteria. The pre-protonation decreased the lanthanides binding above the pre-protonation pH (pH 2). The pre-protonation though, also increased the mass of lighter lanthanides that desorbed in the pH 2 and pH 1.5 washes. In these two pH washes the masses of each lanthanide desorbed were similar, and little differentiation between the lanthanides occurred. Pre-protonation did not significantly change the cumulative mass of lanthanides that were retained by the liposomes. It did, however, increase the cumulative mass of lighter lanthanides and decrease the cumulative mass of heavy lanthanides that were desorbed in those pH washes.(Figure 5.20)

As with the bacteria, pre-protonating of the liposomes prevented the lighter lanthanides from binding to sites with pK_a's higher than the pre-protonation wash. However, after pre-protonation the lighter lanthanides that had adsorbed to higher pK_a sites during filtration without pre-protonation instead adsorbed to lower pK_a sites. While we do not know for sure, it is possible that the pre-protonation wash protonated, and dispersed some of the larger liposomes. These liposomes then reformed and the overall population of liposomes was smaller, but with a larger surface area and more sites. The light lanthanides then outcompeted the heavy lanthanides for these low pK_a sites.

5.7 Summary

We have discovered the individual lanthanides biosorb to multiple sites on the surface of bacteria. It is deduced that the surface sites have various pK_a's and that this differentiates which of the individual lanthanides adsorb. The heaviest, more acidic lanthanides consistently bind to sites with low pK_a's

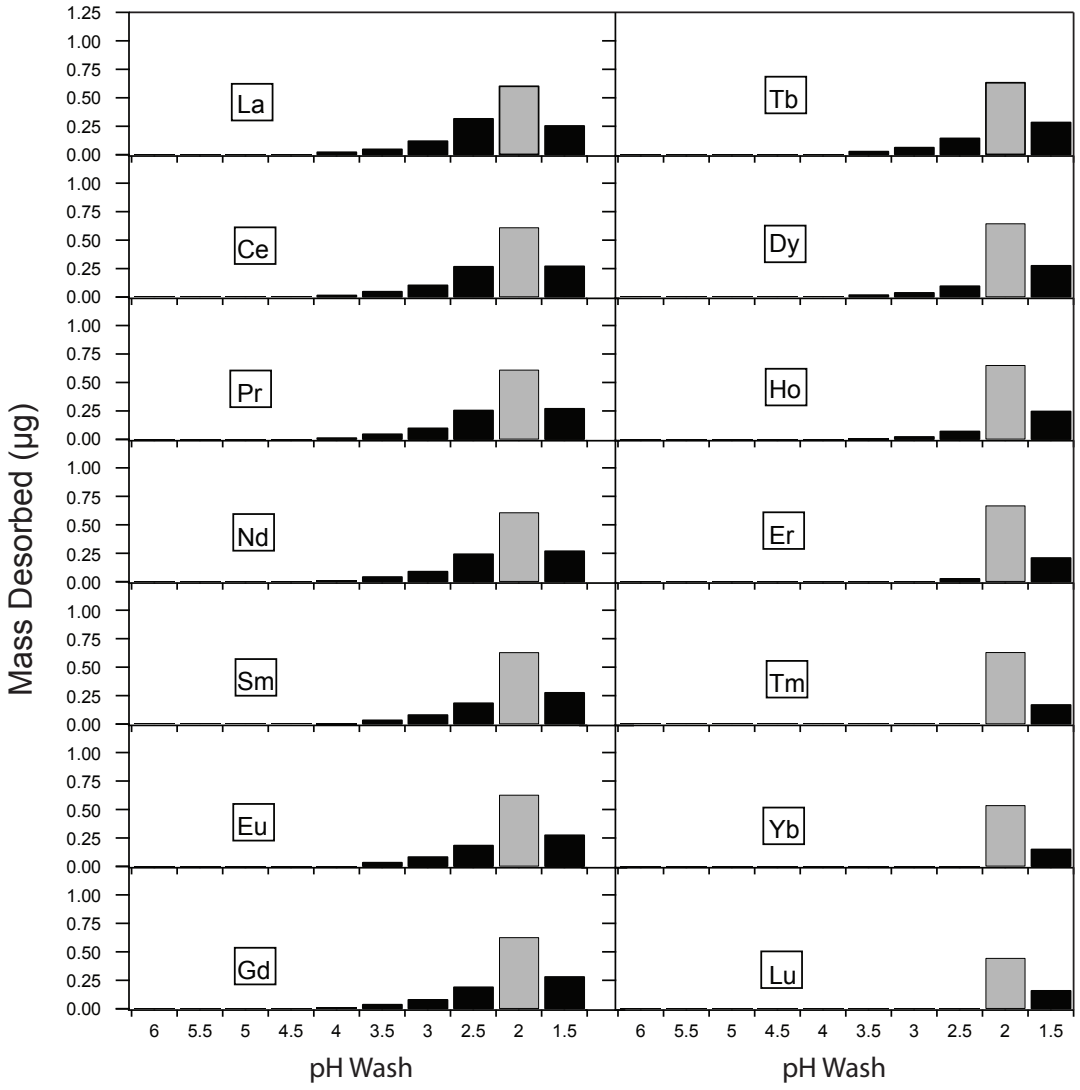

Figure 5.19: The masses of the lanthanides desorbed as a function of pH during the filtration assay after the PA liposomes were first pre-protonated by washing with a pH 2 wash. Compared with the regular filtration (Figure 5.18, there is less overall lanthanide desorption at pH washes that have a higher pH than the pre-protonation wash. At and below the pre-protonation wash there are similar masses desorbed of all the lanthanides. The lowest pH wash desorbed lower levels of the heaviest lanthanides and higher levels of the light lanthanides.

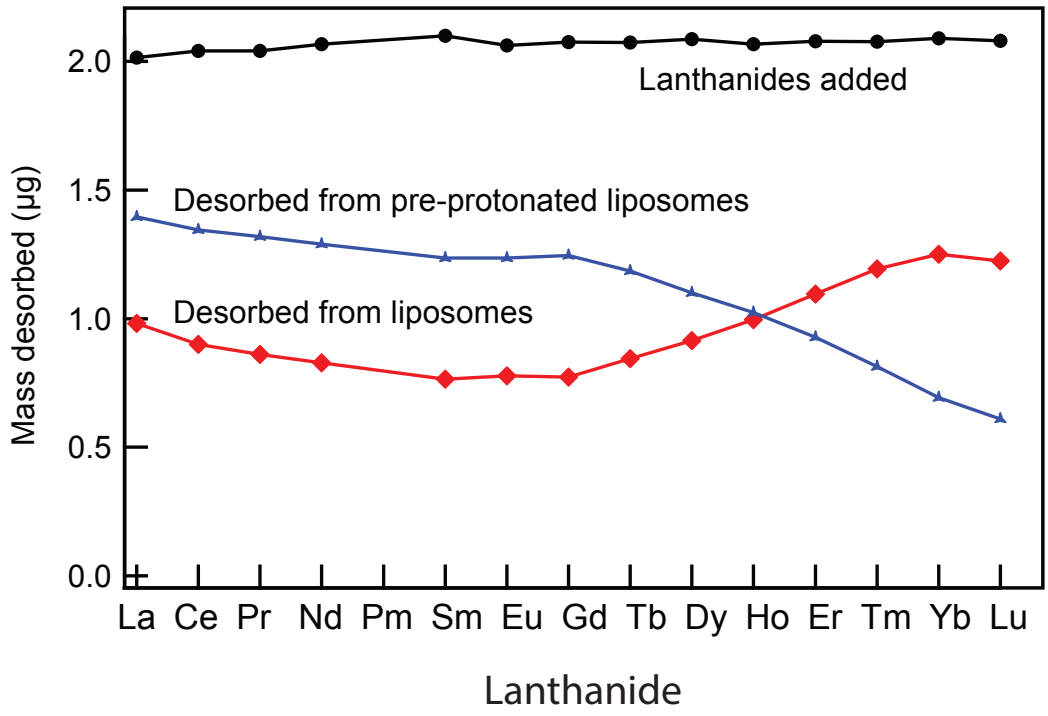

Figure 5.20: Masses of the lanthanides desorbed from regular and pre-protonated liposomes during the filtration assay. The pre-protonated liposomes desorbed higher masses of the lighter lanthanides and lower masses of the heavier lanthanides when compared to the non-pre-protonated liposomes.

whereas the lighter, less acidic lanthanides bind to those sites with higher pK_a's. Furthermore, it is concluded that after these sites are bound by lanthanides they can be protonated by washing with acids, releasing the lanthanides. When the bacteria have a low pH solution passed over them prior to lanthanide adsorption, some of the surface groups become pre-protonated and are no longer available to bind the lanthanides.

Bacterial surfaces are known to consist of lipopolysaccharides with various surface exposed chemical groups, and it is generally understood that two of these, phosphate and carboxyl groups, are the most important to lanthanide binding. The range of pK_a's observed from the bacteria leads us to believe that these surface groups are in different spatial and chemical arrangements that lead to variations in pK_a. We observed the same range of pK_a's from liposomes composed of PA lipids that had only phosphate surface groups, instead of multiple chemical groups like in bacteria. Although further research is needed, we believe that variations in the phosphate group spacing causes the observed pK_a ranges.

In the next chapter the differences in lanthanide desorption will be exploited to concentrate specific lanthanides from a mixed lanthanide solution. In addition, this biosorption-based method is compared to processes that are currently used to separate lanthanides.

6

Lanthanide separation

As discussed in Chapter 2, lanthanide separation is a challenging task because the lanthanides all have similar chemistries (most importantly, they are all trivalent). In this chapter we will apply the differences in lanthanide desorption, observed in the previous chapter, to separate and recover specific lanthanides from a mixed lanthanide solution. First, lanthanide separation is demonstrated using bacteria and liposomes. Then, this separation is compared to one that is calculated based on industrial processes.

Table 6.1: Separation factors for neighboring lanthanide pairs between pH 2.5 and pH 2.0/pH1.5 washes for bacteria and liposomes. Also shown are values from a standard solvent extraction system.

Lanthanide pair	Separation factor		
	Bacteria	Liposomes	Industry*
Ho/Er	1.2	3.4	1.3
Er/Tm	1.3	4.8	1.3
Tm/Yb	1.5	5.5	1.1
Yb/Lu	1.3	2.5	1.1

*Separation using RE(III)-HCL-EHEHPA[38]

6.1 Lanthanide separation from a mixed lanthanide solution using the filtration assay

The variation in desorption of different lanthanides can be quantified by a desorption ratio, R_{AB}, the ratio of the desorbed masses of two different lanthanides, A and B, at the same pH. This naturally leads to the equivalent of a separation factor, S_{AB}, for two different lanthanides, A and B, as the ratio:

$$\frac{R_{AB_1}}{R_{AB_2}}$$

where the subscripts refer to the pH at which the values of the desorptions are being compared. The separation factors between four pairs of neighboring lanthanides are compared in Table 6.1. As evident from the table, the bacterial and liposome systems show higher separations than are achieved in industry.

These separation factors provide the basis for the possible use of bacteria, as well as synthetic liposomes, in separating and recovering individual lanthanides. While the separation factors achiev-

able in a single elution are impressive, it is likely that multiple biosorption-desorption steps will be required to enhance the separation until a desired level of separation (purification) is achieved. Appendix C describes a proposed separation scheme based on a bacterial process. In the following section we demonstrate that system to successfully separate the lanthanides using biosorption to *Roseobacter* sp. AzwK-3b.

6.1.1 Lanthanide separation using *Roseobacter* sp. AzwK-3b

To demonstrate the efficacy of a multiple step process in separating and purifying individual lanthanides, the bacterial surface was first pre-protonated and then washed with the mixed lanthanide solution to adsorb the lanthanides. Then, the bacteria were washed with a pH 1.5 nitric acid solution to desorb the heaviest lanthanides, enriching the filtered solution in Yb and Lu. This filtered solution was then neutralized to pH 5.5 and pumped back over a fresh batch of pre-protonated bacteria and collected. Full details of this procedure and others described in this chapter are explained in full in Appendix C. The mass fractions of the lanthanides in the filtered solution initially, after the first pass, and then after the second pass are shown in Figure 6.1. As can be seen, there is a progressive enrichment of the two heaviest lanthanides, and after the second pass the solution contained nearly 50% Yb and Lu, with 18 wt % Yb and 30 wt % Lu. It is anticipated that even greater separation will be achievable with more passes.

As a further demonstration that different lanthanides can be separated by adjusting the pre-protonation pH, the middle lanthanides were enriched by pre-protonating *Roseobacter* sp. AzwK-3b with a pH 5 wash, followed by a pH 4 wash. This second pH 4 wash was partially enriched in the middle rare earths, and was itself cycled over a new filter with pre-protonated bacteria and the process repeated. The final solution was nearly 20% samarium and europium, in increase from 14% in the initial solution. (Figure 6.2) This recovery is not as stark as with the heaviest lanthanides, but it suggests the filtration assay and a single bacterial strain could be useful in concentrating different sets of lanthanides from a

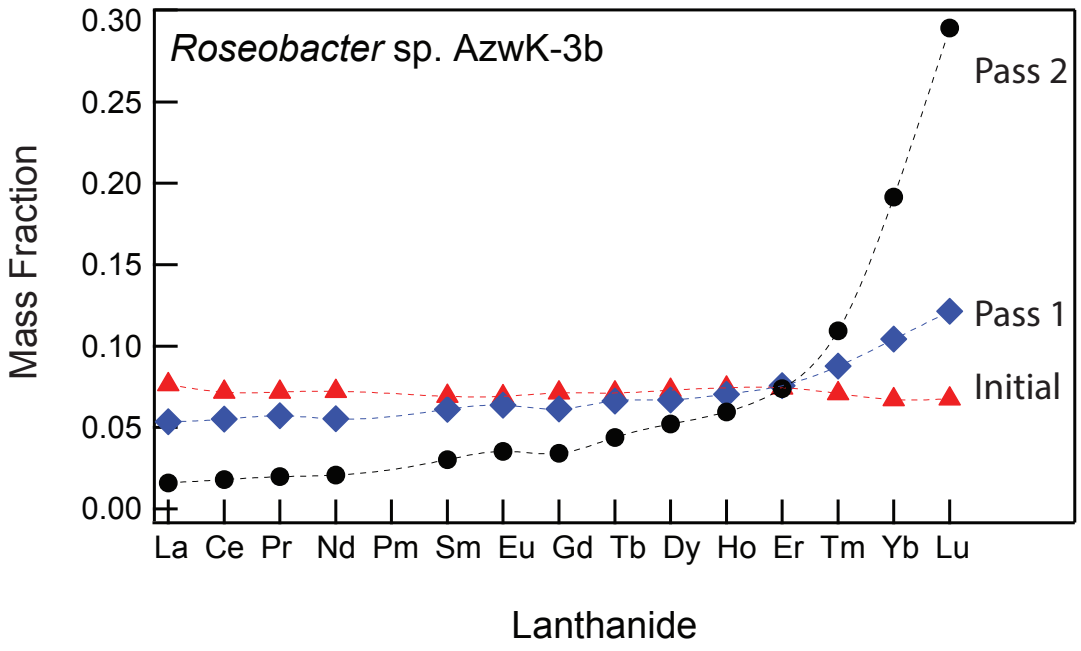

Figure 6.1: Purification of the heaviest lanthanides using *Roseobacter* sp. AzwK-3b. The plot shows the mass fraction of each lanthanide initially in solution and then after the first and second passes of that same solution after being passed over pre-protonated bacteria, illustrating the enrichment of the two heaviest lanthanides, Yb and Lu. After the second pass, the solution contains 48% of these two heaviest lanthanides. Similar enrichment was also exhibited by the liposomes as shown in Figure 6.3, both exceeding the calculated enrichment performed using solvent extraction in industry shown in Figure 6.4. After each pass the bacteria were replaced by a new batch of bacteria, pre-protonated with a wash at pH 2.5.

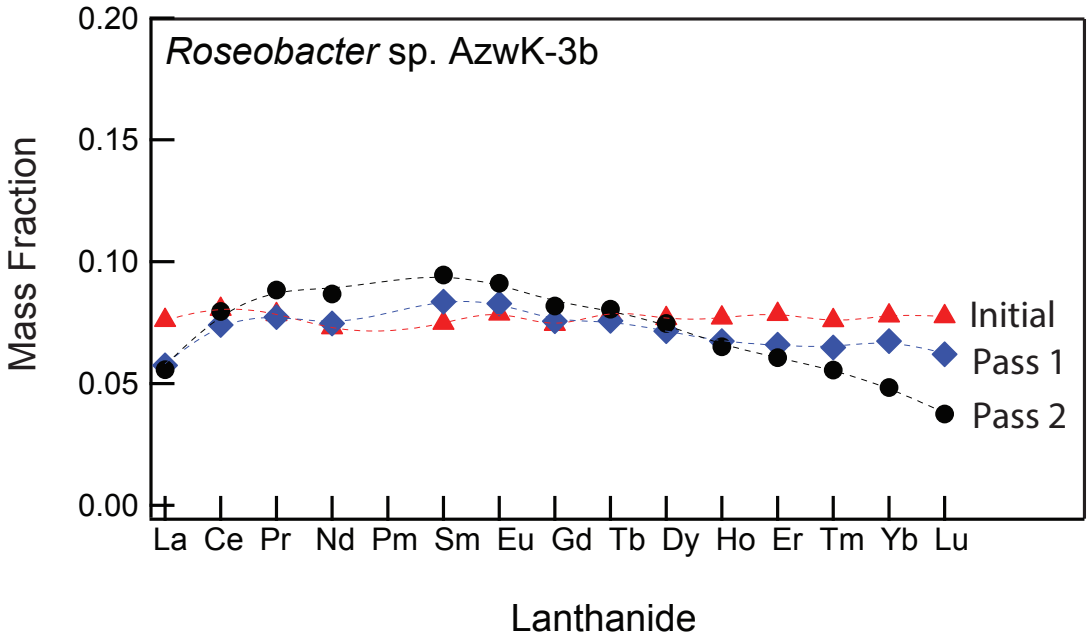

Figure 6.2: Enrichment of the middle lanthanides with Roseobacter sp. AzwK-3b. The mass fraction of each lanthanide is plotted as a function of lanthanide for an initial equal mass mixture of the lanthanides, and then after the first and second passes of that same solution over the bacteria. Enrichment of the middle lanthanides occurs by pre-protonating the bacteria with a pH 5 wash, and then eluting the biosorbed lanthanides with a pH 4 wash. After each pass the bacteria were replaced by new, pre-protonated bacteria, and after the second pass the solution contains 18% of Sm and Eu.

mixed solution.

6.1.2 Lanthanide separation using liposomes

Similar enrichment was observed when the liposomes were used in place of the bacteria, as is shown in Figure 6.3. In this case the two heaviest lanthanides were enriched to 44% of the total lanthanide mass (19% Yb and 25% Lu). While our data has emphasized the heaviest lanthanides, it may be possible to adjust the pre-protonation pH to recover and cycle different washes through the assay in order to recover specific lanthanides other than the heavy ones demonstrated above. In addition, adjusting the

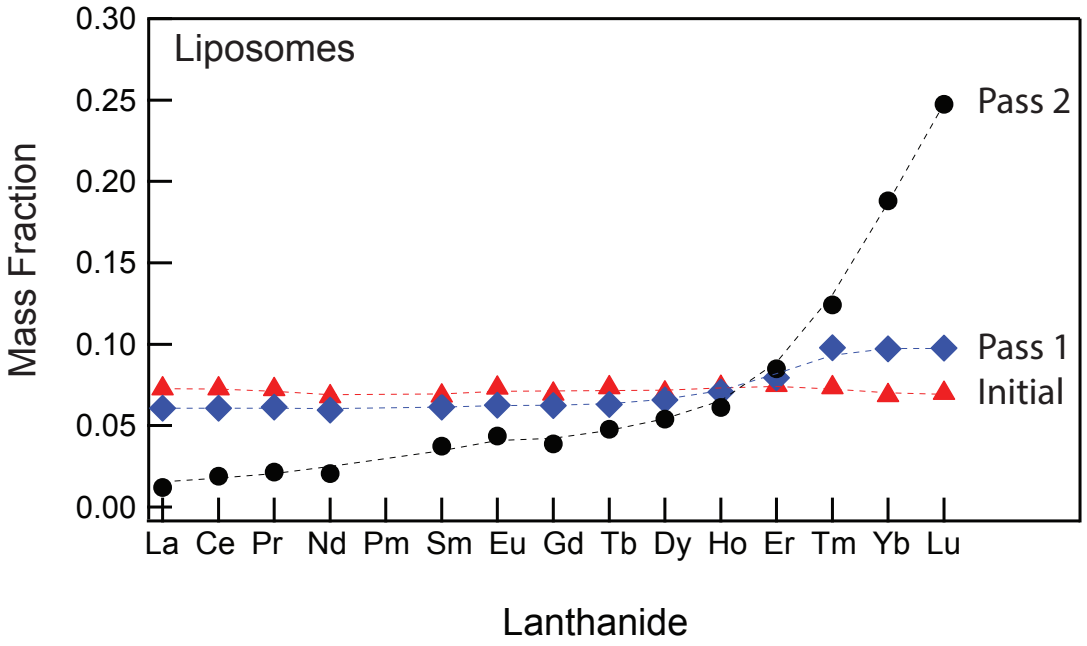

Figure 6.3: Enrichment of heavy lanthanides using liposomes. The mass fraction of each lanthanide initially in solution and then after the first and second passes of that same solution over the liposomes illustrating the enrichment in the concentration of the three heaviest lanthanides. After the second pass, the solution contains 44% of the two heaviest lanthanides, Yb and Lu. After each pass the liposomes were replaced by a new batch of liposomes.

lipid chemistry used to create the liposomes allows for the selection of specific surface groups, and may also allow for the concentration of other lanthanides.

6.2 Comparing adsorption-desorption separations to industrial separations

The industrial liquid-liquid separation and purification of a group of lanthanides from a solution of all the lanthanides can be calculated by using published separation factors. Here we use the separation factors reported for trivalent lanthanides at a concentration of 0.1 M in a mixture of 0.2 M HCl and 1.0 M EHEHPA (2-ethylhexyl phosphonic acid mono-2-ethylhexyl ester), a system commonly used in industry[38], to calculate the purification of Yb and Lu from an equi-mass mixture of all the lanthanides.

The distribution coefficient, D_{Ln_i}, for any lanthanide element, Ln_i, is defined as the ratio of concentrations, C, between two phases, A and B, in a solvent extraction[110].

$$D_{Ln_i} = \frac{C^A_{Ln_i}}{C^B_{Ln_i}}$$

D_{Ln_i} is related to the distribution coefficient, D_{Ln_j}, for another element, Ln_j, by the separation factor $\alpha^{Ln_i}_{Ln_j}$ between elements Ln_i, and Ln_j,[110]:

$$D_{Ln_i} = \alpha^{Ln_i}_{Ln_j} * D_{Ln_j}$$

As the distribution coefficients of the different elements are related in this recursive manner by the separation factor, solutions for each of the elements requires knowledge of the distribution coefficient for one of them, so long as the separation factors are known.

$$D_{Ln_i} = \alpha^{Ln_i}_{Gd} * D_{Gd}$$

Leading to, for instance,

$$D_{Lu} = \frac{D_{Gd}}{\frac{Lu}{Gd}}$$

(By convention, separation factors are always greater than 1).

Based on the reported value for the distribution coefficient for Gd of Log -1.17[41] at similar conditions as the reported separation factors described in Gupta and Krishnamurthy (2009), the distribution coefficients for all the lanthanides in the typical industrial system previously described can be calculated.

The distribution coefficients can then be used to calculate the purities of an initially equi-mass

mixed rare earth solution after successive stages. The equation for the mass fractions of each lanthanide, w_{Ln_i}, for two stages, stage 1 and stage 2, are:

$$w_{Ln_i}^{Stage\ 1} = \frac{1}{(D_{Ln_i}+1)*(\sum_{i=La}^{Lu}\frac{1}{D_{Ln_i}+1})}$$

$$w_{Ln_i}^{Stage\ 2} = \frac{w_{Ln_i}^{Stage\ 1}}{(D_{Ln_i}+1)*(\sum_{i=La}^{Lu}\frac{w_{Ln_i}^{Stage\ 1}}{D_{Ln_i}+1})}$$

Using these relationships, the concentrations after the first and second stage extraction from an initially equi-mass mixed solution are plotted in Figure 6.4.

After the first two stages of the solvent extraction process, it is calculated that the initial, equi-mass solution is enriched to 14% Yb and to 18% Lu. In practice, the solvent extraction scheme is repeated many times with as many as 50 stages to reach accceptable purities[38].

Strikingly, the elution process using both *Roseobacter* sp. AzwK-3b and the PA liposomes results in comparable separation factors to those published for the heavy lanthanides (Table 6.1). Furthermore, our two-pass biosorption-desorption enrichment process achieves better purities than the solvent extraction method used in industry. As indicated in Figure 6.4, it is calculated that after two stages of the solvent extraction method an initially equally mixed lanthanide solution becomes enriched to 18% of Yb and Lu, which is significantly less than the separations we achieved with bacteria and liposomes. In addition, the bacteria and liposomes achieved a higher separation of these two elements from the next heaviest lanthanide, Tm, than the calculated industrial system.

Although our results have been obtained at the laboratory scale, they suggest that the bacterial adsorption-desorption process may be simpler, consume less energy, and use both less expensive as well as less toxic chemicals than current commercial solvent extraction processes for separating the lanthanides. This work used *Roseobacter* sp. AzwK-3b as the biosorbing material but it is anticipated that similar lanthanide separations will be achievable using many other bacteria since the surface groups

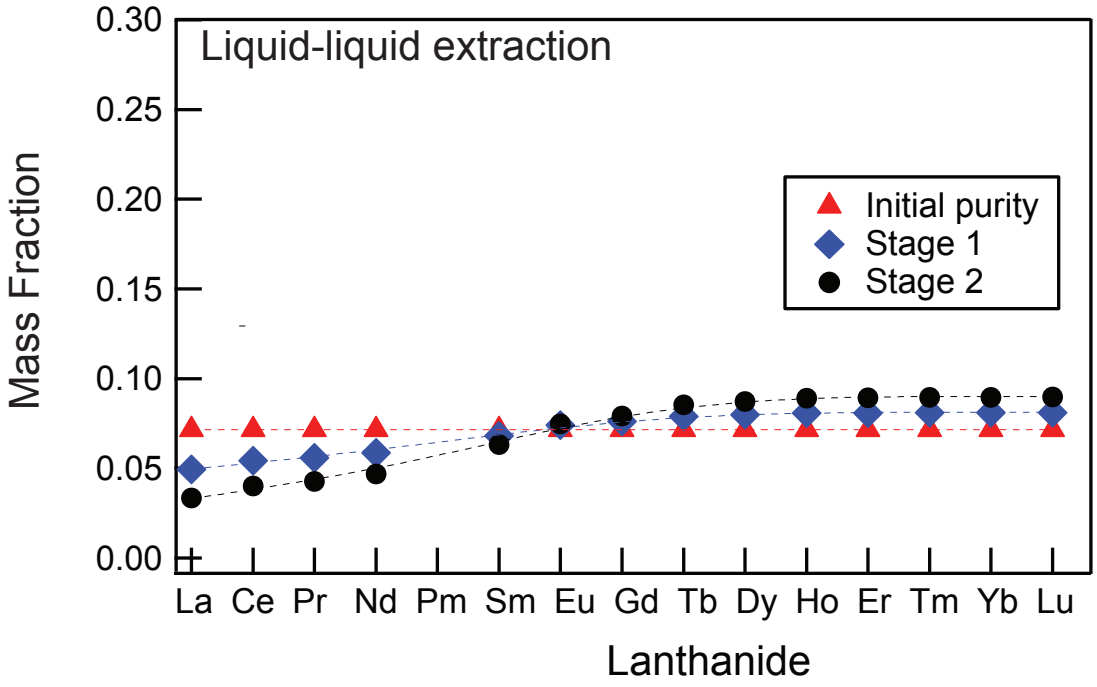

Figure 6.4: The calculated purities of the lanthanides after two stages of solvent extraction using RE(III)-HCl-EHEHPA[38]. Based on reported separation factors for the individual lanthanides in this solvent system, the concentrations as a function of atomic number are calculated after one and then two extraction stages. The separation is not as effective as those found using the *Roseobacter* sp. AzwK-3b and liposomes, shown in Figure 6.1 and Figure 6.3, respectively.

implicated in this thesis commonly occur on the surfaces of other bacteria. Indeed, similar results but differing in separation factors have been obtained with three other bacteria, *Shewanella oneidensis*, *Sphingobacterium* sp. and *Halomonas sp*. Given the large variety of bacterial chemistries, it is also likely that other bacteria may exhibit unique and greater differentiation in lanthanide desorption. Furthermore, it is highly significant that lanthanide separation can also be performed using the liposomes with only phosphate groups, suggesting that synthetic materials may also be used. This provides an opportunity to enhance the separation and recovery of particular lanthanides through adjustments in liposome chemistry. It is also likely that other metals can be separated from one another using similar adsorption-desorption methods. For example, in Appendix E we demonstrate the separation of iron from lanthanides in Nd magnets and Terfenol-d.

6.3 Summary

The filtration separation discussed in this chapter separated biosorbed lanthanides based on the pK_a of the sites to which they are bound. This method was effective in purifying an equally mixed lanthanide solution to 30% Lu in just two passes, exceeding the 9% purification calculated for industrial methods. Also, this separation was not limited to recovering the specific lanthanides, and by simply changing the pH of the washes different lanthanides were recovered. In addition, the procedure was successfully demonstrated using liposomes as an adsorbant, instead of bacteria. This, in principle, should allow for careful selection of liposome surface groups to recover specific lanthanides.

The next chapter of this thesis shifts focus from the lanthanides to tellurium. Unlike the lanthanides, bacteria do actively interact with tellurium, and so Chapters 7 and 8 will be devoted to how these interactions can be exploited to recover tellurium from its compounds.

7

Tellurium microbiology

In the next chapter (Chapter 8), the research performed on bacterial recovery of tellurium will be described. To provide some of the necessary background, this short chapter presents a brief history and background of tellurium microbiology.

Tellurium is the rarest and probably least understood metal that undergoes biogeochemical cycling. It is a metalloid, atomic number 52, which is in the same group of the periodic table as other biologically important elements, such as oxygen and sulfur. It has many accessible oxidation states, the most

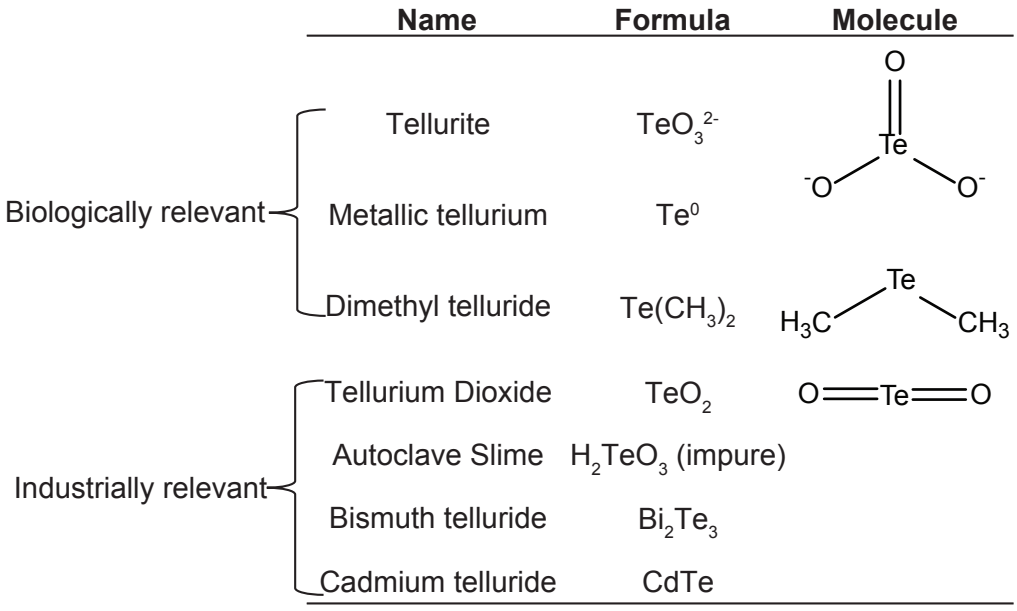

Figure 7.1: Relevant industrial and biological forms of tellurium.

common of which are Te^{6+}, Te^{4+}, Te°, and Te^{2-}. In the earth's crust tellurium takes the Te^{2-} state as it forms tellurides of copper (Cu_2Te), gold (Au_2Te, Au_2Te_3), and bismuth (Bi_2Te_3). In the environment it most often occurs in the 4+ and 6+ states as the tellurite and tellurate oxyanions, TeO_3^{2-} and TeO_4^{2-} respectively. Tellurite is highly soluble, and can be found in earth's waters[45]. For this reason, tellurite has almost exclusively been used to stud tellurium microbiology. This experimentation led to the identification of dimethyl telluride ($Te(CH_3)_2$), a soluble, and volatile form of tellurium created through biomethylation. Other important forms of tellurium are metallic tellurium, Te°, and its oxides, TeO_2, and less commonly TeO_3. Figure 7.1 summarizes the most relevant forms of tellurium discussed in this thesis.

7.1 History of tellurium microbiology

In 1858, Christopher Gmelin injected tellurite into dogs and rabbits[111]. The animals developed a garlic-like odor to their breath, but were otherwise unaffected. In the same era, it was common for people with stomach ailments to take metallic bismuth for relief. These people often developed the same garlic odor on their breaths that Gmelin described in his dogs[111]. This led William Reisert to infer, and experimentally prove in 1885, that trace tellurium impurities in bismuth were responsible for the so called 'bismuth breath'[112]. Shortly thereafter, in the early 20th century, the first microbiological tellurium experiments were performed by scientists. These scientists, including Alexander Fleming, discovered that tellurite was a powerful selection agent for bacteria because its inhibitory concentration spanned many orders of magnitude depending on the specific bacterium[113]. In addition, some bacteria deposited a black material during incubation with tellurite. In 1962 this material was conclusively shown, using X-ray diffraction, to be metallic tellurium[114]. Collectively, these results showed that organisms are able to transform tellurium in two distinct ways, by volatilization to a gaseous species and by precipitation to metallic tellurium. The pathways and mechanisms of these two transformations are still not fully understood, but they are thought to be tellurite detoxification strategies, as will now be discussed.

7.2 Tellurite toxicity to bacteria

Tellurite is highly toxic to bacteria because it is a strong oxidizing agent. Specifically, it has been shown to deactivate cellular thiols by oxidizing disulfide bonds[115,116]. In addition, it is believed that tellurite produces superoxide and other reactive oxygen species (ROS). Many bacteria respond to tellurite exposure by upregulating various oxidative stress proteins like superoxide dismutase (SOD), ibpA, and aconitase[117,118], and based on the similarity between tellurite and selenite (SeO_3^{2-}) chemistry, it is expected that the interaction of tellurite with thiols will produce ROS[119,120]. To this point, superoxide

oxyanions are generated during the first step in abiotic selenite reduction by glutathione (GSH)[121]. Although selenite chemistry suggests that thiol oxidation by tellurite may produce superoxide, this has yet to be definitively proven. Confounding this hypothesis, Tremaroli et al. (2007) observed a temporal de-coupling of ROS production and thiol oxidation in *Pseudomonas pseudoalcaligenes* KF707 cells exposed to tellurite, indicating that the relationship may be more complicated than selenite chemistry would suggest[122].

If superoxide is generated by tellurite, then it is likely that it too contributes to toxicity. Superoxide potentially damages cell proteins, membranes, and DNA. In addition, the generated superoxide can damage [Fe-S] clusters in metabolic enzymes such as aconitase and fumarase, and the released iron can generate additional ROS (i.e., hydroxyl radicals) through Fenton or Haber-Weiss reactions[123]. Although the relationship between tellurite reduction and oxidative stress is well established, definitive *in vivo* evidence of superoxide as the ROS product remains lacking.(Figure 7.2)

Because tellurite is so dangerous to cells, its precipitation to metallic tellurium and methylation to a gaseous tellurium species are generally considered to be detoxification strategies used by the cell. Methylation to a volatile species allows for the removal of tellurium by escaping from the cell and its environment. In contrast, precipitation of an insoluble species (i.e. metallic tellurium) also removes the oxidative stress. Of course, this reduction and precipitation may partly be the unintended consequence of harmful tellurite oxidation of thiols, as discussed above.

7.3 Bacterial volatilization of tellurite

As mentioned, some bacteria effuse a garlic-like odor during incubation with tellurite. Mass spectrometery analysis confirms the existence of a gaseous tellurium species in the headspace of these bacteria, but the composition of this species is not well-defined. It is also possible that it varies between bacterial strains. It consists of various organotelluride species such as dimethyl telluride, dimethyl ditel-

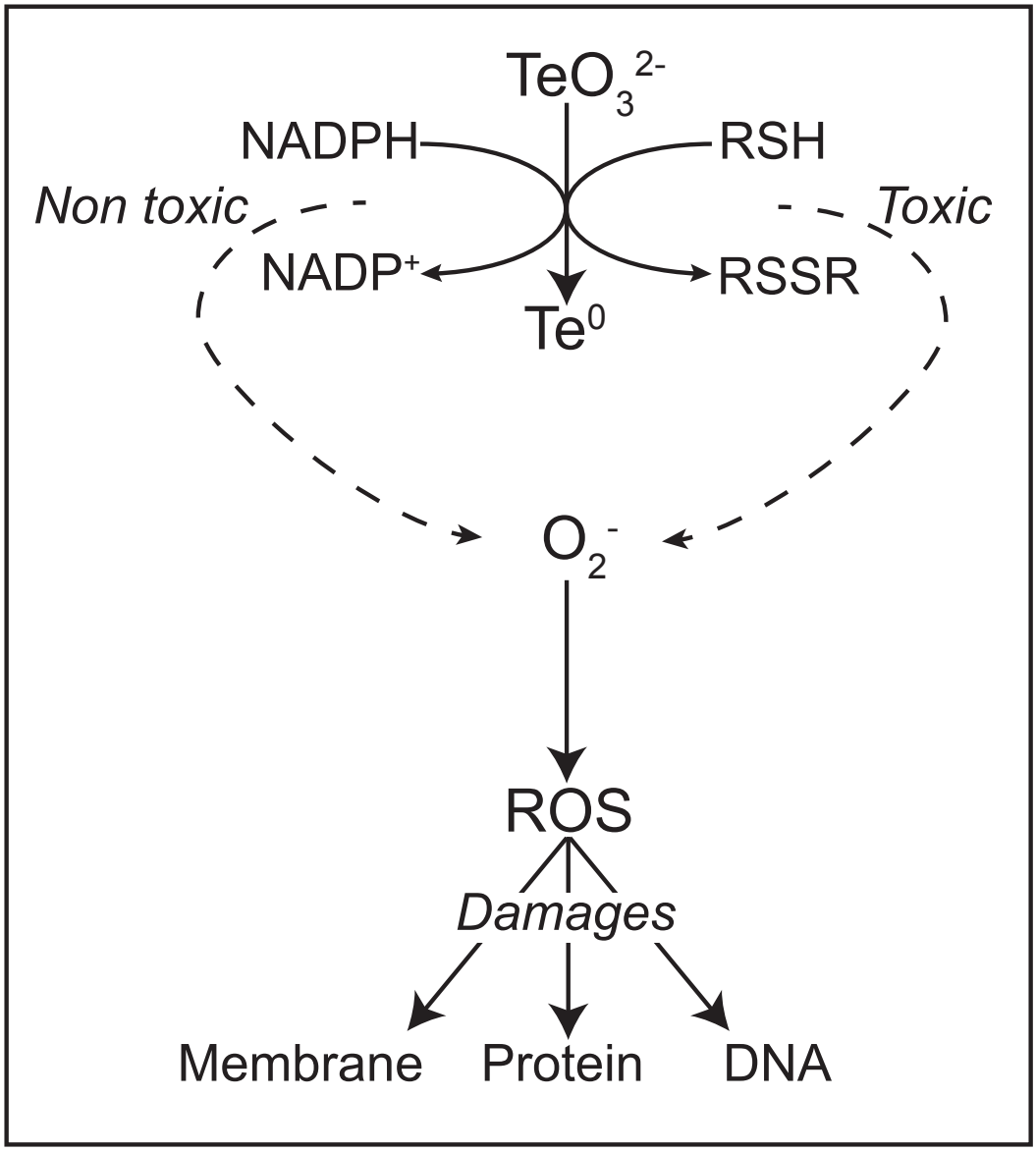

Figure 7.2: Schematic of bacterial precipitation of metallic tellurim (Te^0) from tellurite (TeO_3^{2-}). Tellurite enters the cell and is reduced by cellular reducing agents such as NADP+ or thiols. Reduction by nicotinamide adenine dinucleotide phosphate ($NADP^+$) would not be toxic, but reduction by cellular thiols may harm the cell. Any reduction of tellurite may also form superoxide (O_2^-) which is a reactive oxygen species (ROS) that has the ability to form other ROS. ROS are known to damage the cellular membranes, proteins, and DNA.[111]

luride, dimethyl tellurenyl sulfide, and methane tellurol, along with other disulfide species[124]. The most abundant organotelluride produced by bacteria is dimethyl telluride, which gives the gaseous species its garlic-like smell. It is also the only volatile tellurium species produced by bacteria for which there is an accepted bio-formation mechanism. Specifically, Challenger and Bird published, in 1939, a methylation mechanism for tellurium by microorganisms that has come to be known as the 'Challenger mechanism'[125]. It consists of a series of consecutive reductions and methylations of tellurite through four intermediates until dimethyl telluride is formed.(Figure 7.3) While this mechanism has yet to be proven for tellurium methylation, it is generally regarded as being correct because it has been scrutinized for selenium methylation, an analogous transformation (based on the similarity of tellurium's and selenium's chemistries).

Additional research on dimethyl telluride suggests that ubiquinone, an enzyme, transfers a methyl group from S-adenosyl-L-methionine (SAM) during the methylation of tellurite[127]. Other experiments have shown that aerated bacteria produce more dimethyl telluride than unaerated controls[128].

7.4 Bacterial precipitation of tellurite

Many strains of bacteria, especially Gram-negative ones, are able to precipitate metallic tellurium from tellurite. This precipitation is reported to occur both intra- and extra-cellularly, and result in both crystalline and amorphous metallic tellurium[129,130]. Some researchers have shown that nitrate reductases may be partially responsible for reducing tellurite to metallic tellurium through *in vitro* and histadine tagging studies[129]. Mutated *E. Coli* that lacked specific nitrate reductases decreased tellurium precipitation, while promoted nitrate reductases increased tellurite resistance[131]. Similar experiments have shown that catalases may also be important to tellurium precipitation. Again, knocked out catalase genes decreased precipitation of tellurium, and promoted catalase genes increased tellurite resistance[132]. These researchers also showed abiotic reduction of tellurite with catalase, but only in the

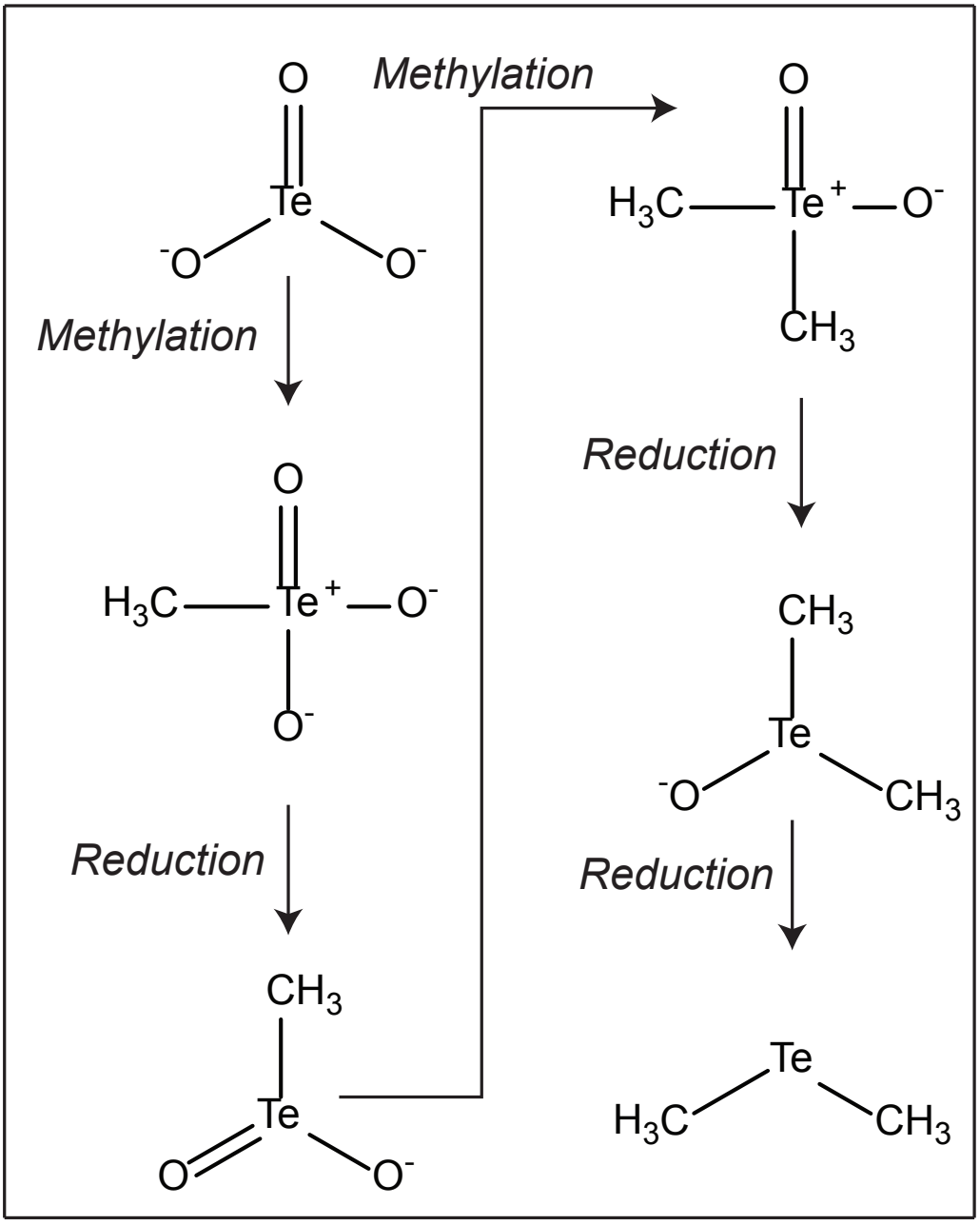

Figure 7.3: The Challenger mechanism for the biological conversion of tellurite to dimethyl telluride. Through a series of reductions and methylations oxygen is removed and methyl groups are added to the central tellurium atom [126]

.

presence of reduced nicotinamide adenine dinucleotide phosphate (NAD(P)H). This led them to believe that NAD(P)H is the relevant reducing agent, with catalase serving an enzymatic role. In addition, tellurite reduction has been coupled to the oxidation of cellular thiols (RSH), primarily cysteine and GSH, which can be re-reduced via NAD(P)H oxidation and thiol reducers such as glutathione reductase[115,116]. Based on these studies, it is not clear if the precipitation of metallic tellurium is the result of specific binding proteins like catalase, the consequence of general cellular reducing agents like nitrate reductase, or some combination of these. Whichever the case, a detailed and comprehensive mechanistic basis of the transformation has yet to be demonstrated.

7.5 Hydrothermal vent bacteria and tellurium

As mentioned in Chapter 3, hydrothermal vent bacteria are of particular interest because vent chimneys are amongst the world's most concentrated sources of tellurium (ζ_{Te}=50 ppm)[46,31]. The high pressure (250 atm) and temperature (400 °C) of vent walls allows tellurium from the vent fluid to substitute for sulfur. The microbes that occupy these vents are exposed to high concentrations of tellurium[45]. In fact, vent microbes from the genus *Pseudoalteromonas* are relatively resistant to tellurium[48,51,52], and bacteria in vents may have evolved the ability to use tellurite as a terminal electron acceptor during metabolism[133,49]. For these reasons, the bacterial strain used in the tellurium studies is a bacterium from the East Pacific Rise vent fields: *Pseudoalteromonas* sp. EPR3[50].

7.6 Summary

Many bacteria interact with environmental tellurite by reducing it to metallic tellurium and methylating it to a gaseous tellurium species that contains dimethyl telluride. These transformations are considered to be detoxifications strategies by the bacteria because they reduce the abundance of tellurite, an oxidizing agent, in the cell. The next chapter describes how these naturally occurring phenomena

can be utilized to recover tellurium from its sources and devices.

8

Bacterial transformation of tellurium compounds

As discussed in the previous chapter, some bacteria can actively transform tellurite to either metallic tellurium or dimethyl telluride. In this chapter, we will demonstrate how these transformations may have utility in tellurium recovery and recycling, especially from tellurium sources that have not yet been studied in relation to bacteria. In addition, this chapter aims to elucidate the tellurium specia-

tion mechanisms within the cell, and how the transformation mechanisms to dimethyl telluride and metallic tellurium are connected. Throughout this chapter the bacteria used for experimentation was *Pseudoalteromonas* sp. EPR3.

8.1 EPR3's response to tellurite

EPR3 was inoculated in liquid artificial seawater (ASW) containing tellurite at concentrations of 8 nM to 0.8 mM. EPR3 grew at all but the highest concentration of tellurite, and subsequent experiments showed that EPR3 grew at all tellurite concentrations below approximately 0.3 mM. Growth curves were then created to measure the effect of tellurite concentration on EPR3 growth. In order to generate the curves, absorbance at 600 nm was measured over the course of one day. The absorbance data was confounded by the presence of precipitated metallic tellurium which also absorbs at 600 nm. In addition, the cell density as a function of tellurite concentration was not measured, so the relative optical densities of the curves cannot be accurately compared. Nevertheless, it appeared that increasing tellurite concentration decreased growth rate from approximately 30 generations per day to 25.(Figure 8.1)

EPR3 formed black colonies in the presence of tellurite, even at concentrations as low as 8 nM. This darkening of colonies was indicative of metallic tellurium precipitation. To verify the presence of metallic tellurium these experiments were repeated on solid media, and darkened bacterial colonies were probed using confocal Raman spectroscopy. These colonies showed the same characteristic Raman pattern as metallic tellurium standards.(Figure 8.2)

In addition, a garlic odor was detected in the headspace of the bacteria. The garlic odor, which is characteristic of bacterial volatilization of tellurite to a gaseous tellurium species[135], was confirmed to contain tellurium by analyzing the bacterial lawn's headspace using ICP-MS.(Figure 8.3) On solid agar, those portions of the bacterial lawn where metallic tellurium precipitated and became dark brown after

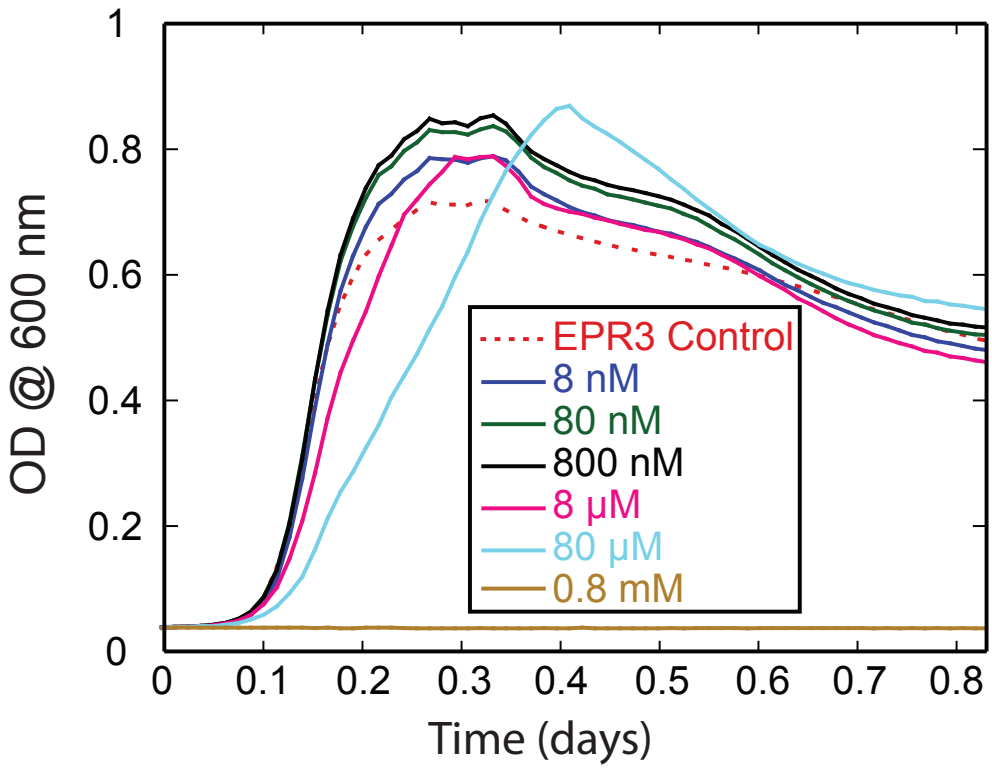

Figure 8.1: Growth curves of EPR3 with different concentrations of tellurite. EPR3 grows in all by the highest concentration of tellurite (0.8 mM), and the growth rate appears to decrease with concentration. Metallic tellurium, which absorbs at 600 nm, was produced by the growing bacteria which confounds the data.

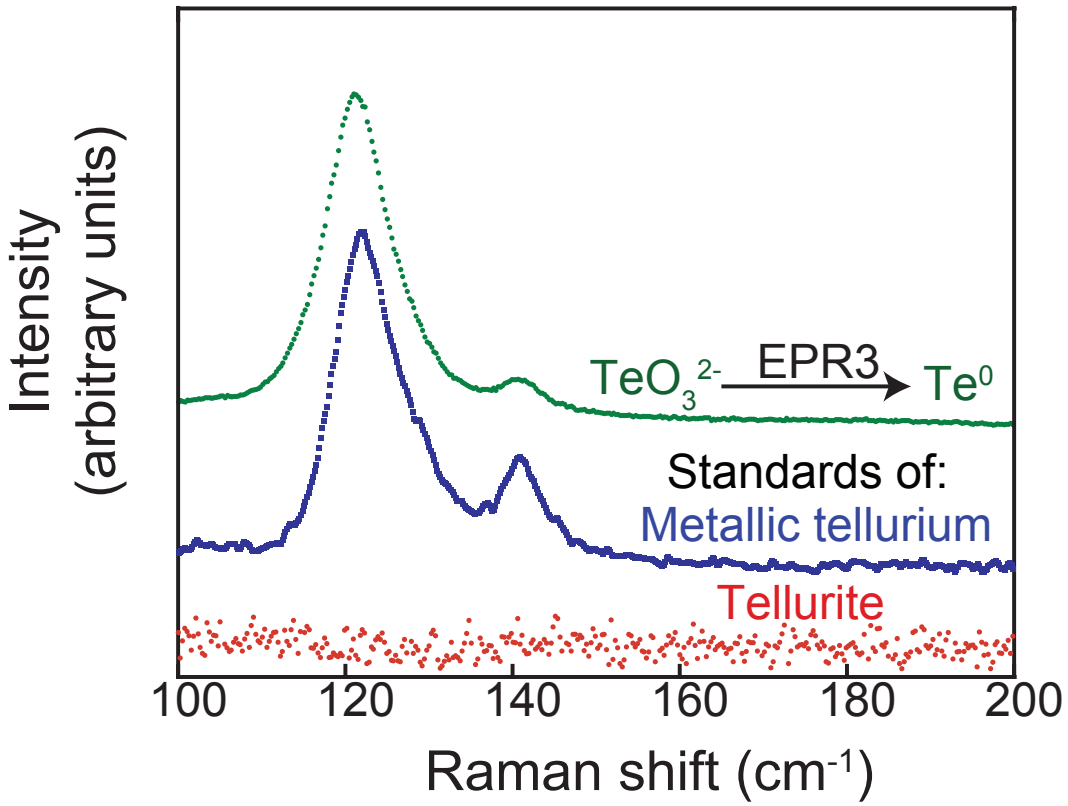

Figure 8.2: Raman spectrum of tellurite transformed into metallic tellurium by EPR3. The top green plot shows the existence of metallic tellurium, which is evident by comparing it to the middle blue plot of a metallic tellurium standard. Tellurite itself (the bottom red plot) does not produce a Raman signal in the given range. Used with permission [134].

48 h gradually faded to a lighter brown after an additional 120 h.(Figure 8.4) As the dark color of the bacterial lawn faded there was a concurrent decrease in the Raman intensity of the metallic tellurium Raman spectrum until, when there was no color remaining, no Raman peaks were distinguishable.

Furthermore, measurements of the dissolved tellurium concentration in tellurite-amended liquid ASW decreased 93% when inoculated with EPR3.(Figure 8.5) This loss was attributed to the precipitation of tellurite to metallic tellurium and the volatilization of the gaseous tellurium species. Sterile tellurite controls exhibited no turbidity, darkening, or decrease in tellurium concentration from metallic tellurium precipitation as measured by spectrophotometry and ICP-MS. In addition, no volatile tellurium species were detected in the headspace of the controls.(Figure 8.3)

8.2 EPR3's interaction with metallic tellurium and tellurium dioxide

EPR3 was incubated in liquid ASW containing metallic tellurium and tellurium dioxide. Despite the insolubility of these sources, metallic tellurium was precipitated during incubation. In order to measure the tellurium transformation, photographs and visible light spectrophotometry data were taken over 168 h.(Figure 8.6) As both the bacterial population and the effect of metallic tellurium on them could not be separated, the spectrophotometry data represents their combined effect on light absorption. Even so, the photographs and absorption data show that EPR3 produced metallic tellurium within the first 24 h of growth, which then diminished over the next 140 h. Controls of each tellurium compound in sterile ASW showed no change in optical absorbance over the course of the measurement time.

These experiments were repeated on solid agar to determine whether direct contact between the bacteria and solid tellurium sources was necessary for the tellurium precipitation. When fine metallic tellurium and tellurium dioxide particles were placed at the center of an agar plate inoculated with EPR3, metallic tellurium was discovered to precipitate even at a distance away from the original tel-

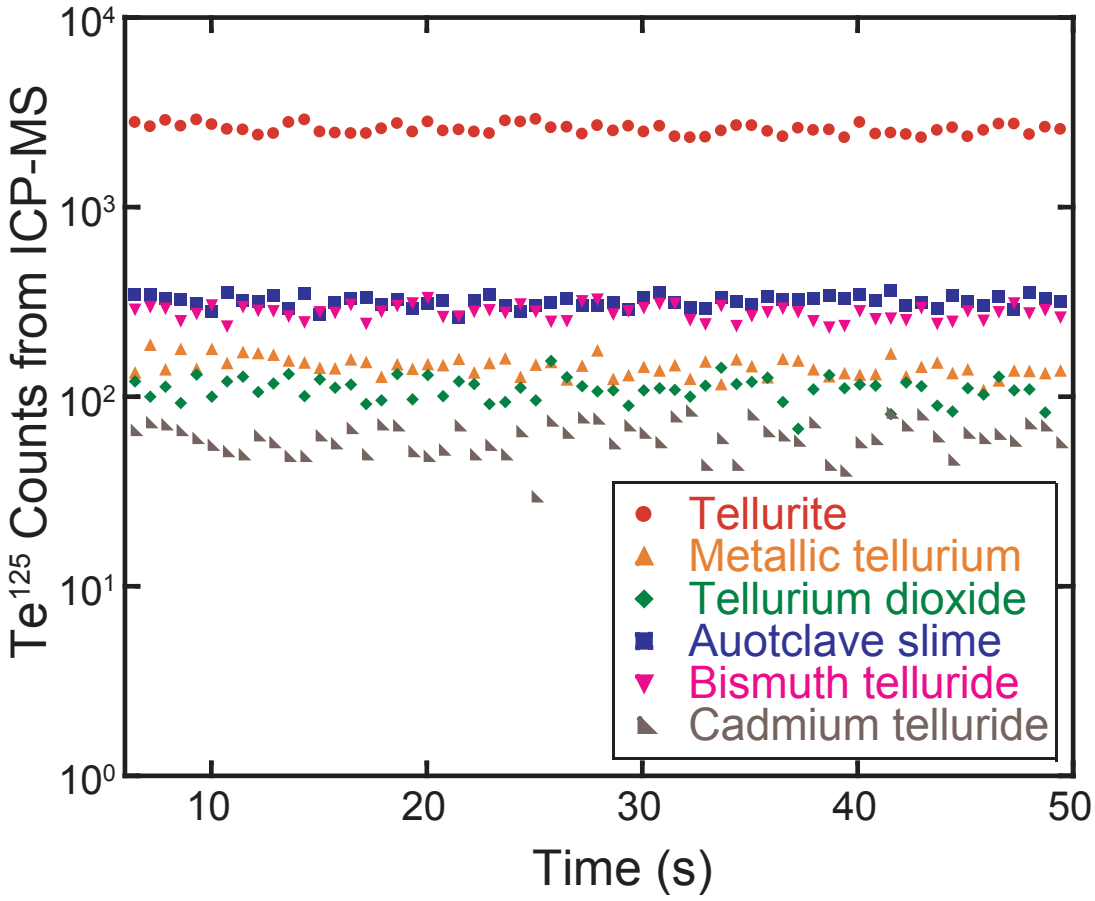

Figure 8.3: ICP-MS results for headspace sampling of Te^{125} above EPR3. Samples of tellurite, metallic tellurium, tellurium dioxide, autoclave slime, bismuth telluride, and cadmium telluride were incubated aerobically with EPR3 on solid ASW for 48 h. In the headspace of each sample a gaseous tellurium species was detected. In controls of the tellurium compounds incubated on sterile solid ASW without EPR3, zero tellurium was detected. Used with permission [134].

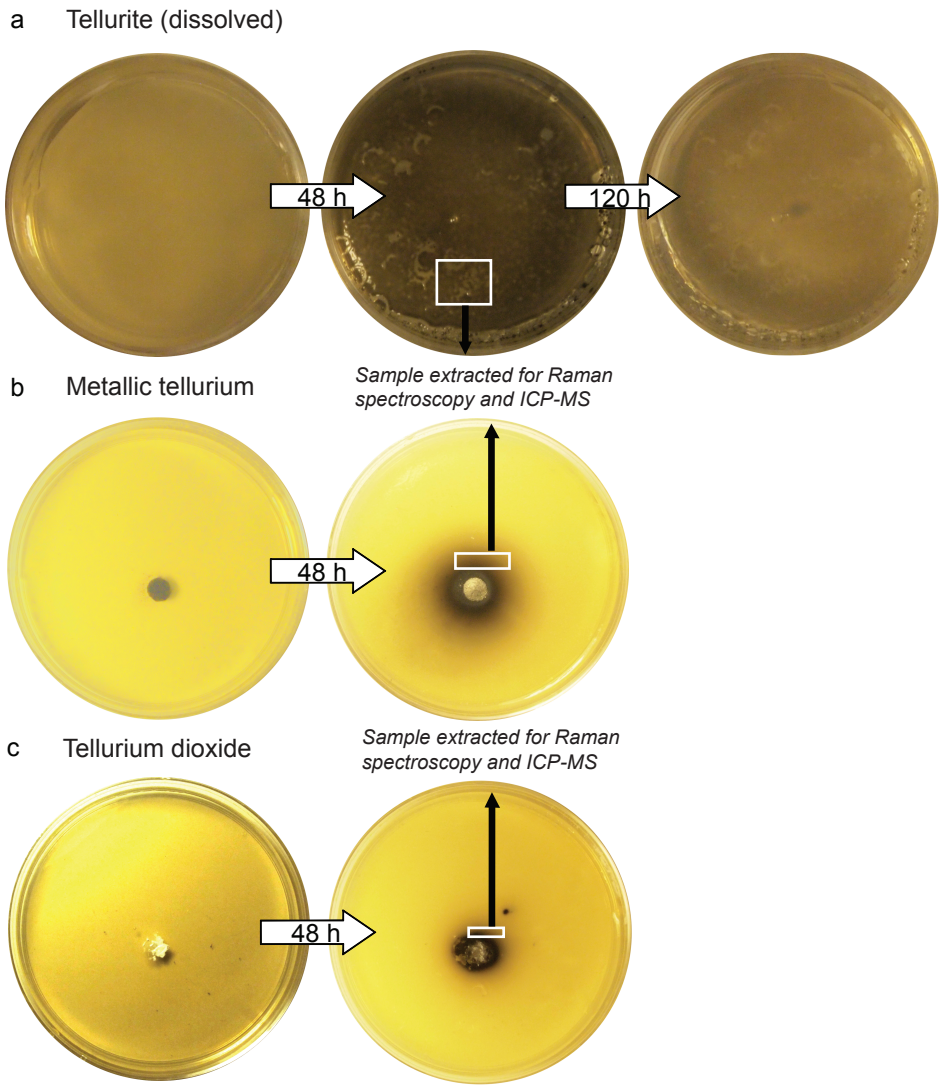

Figure 8.4: a) Photographs of ASW agar plates amended with 0.1 mM tellurite and inoculated with EPR3. After 48 h, bacterial colonies are dark brown, indicative of metallic tellurium precipitation. The plate was aged an additional 120 h. In these plates the dark brown colonies faded to a lighter brown. b,c) Photographs of EPR3-inoculated ASW plates after addition of b) metallic tellurium and c) tellurium dioxide. The colonies in contact with the tellurium compounds and their surrounding colonies turned dark brown, indicative of metallic tellurium precipitation. Those colonies closest to the tellurium source were darkest brown, fading to lighter brown the further the colonies were from the tellurium source. The boxed region in each sample was extracted for Raman and ICP-MS analysis. Used with permission [134].

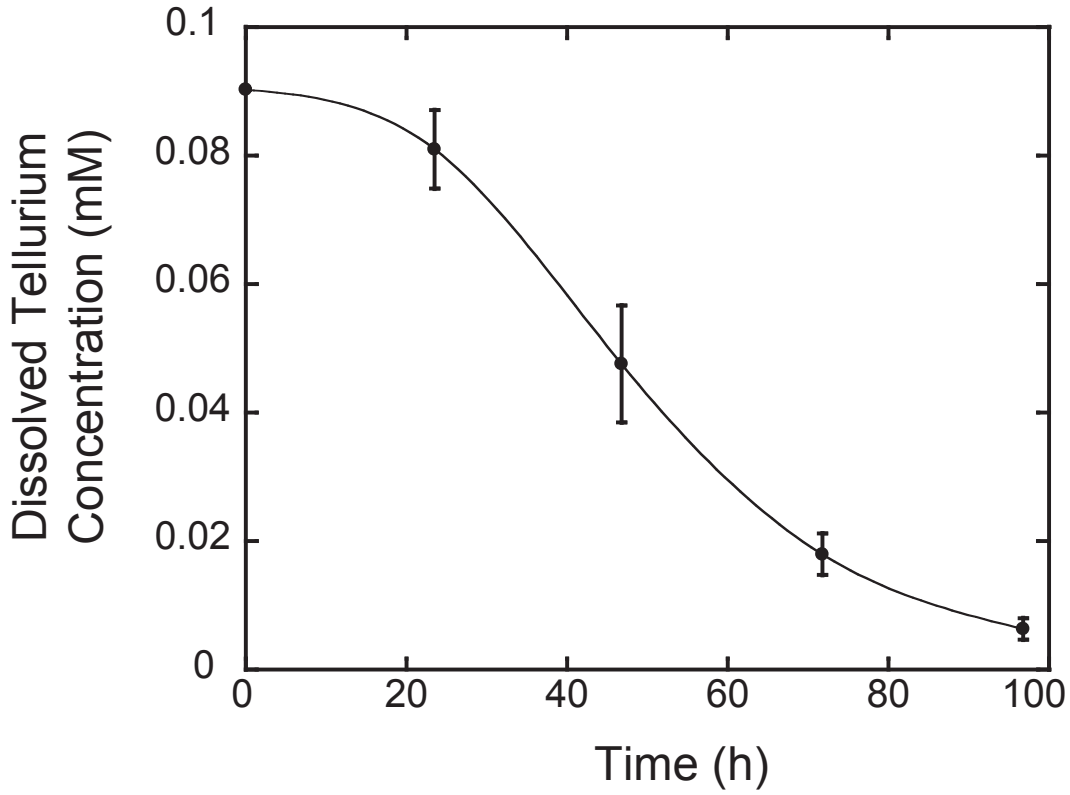

Figure 8.5: The change in soluble tellurium concentration over time during incubation with EPR3, as measured by ICP-MS. The points on the plot are the average of three replicates and the error bars are the standard deviation of the three measured values. A cubic spline fit line is drawn through the points. Used with permission [134].

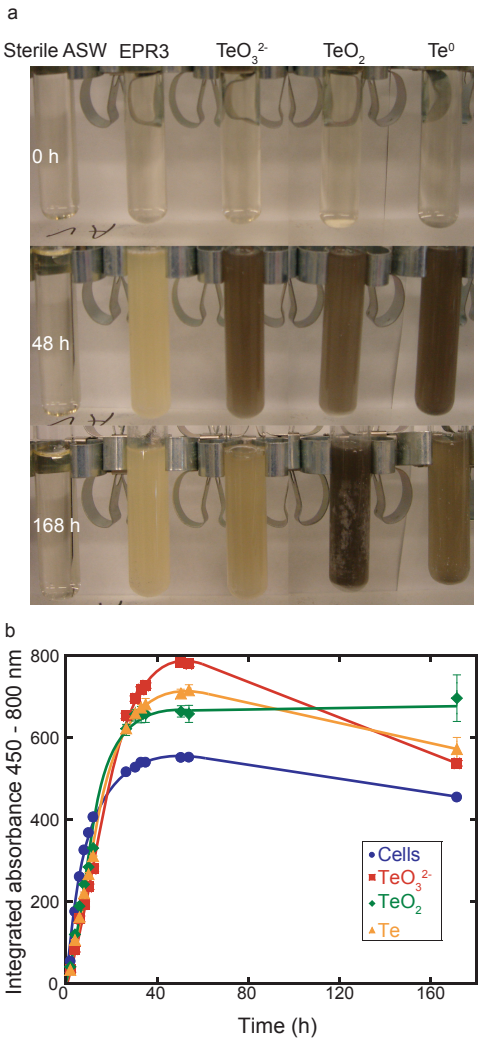

Figure 8.6: EPR3 precipitation of tellurium from dissolved tellurite, metallic tellurium, and tellurium dioxide over time. a) Photographs of ASW tubes, with the three rightmost samples amended with 0.1 mM tellurite, 0.1 g tellurium dioxide, and 0.1 g metallic tellurium, and all but the leftmost sample inoculated with EPR3. After 48 h, bacterial colonies exposed to tellurium compounds are dark brown, indicative of metallic tellurium precipitation. The samples were aged an additional 120 h during which the dark brown colonies faded to a lighter brown for the tellurite and metallic tellurium samples, which at that time resemble the tellurium-free EPR3. b) Plot of integrated absorption between 450-800 nm wavelengths as a function of time for the samples. Note: An ASW sample in which EPR3 precipitated metallic tellurium from telluric acid ($Te(OH)_6$), which is not discussed in this thesis but was included in the assay, was spliced from the images using Adobe Photoshop CS3, otherwise minimal processing was performed on the images. Used with permission [134].

Table 8.1: Soluble tellurium from 0.1 g of various tellurium compounds in liquid ASW after 48 h at 37°C. Used with permission [134].

Tellurium source[a]	Soluble tellurium concentration (mM)[b]
Metallic tellurium	0.038
Tellurium dioxide	0.063
Autoclave slime	0.066
Cadmium telluride	0.001
Bismuth telluride	0.037

[a]Incubated in the absence of EPR3

[b]ICP-MS sensitive to 20 nM

lurium source. (Figure 8.4) This was not only seen by color changes but also by confocal Raman spectroscopy. (Figure 8.7) In addition, ICP-MS analysis showed these bacteria evolved volatile tellurium (Figure 8.3). In the cases of tellurium dioxide and metallic tellurium, bacteria grew right next to the source, making it unclear whether the bacteria in contact with tellurium dioxide were directly reducing it, or the tellurium dioxide was passing through an intermediate soluble phase before it was reduced.

To confirm the possibility of the dissolution of metallic tellurium and tellurium dioxide, both components were added to sterile liquid ASW. After 48 h, the amount of dissolved tellurium, measured using ICP-MS, was 0.038 mM and 0.063 mM for metallic tellurium and tellurium dioxide, respectively. (Table 8.1) This indicates that, contrary to reports in the literature[132], tellurium has a non-negligible solubility in water and that there is a possibility of ion transport in aqueous solutions.

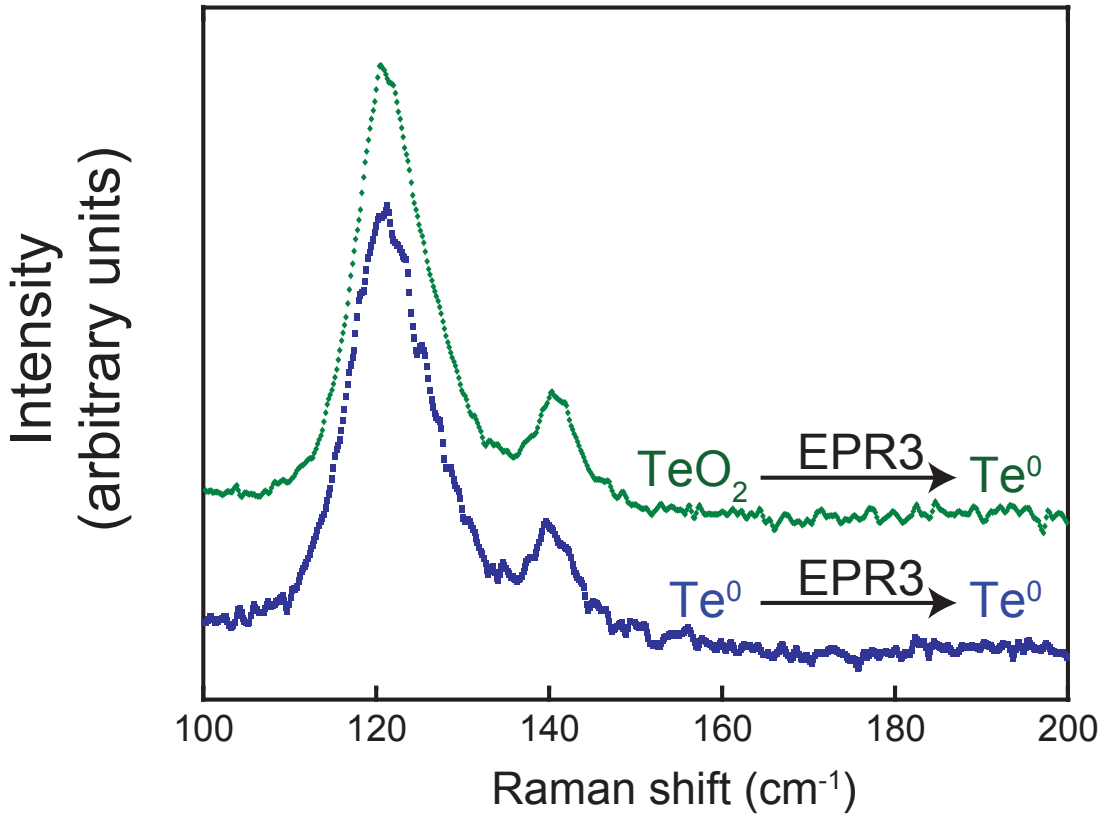

Figure 8.7: Raman spectra of EPR3 precipitations after incubation with tellurium dioxide and metallic tellurium on solid media. Each precipitation exhibits Raman peaks distinctive of metallic tellurium, at 122 cm^{-1} and 141 cm^{-1}. These spectra were recorded from the boxed region shown in Figure 8.4, suggesting that EPR3 is precipitating metallic tellurium away from the tellurium sources indicated. Used with permission [134].

8.3 Demonstration of tellurium recovery from industrial sources

Copper autoclave slime was obtained from Freeport McMoran Copper and Gold El Paso refinery. Normally an effluent from copper and tellurium production, it is a potential source for bacterial recovery to improve current processing methods. To evaluate EPR3's efficacy in interacting with industrially relevant tellurium sources, a similar set of experiments was performed as before. Autoclave slime, an insoluble powder, was added to the center of a dish plated with EPR3 and the plates were incubated as described previously. After 48 h, bacterial colonies darkened to a light brown in a similar manner characteristic to tellurium precipitation. The presence of both metallic tellurium and a gaseous tellurium species in bacteria distant from the autoclave slime were confirmed via Raman spectroscopy and ICP-MS (Figure 8.8, Figure 8.3). Slight dissolution of the slime also occurs in liquid ASW, reaching a tellurium concentration of 0.066 mM. (Table 8.1) For recovery purposes, a slurry of autoclave slime could be added to batch culture for further tellurium recovery, increasing production efficiencies.

To simulate PV and thermoelectric waste recycling, EPR3 was exposed to cadmium telluride and bismuth telluride in agar plates, and incubated at 37°C for 48 h. During that time darkened colonies indicative of tellurite reduction to metallic tellurium appeared and the existence of metallic tellurium was confirmed with Raman spectroscopy.(Figure 8.8) In addition, gaseous tellurium was detected in the headspace of these bacteria using ICP-MS.(Figure 8.3 Incubating cadmium telluride in liquid ASW and measuring the amount of dissolved tellurium confirmed the presence of tellurite at a concentration of 0.001 mM.(Table 8.1) Given the toxic nature of cadmium, any more than 0.1 g of cadmium telluride was lethal to all the cells on the plate, thus only minimal amounts could be used for biogenic recycling.

The cells were more resilient in the presence of bismuth telluride. When bismuth telluride was added to the center of EPR3 plates and incubated the cells near the bismuth telluride turned black,

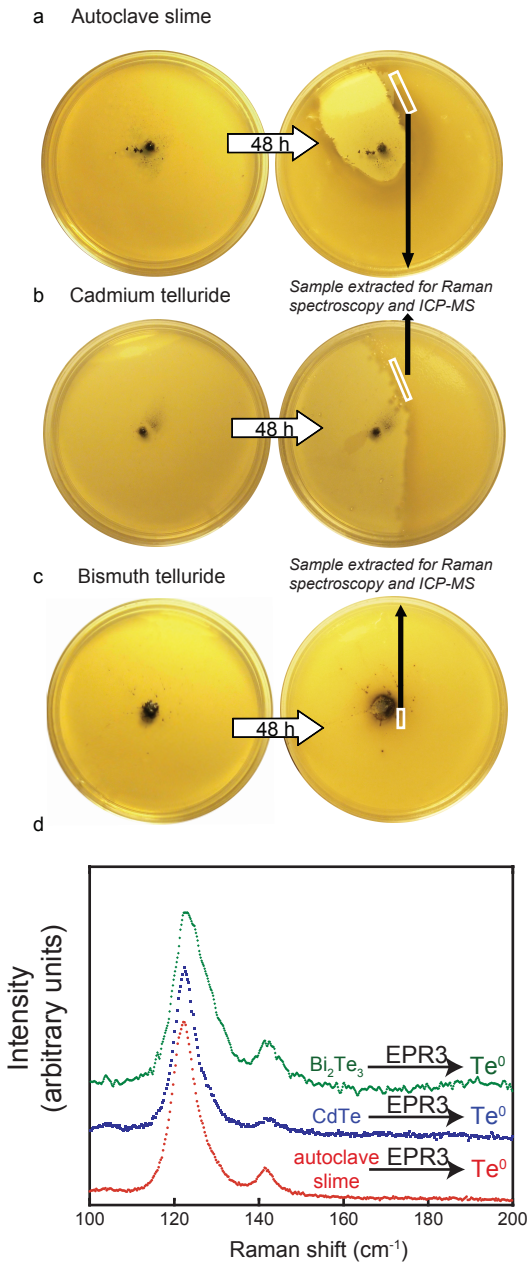

Figure 8.8: Photographs of a) autoclave slime, b) cadmium telluride, and c) bismuth telluride after addition to the center of dishes inoculated with EPR3. After 48 h the surviving cells closest to the tellurium compounds were brown, indicative of metallic tellurium precipitation. Used with permission [134].

indicating metallic tellurium formation.(Figure 8.8) Tellurium precipitation was again accompanied by tellurium volatilization. Both these transformations were verified by Raman spectroscopy and ICP-MS.(Figure 8.8, Figure 8.3) Again, bismuth telluride was slightly soluble, with 0.1 g dissolving in liquid ASW to form 0.037 mM tellurite. (Table 8.1).

8.4 Tellurium speciation by EPR3

Despite the chemical differences between the solid tellurium compounds used as sources in the experiments, EPR3 was found to be effective in converting each of them to metallic tellurium and a gaseous tellurium species. Significantly, the conversion occurred at bacterial cells located a distance from the surface of the solid sources, as evidenced by the precipitation of metallic tellurium, confirmed by Raman spectroscopy, well away from the powders used as the sources. Consequently, it is concluded that all the solids exhibit some solubility and that the tellurium is transported as a soluble ion from the source particles to the bacteria which, in turn, act to reduce the anion to metallic tellurium as well as a gaseous tellurium species, detectable by Raman and ICP-MS, respectively. It is likely, based on the circumneutral pH's we have measured and the tellurium Pourbaix diagram[35], that the soluble anion is the tellurite oxyanion, but the identity of the gaseous tellurium species has yet to be established. Based on the distinctive garlic odor accompanying the bacterial action, however, we believe it to include dimethyl telluride.

In order for some of the tellurium compounds to dissolve, a 4 or 6 electron oxidation process is required, for instance, to convert Te^{2-} in tellurides and Te^{0} in metallic tellurium to Te^{4+} in tellurite. We propose that molecular oxygen provides the necessary oxidization potential to transform these compounds. Our observations that metallic tellurium precipitates faded away faster on agar than in liquid media supports this. On agar, the metallic tellurium is exposed to more oxygen, which favors dissolution to tellurite. Consequently, this tellurite is converted to a gaseous tellurium species and

leaves the system faster than in samples exposed to less oxygen. This hypothesis is consistent with conclusions from Ollivier et. al. (2011) that aeration increases volatile tellurium formation and inhibits metallic tellurium formation in a marine yeast.

Alternatively, it is possible that the tellurium compounds, especially those in liquid media which are exposed to less oxygen and more reduced carbon, are being reduced to hydrogen telluride, and this is the compound which the bacteria act upon. However, no volatile tellurium species, including hydrogen telluride, were detected by ICP-MS from the headspace of sterile tellurium amended ASW plates. For this reason we believe that this alternative is less likely.

8.5 EPR3's tellurium transformation mechanism

Based on our experimental observations, we propose that several inter-related and coupled processes occur during the bacterial speciation of tellurium and its compounds. These are illustrated schematically in Figure 8.9. When the solid tellurium sources are added to agar and liquid ASW, they dissolve until the solubility limit is reached, local equilibrium is established, and no further net dissolution occurs. This solubility, given by the reaction rate constant, is low and, indeed, tellurium solids are generally considered to be insoluble in aqueous solutions[84]. However, when EPR3 is present, the soluble ion diffuses across the cell membrane. Inside the cell, two coupled reactions occur concurrently. One, we infer from our data, is a reversible reduction-oxidation reaction between the tellurite ion and metallic tellurium that is responsible for the internal bacterial precipitation of metallic tellurium. The other we suggest, is methylation by the Challenger mechanism to a gaseous tellurium species that can diffuse out of the cell membrane and either volatize to the air atmosphere or reform the soluble tellurite ion in the solution.

After an initial incubation period, while there remains a solid tellurium source and the cells are active, we believe that a steady state is established. During this steady state, the soluble tellurite oxyan-

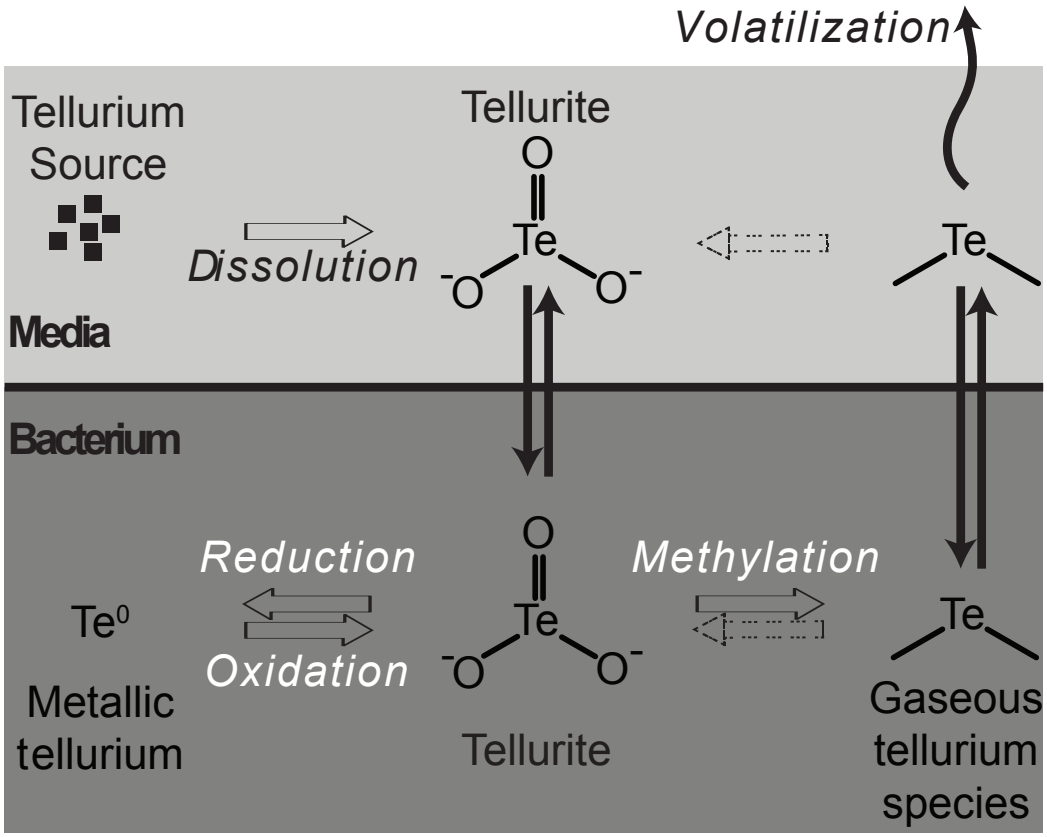

Figure 8.9: Schematic of proposed tellurium speciation in a bacterium and its media. Diffusion is represented by solid arrows and chemical changes are represented by hollow arrows. We propose that a solid tellurium source (e.g. tellurium dioxide, autoclave slime, cadmium telluride, and bismuth telluride) dissolves in the media to yield soluble tellurite. The tellurite crosses the cell wall and the bacterium transforms it to either metallic tellurium or a gaseous tellurium species (for instance, dimethyl telluride by way of the Challenger mechanism). While there is undissolved tellurium source, the metallic tellurium - tellurite - volatile tellurium system is in steady state; solid tellurium dissolves to tellurite, which can be converted to a gaseous tellurium species, which escapes to the environment by volatilization. Volatile tellurium species may also be transforming back to tellurite (represented by dotted hollow arrow). Used with permission [134].

ion formed by dissolution of the source is transported and converted by the cells to metallic tellurium and, a yet unidentified, gaseous tellurium species, most likely including dimethyl telluride. In essence, in steady state the solid dissolution rate is equal to the volatilization rate buffered by the precipitated metallic tellurium produced by the cell, with the rates being dependent on temperature, pH, partial pressure of oxygen, and the cell concentration. Once the source of tellurium is consumed, the metallic tellurium buffer in the cells is depleted and the overall reaction ceases. The changes observed on the agar plates are visible evidence of these reactions: the darkening due to the precipitation of metallic tellurium at distances away from the powder sources and the subsequent lightening in color as the amount of tellurium decreases until none remains and the agar returns to its initial color. The observed color changes when the bacterial reaction occurs in the liquid medium is also consistent with this overall reaction, although less vivid.

It is possible that other soluble and volatile tellurium compounds, not shown in Figure 8.9, may also be present and contribute to the overall tellurium cycling. However, the similarity of EPR3's response to the different solid compounds leads us to conclude that EPR3 is acting on the same tellurium containing molecule which we believe is the tellurite oxyanion. This conclusion can be applied to other tellurium compounds that can be transformed by bacteria but are not discussed here, such as bacterial tellurate (TeO_4^{2-})[127,133,49], and telluric acid ($Te(OH)_6$) (transformation by EPR3 observed during the course of experimentation, but no measurements were taken), as well as anecdotal studies on tellurium transformation by mammals ingesting metallic tellurium[111]. It is also consistent with the work of Ollivier et. al. (2011) which shows that a marine yeast precipitated metallic tellurium from a biologically evolved gaseous tellurium species. We also suggest that there is a concurrent reaction between the gaseous tellurium species being oxidized to tellurite and precipitating as metallic tellurium. This reversible reaction of gaseous tellurium species to tellurite is represented in Figure 8.9 by the dotted arrows. It is shown dotted because of our uncertainty of the actual mechanism.

8.6 Summary

In this chapter we found that EPR3 transformed a variety of tellurium containing compounds including cadmium telluride, bismuth telluride, autoclave slime (a waste product of tellurium production), and tellurium dioxide (an intermediate in tellurium production) to metallic tellurium and a gaseous tellurium species. Each of these compounds are generally considered to be insoluble, but our experiments suggest that EPR3 acts on a dissolved tellurium species to precipitate and methylate tellurium from these compounds. These findings led to the conclusion that precipitated tellurium within the cell should also be dissolving to tellurite, and that this tellurite can be transformed into a gaseous tellurium species which eventually leaves the cell. This was confirmed by experiments that showed the total amount of tellurium in the bacteria and its media decreases over time, as it is lost to the environment by volatilization. In addition, EPR3's ability to transform these various compounds to metallic tellurium lends itself to tellurium production. By simply incubating EPR3 in non-lethal concentrations of these compounds, such as autoclave slime, PVs, or thermoelectric devices, direct transformation and recovery of metallic tellurium should be possible. Overall, these results introduce new insights into tellurium speciation in bacteria, and demonstrate the potential for bacteria in tellurium recovery.

9

Conclusion

This thesis has demonstrated various microbiological methods to separate the lanthanides and recover tellurium from many of their sources and devices, and through pursuing these methods new discoveries were made regarding the mechanisms by which these metals interact with bacteria. In this final chapter we will summarize and discuss conclusions from the experimental work presented in this thesis.

9.1 Lanthanide recovery and potential for recycling

9.1.1 Summary and conclusions

Despite the lanthanides' value and increasing pervasiveness in our lives, little attention is paid to their production and recycling, which are costly and harmful to the environment because of inefficient lanthanide separations. Biosorption has long been considered as a potential method for valuable metal recovery. The primary problem though, is that biosorption is not normally selective towards specific metals, and most research demonstrates biosorption from a single element solution when other methods of recovery are better suited.

This thesis discussed the separation and recovery of individual lanthanides from a lanthanide mixture through biosorption to *Roseobacter* sp. AzwK-3b and subsequent selective desorption. The bacterial surface sites, which ranged in pK_a from 1.5 to 6, bound the lanthanides differently according to the lanthanides' basicities. The lighter lanthanides bound higher pK_a sites, while the heavier lanthanides bound lower pK_a sites. Bacterial surfaces are known to consist of lipopolysaccharides with various surface exposed chemical groups, and it is generally understood that two of these, phosphate and carboxyl groups, are the most important to lanthanide binding. The range of pK_a's observed from the bacteria leads us to believe that indeed these surface groups are responsible, and their different spatial and chemical arrangements lead to variations in pK_a. We observed the same range of pK_a's from liposomes composed of PA lipids that had only phosphate surface groups, instead of multiple chemical groups such as those that are on the surface of bacteria. Although further research is needed, we believe that variations in the phosphate group spacing causes the observed pK_a ranges.

The lanthanide adsorption differences were utilized to concentrate a solution in the heaviest lanthanides. A mixed lanthanide starting solution was adsorbed to liposomes and pre-protonated bacteria and selectively washed with low pH washes so as to recover only the heaviest lanthanides. This process was repeated 2 times until the final solution was nearly 50% concentrated in these two lan-

thanides. The process occurs at room temperature and pressure and does not involve the use of any harsh chemicals (only low pH acids), so it confers advantages to many of the industrial metal refining and production methods that are currently used. Some disadvantages are apparent though. The process, so far, has only been tested on small masses of the elements and may not be effective at an industrial scale. Also, even with these small amounts there was still a loss in mass of each element throughout each step in the process. Finally, the process is presently only semi-continuous, rather than fully continuous, and the pH values needed to be decreased in steps rather than over a gradient. Even with these drawbacks though, this adsorption-desorption method is a promising strategy to recover metals from solution.

The favorable lanthanide separations demonstrated in this thesis were observed using various bacteria and liposome surfaces, without controlling for their compositions. Once the lanthanides adsorbed to these surface, eluting them with a gradient of pH solutions tended to separate each one according to atomic number. It appears, then, that once the lanthanides are in solution their adsorption behavior is a powerful property that can be used to differentiate them. Tuning adsorption surfaces through bioengineered bacteria or chemically engineered substrates should allow for enhanced lanthanide separations and improved recovery systems.

9.1.2 Future work

The bacterial based lanthanide recovery has further experimentation that should be carried out in future work. In this thesis, the identification of surface groups was done by matching observed pK_a's with the published pK_a's. This is not always accurate and limits the analysis to well studied surface groups. Future investigations could verify these identities by characterizing these surface groups using X-ray absorption spectroscopy (XAS). In addition, the observed lanthanide binding pk_a's were confounded by the complexity and variation in spacing of the surface groups on the bacterial surface, and by the dynamism of the liposomes. Experiments should be carried out in which lanthanides are

adsorbed and desorbed from rigid surfaces with known compositions and spacings between groups. This simpler, well defined surface should help verify the model. Also, with respect to the liposomes, it is assumed that lanthanides are not entering inside of them. This could be verified by performing the filtration assay with various sets of homogeneously sized liposomes. If the lanthanides are adsorbed to the surface of the liposomes, their desorption should increase quadratically as a function of liposome radius, whereas if they are entering the liposomes their release should increase cubically as a function of liposome radius.

Regarding lanthanide separation, the recoverability of all the lanthanides that are added to the system needs to be addressed. In the current filtration assay some of lanthanides' mass flows right past the adsorbant. In addition, there appears to be some lanthanide that does not desorb even with the low pH 1.5 washes. These lanthanides are only removed with a 70% nitric acid wash. In both these cases these lanthanides would need to be recovered and recycled in any future system, but no such work on recovering them was performed. Also, further work is needed to characterize the bacterial surfaces, especially as a function of growth rate. During experimentation it appeared that the growth phase of *Roseobacter* sp. AzwK-3b affected lanthanide biosorption, and different desorption results were measured when one day old versus two month old batches of the bacteria were used. There have been some studies on the surface changes in bacteria throughout their growth[136], but nothing related to lanthanide biosorption.

9.2 Tellurium Recovery

9.2.1 Summary and conclusions

Tellurium is produced as byproduct of copper refining, and exists in the anode slime of any refinery. Despite this, of the three major copper refineries in the United States, tellurium is only produced at one of them, the ASARCO copper refinery in Amarillo Tx. The others, the Rio Tinto refinery in Salt

Lake County, Utah, and the Freeport McMoran refinery in El, Paso Tx, do not choose to recover their tellurium.

This thesis discussed the recovery of tellurium from a common mining effluent, called autoclave slime, in addition to materials used in devices, such as cadmium telluride and bismuth telluride. Each tellurium compound exposed to the hydrothermal vent bacteria *Pseudoalteromonas* sp. EPR3 was converted to metallic tellurium and a gaseous tellurium species. Based on the observation that precipitation of metallic tellurium occurs in cells located well away from these tellurium sources in agar, it is concluded that some soluble tellurium species, likely to include the tellurite oxyanion, forms despite the reported insolubility of the solid sources, and diffuses to the cells. There the soluble tellurium is taken up by EPR3, precipitating metallic tellurium within the cell and more slowly converting, possibly by the Challenger mechanism, to a volatile tellurium species that diffuses out of the cell and escapes. Interestingly, the slight solubility of metallic tellurium suggests that metallic tellurium precipitating in the cell should be dissolving to tellurite as well. This produces a steady state between undissolved tellurium compounds and gaseous tellurium volatilization. Evidence for this mechanism comes from the observation that metallic tellurium precipitated by the bacteria is gradually degraded over time, as it is eventually converted to gaseous tellurium and volatilized to the environment.

Irrespective of whether bacterial transformation of tellurite is a detoxification strategy or an 'unintended' byproduct of cellular reducing agents, more work is necessary to understand the complex interactions, including the enzymatic reactions, between bacteria and tellurium. Despite this we have demonstrated that EPR3 may be a useful bacterium in the recovery of tellurium because it is shown to be a versatile bacterium in the reduction and methylation of tellurium from a wide variety of solid tellurium compounds. Notably, EPR3 shows resilience to the soluble tellurite oxyanion at concentrations of 0.3 mM, significantly higher than reported in vent fluid[45]. Consequently, there is potential in using EPR3 to recover tellurium industrially, bypassing some of the existing processing steps, and, possibly, also in recycling. This will involve handling the volatized tellurium species and, in the case of

processing cadmium telluride, special care in capturing the highly toxic dimethylcadmium[137,138] if any were to evolve. Further research into purities, yields, and flow-through processes are clearly needed, but EPR3 and possibly other vent bacteria show considerable promise for both higher efficiency tellurium recovery and simpler processing.

Many bacteria transform tellurite to metallic tellurium and the gaseous tellurium species, even though tellurium is one of the scarcest elements in the earth's crust. It is likely then, that the molecules that are acting on tellurite are not specific to this element, as it would be improbable for so many species to have evolved enzymes that use this scarce metal as a substrate. This is evidenced by the similar transformations that occur with selenite, which is chemically similar to tellurite. This transformation process and the molecules involved may have broad value then, in recovering various cations from solution. This underscores the need to better understand the interactions between metals and bacteria, because they could serve as the basis for new metal recovery and recycling methods.

9.2.2 Future work

Further tellurium experimentation will be necessary to better support the proposed speciation model. The ICP-MS measurements of soluble tellurium only detected nominal tellurium concentration, and no distinction could be made between tellurite and the gaseous tellurium. To this end, the most important work needed is *in situ* monitoring of the gaseous tellurium species while tellurite is being acted on by the bacteria. This would shed light on the overall kinetics of tellurium transformation and allow for reaction rates to be calculated. In addition, this would convincingly demonstrate whether or not the gaseous species is directly oxidizing to tellurite, something that is suggested with uncertainty in the model. Also, the composition of the gaseous tellurium species should be determined. Attempts at doing this using gas chromatography - mass spectrometry failed because the gas concentration was too low, but sophisticated sample preparation techniques, such as solid phase microextraction, may be successful.

Optimal recovery of metallic tellurium after bacterial transformation from tellurite needs to be investigated as well. For example, techniques to increase the bacterial precipitation of tellurite, rather than methylation of tellurite to the gaseous species, should be studied. Based on the tellurium speciation model, after metallic tellurium is formed within the cell it can be be oxidized to tellurite and then converted to the gaseous species. Therefore, limiting the oxygen in the media or performing the bacterial transformation in an anaerobic environment are potential strategies to enhance metallic tellurium formation. In addition, the purity of metallic tellurium produced by bacteria needs to be measured, and techniques to physically or chemically remove it from the cell should be explored. Finally, the bacteria should be tested for their ability to recover tellurium from other sources like copper mine tailings and smelting filters.

9.3 Closing remarks

In this dissertation we have demonstrated simple and effective methods to recover the lanthanides and tellurium using biological processes. Ours and other investigations of new recovery methods for many of the scarcest metals are important endeavors, so we hope this dissertation serves as a meaningful and impactful advancement in this field.

A

Materials and methods for lanthanide experiments

This appendix shows the experimental methods used for the lanthanide experiments discussed in Chapters 4, 5 and 6.

A.1 Media and Reagents

A mixed lanthanide calibration standard (Accutrace, New Haven, Ct) used for inductively coupled plasma - mass spectrometry (ICP-MS) was used as the mixed lanthanide solution unless otherwise described. This standard solution contains 10 μg/mL of each lanthanide (except Pm) as well as Sc, Y, and Th all dissolved in 2% nitric acid. It was then diluted with deionized water and neutralized to pH 6.0 to an approximate concentration of 2 μg/mL. It was also diluted with trace metal free 2% nitric for use as the lanthanide standards for ICP-MS analysis. Lanthanum (III) nitrate hexahydrate (Alfa Aesar, Ward Hill, MA), and lutetium (III) chloride hexahydrate (Alfa Aesar, Ward Hill, MA) were used to create individual lanthanide solutions. These chemicals were diluted in deionized water to a concentration of approximately 30 μg/mL.

Dipiciolinic acid was purchased from Spectrum Chemicals (Gardena CA). It was used to chelate the Nd and Pr to form Nd(III) and Pr(III) dipicolinate. First 0.003 moles (∼0.5 g) of dipicolinic acid were added to 10 mL of vigorously mixed DI water. Then 0.001 moles of the Nd or Pr (as $Pr(NO_3)_3 \cdot 5H_2O$, or $Nd(NO_3)_3 \cdot 6H_2O$) were added to the solution. After, while still mixing, the pH of the solution was raised to pH 8.0 by adding 2.0 M NaOH drop by drop. Then the solution was allowed to evaporate slowly, creating large crystals of Pr(III) and Nd(III) dipicolinate. These crystals were then redissolved in deionized water to a lanthanide concentration of approximately 2 μg/mL.

Roseobacter sp AzwK-3b was donated by C. Hansel who isolated it from Elkhorn Slough, a coastal estuary adjacent from Monterey Bay, CA[57]. EPR3, EPR7, and EPR174 were obtained from Costantino Vetriani who isolated them from the East Pacific Rise hydrothermal vent field[50]. *Halomonas* sp. *Sphingobacteria* sp., and *Pseudoaltermonas* sp. were isolated from cheese rinds by Rachel Dutton[139]. The growth media for these bacteria was artificial seawater (ASW) which was sterilized by autoclaving at 120°C for 15 min. *Escherichia coli* and *Shewanella oneidensis* were purchased from the ATCC. The growth media for these was autoclaved tryptic soy broth (TSB), which was sterilized at the same con-

ditions as the ASW.

A.2 Preparation of the bacteria

Each strain was inoculated from a frozen stock into 5 mL of its media and grown for 24 h at 37°C. Each was then individually transferred to 5 mL of media and grown for 24 h at 37°C which provided the source bacteria for each experiment. The filtration assay experiments that used AzwK-3b as the adsorbant were incubated for a longer time before use. A single stock of AzwK-3b was created by inoculating 1 L of sterile ASW with AzwK-3b and allowing it to incubate for approximately 2 months. Then, AzwK-3b biomass was kept refrigerated, and was sterilely removed from this stock throughout the experiments.

A.3 Liposome Formation

The following saturated phosphatidic acid (PA) lipids were procured from Avanti Polar Lipids (Alabaster, AL) to create liposomes: 10:0 PA 1,2-didecanoyl-sn-glycero-3-phosphate (sodium salt) (25 mg in chloroform solution, part number: 830843C).(Figure 5.16) Liposomes were created from the PA lipids following the standard protocol outlined by the lipid manufacturer, Avanti Polar Lipids[140]. In each case, 5 μg of the lipid dissolved in chloroform was transferred with a glass pipette to a 10 mL glass vial. The chloroform was then dried by a steady stream of nitrogen gas to form a lipid film. The film was subjected to vacuum for 2 hours, and then suspended in deionized water to a concentration of 1 μg/mL. The resultant solution was shaken at 240 rpm for 1 hr to form liposomes. The liposomes were sized using a dynamic light scattering (DelsaNano C, Beckman Coulter) and found to range in size between 0.25 μm and 50 μm diameter with an average size of 1.2 μm.(Figure A.1 They were stored at 4°C and always used within 3 days of their formation.

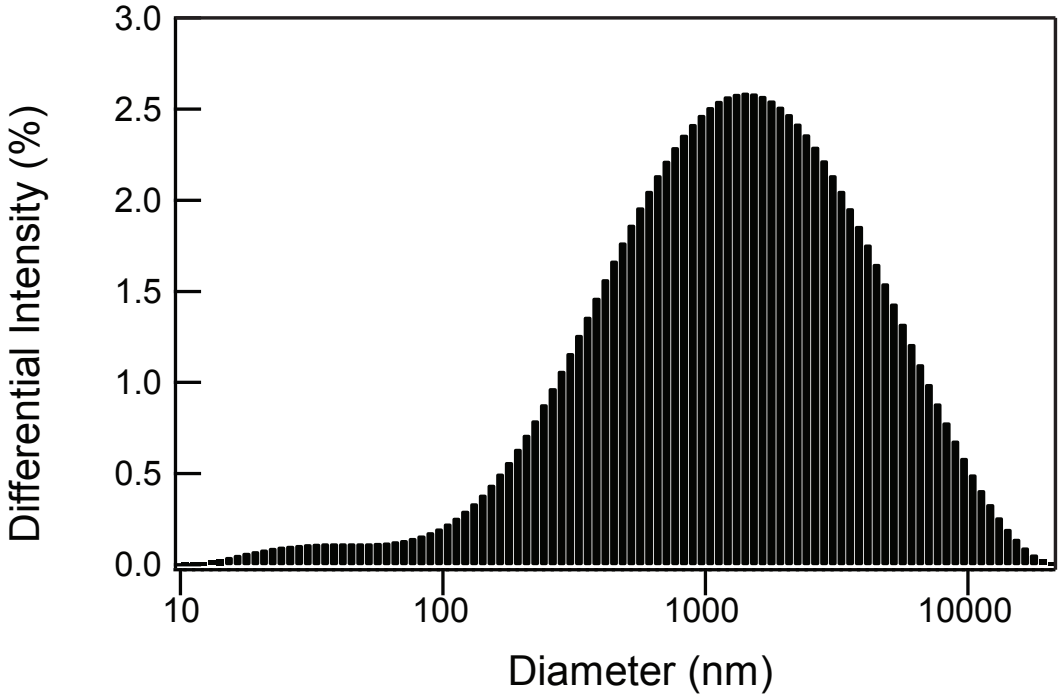

Figure A.1: Differential intensity as a function of diameter for the liposomes used in this study. As shown in the plot, the liposomes had an average diameter of 1.2 µm.

A.4 Batch studies

Three batch studies were conducted by incubating bacteria in media amended with the lanthanide cocktail. In the first experiment individual samples of each strain were inoculated into media that had a concentration of 0.1 μg/g of each lanthanide. These were then incubated at 37°C with continued shaking for 11 days. In the second experiment each strain was grown individually in lanthanide-free media for 10 days at 37°C with continued shaking. At that point the media was amended with the lanthanide cocktail and brought to a concentration of 0.1 μg/g. These samples then incubated with continued shaking for 1 additional day. In the third experiment two samples of EPR3 were inoculated then incubated in ASW for 10 days at 37°C with continued shaking. At that point the media was brought to a concentration of 0.1 μg/g of each following lanthanides: sample 1, a combination of Pr(III) and Nd(III) cations in solution, and sample 2, a combination of Pr(III) and Nd(III) dipicolinate in solution. These samples were then incubated at 37°C with continued shaking for an additional 1 day. After incubation each of the samples described above were centrifuged at 8000 rpm for 60 min to form a cell pellet, isolated from the media. Then, the supernatant media was removed from each sample, diluted in 2% trace metal free nitric acid, and analyzed for its lanthanide content by ICP-MS. Sterile controls of media that contained the lanthanides were prepared as well, and showed no difference in lanthanide mass before and after incubation.

A.5 Filtration Based Assay

A filtration assay was developed to measure lanthanide adsorbtion and then to expose adsorbed lanthanides to various pH washes. The assay consisted of a syringe pump pumping liquids from a syringe past a 25 mm diameter hydrophilic filter (Pall, Port Washington, NY, GHP Acrodisc) at a rate of 2.5 mL/min. The average pore size of the filter (0.2 μm) was selected to be smaller than the diameter of the bacteria (0.8 μm). First, 5 mL of water was passed through the filter to wet it. This was then followed

by approximately 0.1 mg of the bacteria or 2.0 μg of liposomes in solution.(Figure 5.1) Then, 1 mL of the 2.0 μg/mL solution of mixed lanthanides was pumped through the filter enabling the lanthanides to adsorb to the bacteria or liposomes. This was followed by a deionized water wash (pH 7) to remove any unbound lanthanides. Then, a series of nitric acid solutions, from pH 6 to pH 1.5 in intervals of pH 0.5, was pumped past the bacteria on the filter. These nitric acid solutions desorbed the adsorbed lanthanides depending on the pH of the wash. Each of the nitric acid washes was analyzed by ICP-MS after passage across the filter to quantify the concentrations of the individual lanthanides desorbed as a function of pH wash.

Several modifications of the titration assay were also developed as controls in the experiments. One modification using bacteria as the adsorbant involved collecting a single drop from the syringe every 500 μL of liquid pumped through the filter, and analyzing each drop for lanthanide content, rather than collecting the entire 5 mL fraction. In this version only two pH washes were used, a pH 3.5 wash and a pH 1.5 wash. This modification showed that the wash volume and pump rate were sufficient for complete lanthanide desorption because a negligible mass of lanthanides were detected in drops obtained following the passage of 5 mL past the filter.(Figure 5.3) Another modification involved passing the lanthanides through a new filter absent bacteria to show that the filter itself was not a sorbent of the lanthanides.(Figure 5.2)

The filtration assay was also used to study the effect of pre-protonation of the bacterial surfaces. After the filters have been coated with the bacteria, a solution of nitric acid of either pH 2.5 for the bacteria or pH 2 for liposomes was pumped through the filter. Then, the lanthanide solution (at circumneutral pH) and subsequent nitric acid washes were passed through the filter as described in the basic assay experiment. An alternate version of this assay used a lanthanide solution that was decreased to pH 3.0 using 2% nitric acid.

In a final modification, individual lanthanide solutions consisting of either 30 μg/mL of La (III) or Lu (III) were substituted for the combined lanthanide mixture in order to measure the biosorption

behavior of these individual lanthanides.

A.6 Reversibility

The reversibility of biosorption with changes in pH was studied using a modified biosorption reversibility assay adapted from Ngwenya *et. al.*[71]. A 100 mL volume of a grown culture of AzwK-3b was centrifuged (8000 rpm, 30 min), and the supernatant media removed. The culture was then mixed with 200 mL of deionized water and 3.3 mL of the ~30 μL/ml lutetium (III) chloride solution. The solution was equilibrated for 2 h while mixing, and the pH was then measured and a 500 μL sample was removed. The pH of the solution was then reduced by successively adding drops of nitric acid of varying concentration. At each step in pH the solution was allowed to equilibrate for 30 min, and thereafter the pH was measured and a 500 μL sample was removed. After reaching the lowest pH value (1.99) the pH was then increased using various concentrations of sodium hydroxide. At each pH step the solution was equilibrated, its pH measured, and a 500 μL sample was removed for analysis. These samples were then further diluted with nitric acid for analysis of their Lu content by ICP-MS.

A.7 ICP-MS Analysis

ICP-MS (Agilent Technologies 7700x, Figure A.2) was used to measure the concentration of lanthanides in all the solutions analyzed. The instrument used calibrations standards spanning a concentration range from 0.1 ng/mL to 1 ug/mL, with routine detectabilities of 0.1 ng/mL. It was used to detect the most abundant naturally occurring isotope for each lanthanide (mass-to-charge ratio equal to mass of most abundant isotope), except for the following masses Nd^{146}, Sm^{147}, Gd^{157}, Dy^{163}, Yb^{172}. The instrument calculated the concentration of lanthanides in each sample, and based on the volume of each sample the absolute mass of the lanthanides was calculated. A background on the ICP-MS and its functions will now be discussed.

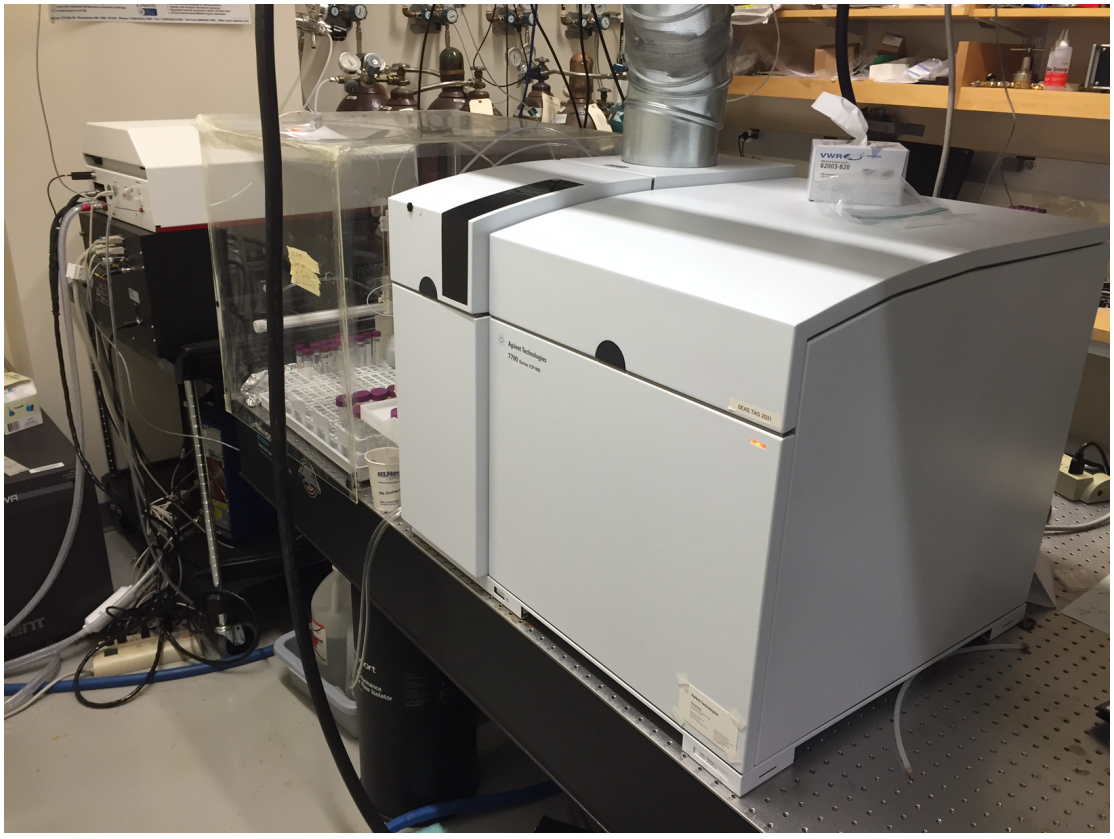

Figure A.2: Photograph of the ICP-MS used in the experimentation

ICP-MS is one of the most sensitive instruments used to detect trace metals and is regularly used to quantify part per trillion concentrations of metals in aqueous solution. An ICP-MS functions by ionizing a sample in a plasma torch prior to introduction into a mass spectrometer. Specifically, a liquid sample is nebulized and sprayed into an argon plasma torch. The torch ionizes the aerosolized sample which is then physically and electromagnetically focused into a mass spectrometer. Prior to nebulization an internal standard is automatically spiked in each sample so that the samples can be compared. The instrument calculates the concentrations of specific trace elements in samples by comparing their mass-to-charge ratio (m/Z) signals to calibration standards of known concentrations of that element. The internal standards correct for differences between the calibration standard and sample matrix solutions (i.e. solutions in which the element is dissolved). A schematic of an ICP-MS is shown in Figure A.3. The ICP-MS can be converted to detect gaseous samples by bypassing the nebulizer and carrying a gas sample directly into the plasma torch. In this instance it is difficult to quantify metal concentrations because calibration standards and internal standards are fundamentally difficult to introduce into the instrument.

An Agilent 7700x ICP-MS with a Cetac ASX-520 autosampler was used for the experimentation. The instrument included a micromist nebulizer, x-lens ion lens, nickel sampling cone, and platinum skimmer cone, but otherwise used standard components included with the instrument. Upon start-up the automated tuning steps were performed. These include: torch axis alignment, electron multiplier detector tune, plasma correction, standard lens tune, axis and resolution adjustments, full spectrum sensitivity tune, and pulse/analog factor setting. Samples were pumped at 50 rpm for 25 seconds and then stabilized at 10 rpm for 55 seconds. Each sample had its elements measured in a 3 peak pattern over 6 replicates with 100 sweeps per replicate. Data analysis was performed using a linear calibration curve, and the origin was offset by the zero concentration blank.

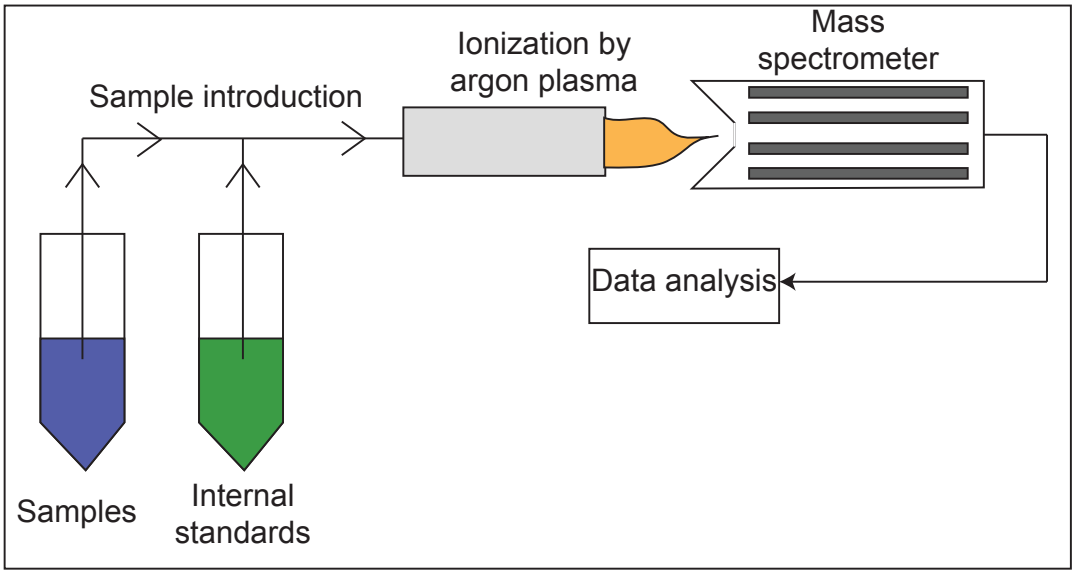

Figure A.3: Schematic of an ICP-MS

B

Supplemental lanthanide desorption data

This appendix includes additional plots to those shown in Chapter 5. This data was not included in Chapter 5 because it is similar to data that was presented there. The plots below show the lanthanide desorption as a function of pH wash by the filtration assay from the following bacteria: *Pseudoalteromonas* sp., *Alcanivorax* sp. EPR7, *Acinetobacter* sp. EPR174, *Sphingomonas* sp., and *Shewanella oneidensis*. The first three strains show similar, broad lanthanide desorption at high pH washes. The last two show preferential light lanthanide desorption at high pH washes and heavy lanthanide des-

orption at low pH washes. The differences seen in these last two plots show the potential of using different bacteria for lanthanide separation.

Figure B.1, Figure B.2, and Figure B.3 show lanthanide desorption from *Pseudoalteromonas* sp., *Alcanivorax* sp. EPR7, and *Acinetobacter* sp. EPR174, respectively. These strains appear to have a single primary binding site with broad pK_a's centered around 5. The *Acinetobacter* sp. EPR174 appears to have an additional binding site with a lower pK_a of approximately 3.

Figure B.4 and Figure B.5 show lanthanide desorption from *Sphingomonas* sp. and *Shewanella oneidensis*, respectively. *Sphingomonas* sp. appears to have five binding sites with pK_a's of approximately 6, 4, 3.5, 3, and 2.5. The latter four binding sites bind the lanthanides as a function of atomic number according to their pK_a's. A similar phenomenon is seen with *Shewanella oneidensis*, which has binding sites with pK_a's if approximately 4.5, 3.5, 3, 2.5, and 2. As before, the lower the pK_a of the site, the greater affinity that site has to preferentially bind the heavier lanthanides.

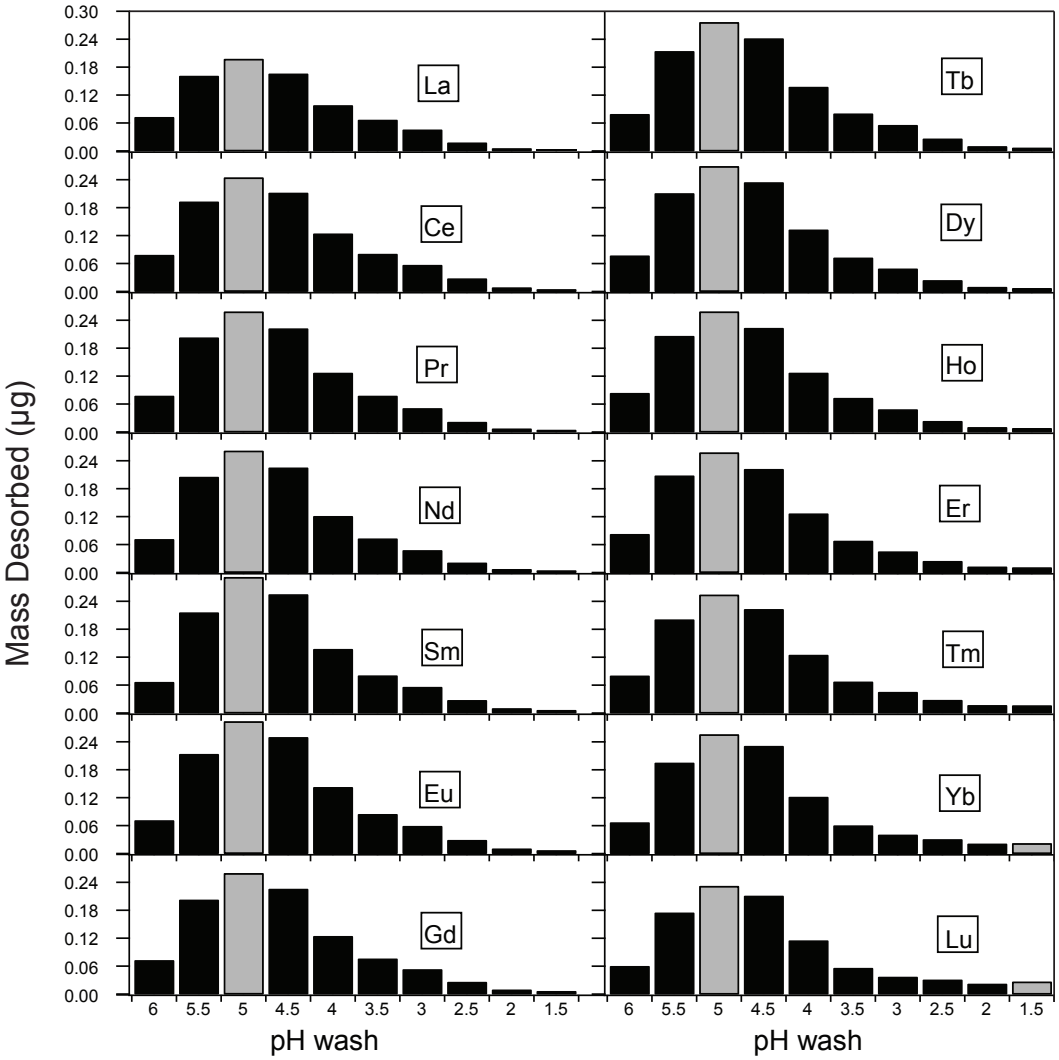

Figure B.1: Lanthanide desorption from *Pseudoalteromonas* sp. using the filtration assay. The lanthanides behave similarly, with most being desorbed with the pH washes around pH 5. The gray bars show local maxima of masses desorbed.

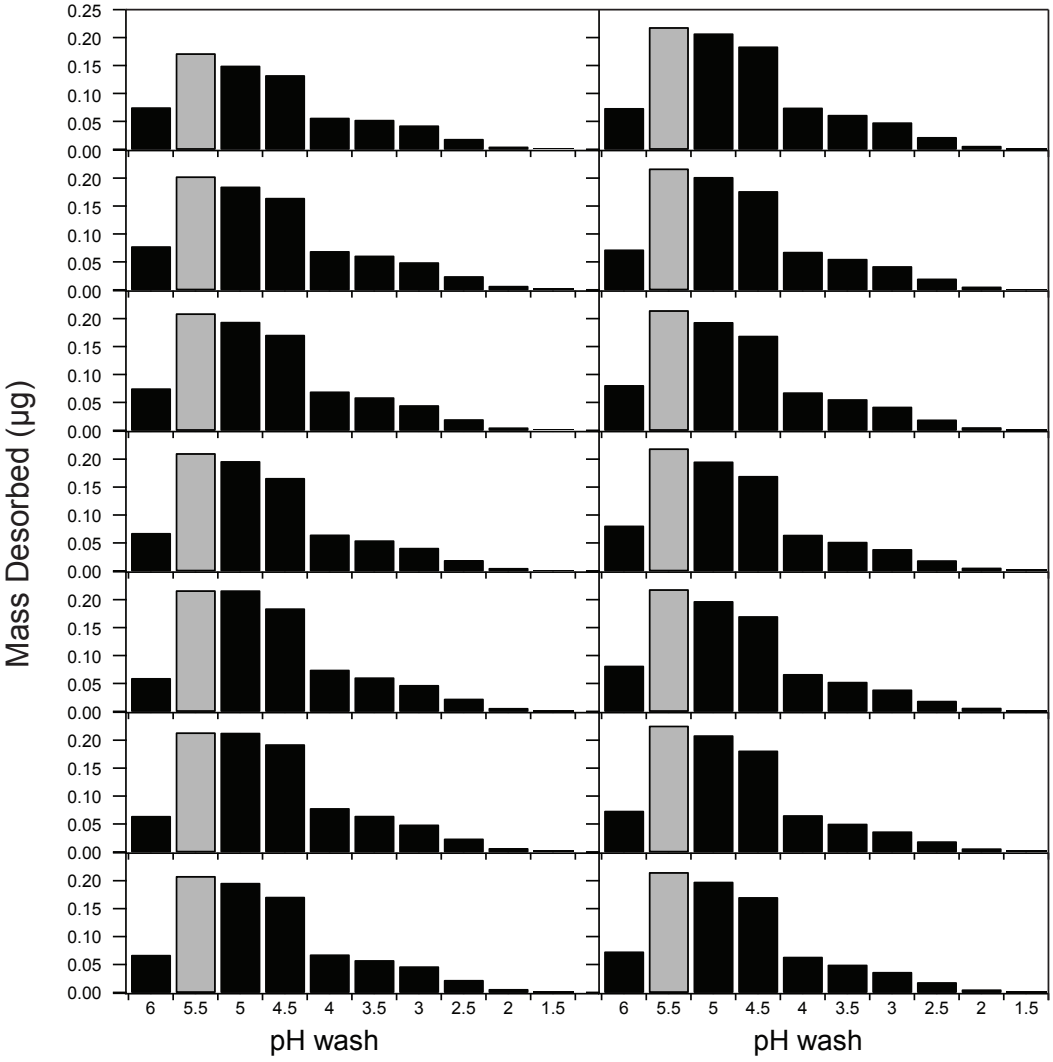

Figure B.2: Lanthanide desorption from *Alcanivorax* sp. EPR7 using the filtration assay. The lanthanides all desorb similarly, with most lanthanides desorbing with the pH 5.5, pH 5, and pH 4.5 washes. The gray bars show local maxima of masses desorbed.

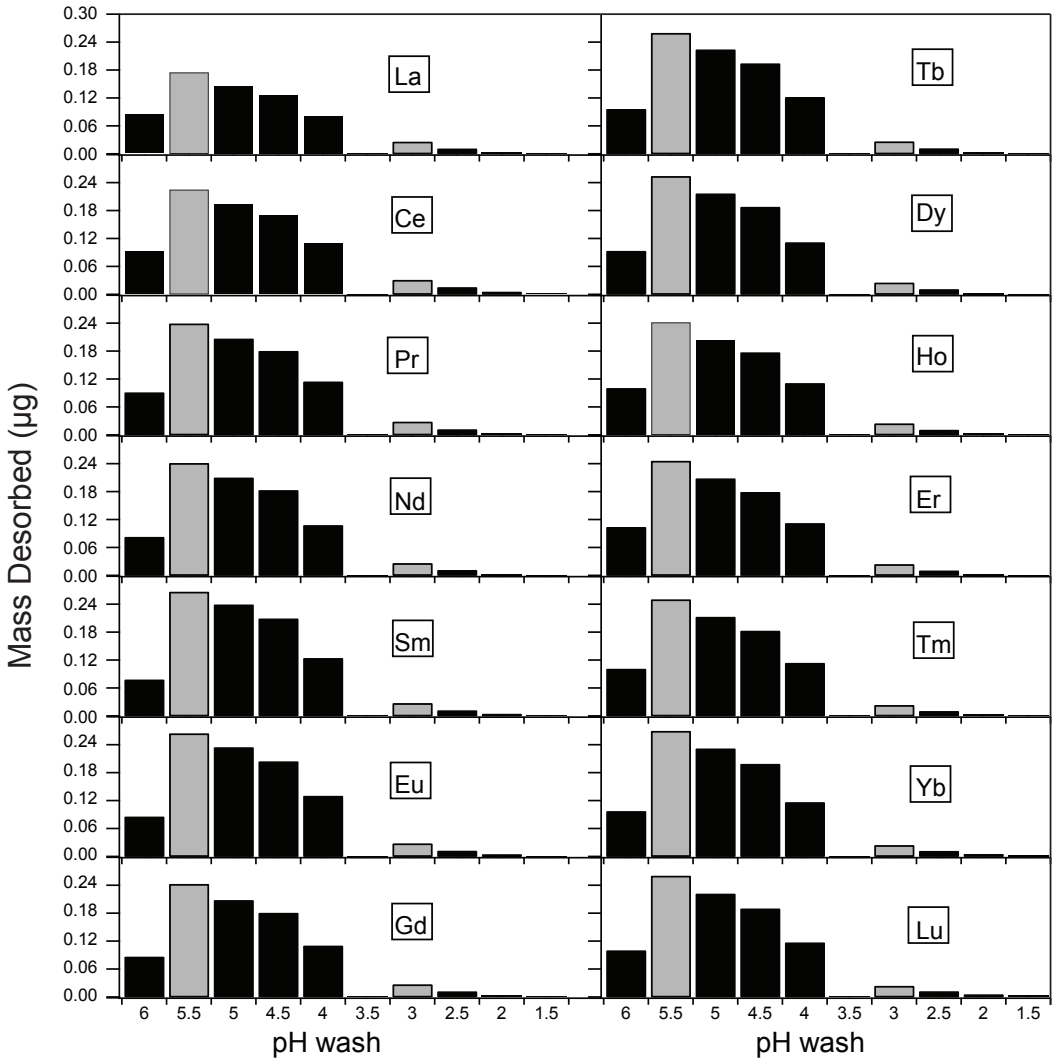

Figure B.3: Lanthanide desorption from *Acinetobacter* sp. EPR174 from the filtration assay. The lanthanides desorb similarly, with most being removed with the pH 5.5 wash. The gray bars show local maxima of masses desorbed.

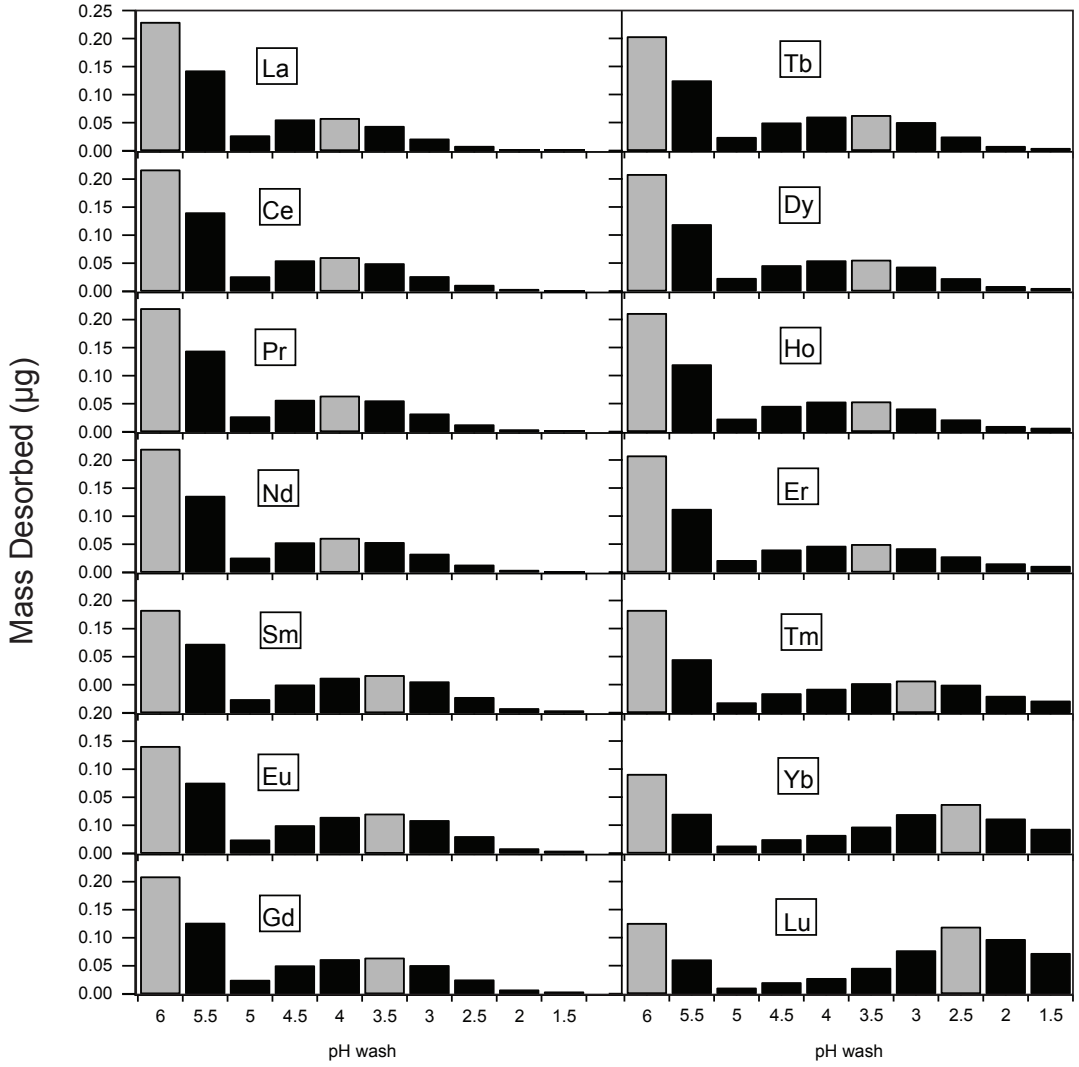

Figure B.4: Lanthanide desorption from *Sphingomonas* sp. using the filtration assay. All of the lanthanides had large masses desorbed from the pH 6 wash. In addition, the heavy lanthanides tended to have larger masses desorb from the lower pH washes than the lighter lanthanides, which had larger masses desorbed from the middle pH washes. The gray bars show local maxima of masses desorbed.

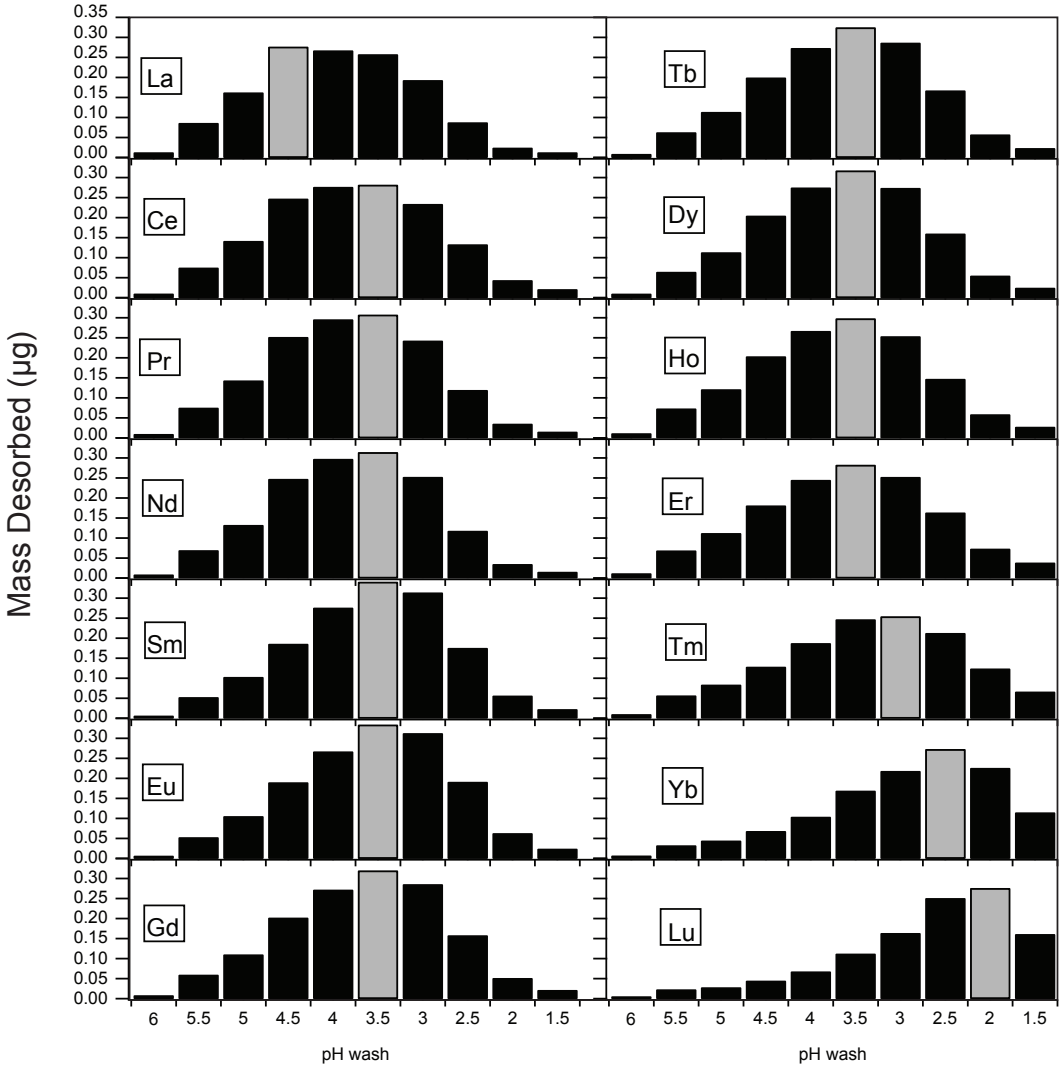

Figure B.5: Lanthanide desorption from *Shewanella oneidensis* using the filtration assay. While each lanthanide desorbed broadly around the middle to low pH washes, the heavy lanthanides had greater total masses desorbed with lower pH washes while the lighter lanthanides had greater total masses desorbed from the middle pH washes. The gray bars, which are local maxima of desorption masses, illustrate this. For example, more Lu mass desorbed with the pH 2 wash than any other wash, while more La mass desorbed with the pH 4.5 wash than any other wash.

C

Flowchart for lanthanide recovery using bacteria

This appendix shows a possible flow chart for a bacterial - based system to recover specific lanthanides. It is included in order to show what a potential recovery scheme might consist of, as well as to help visualize the lanthanide recovery steps performed in Chapter 6.

sectionFlow chart for lanthanide recovery from a mixed solution

The heavy lanthanides can be recovered using the filtration assay and pre-protonated bacteria because biosorbed Yb/Lu will desorb more than any other element during a pH 1.5 nitric acid wash. Therefore, to achieve an enriched Yb/Lu solution from a mixed lanthanide chloride solution, two steps are needed: first, biosorb lanthanides to pre-protonated *Roseobacter* sp. AzwK-3b and second, desorb the lanthanides using a pH 1.5 nitric acid wash. Now enriched with Yb/Lu, this wash is repeatedly biosorbed to new pre-protonated *Roseobacter* sp. AzwK-3b and washed with pH 1.5 nitric acid until it is the desired Yb/Lu purity. After each step the unused solutions that contain lanthanides are collected for future lanthanide recovery. The following flow chart, Figure C.1, illustrates this process.

The process can be adjusted to recover multiple elements from the same lanthanide mixture, such as middle and heavy lanthanide recovery, shown in Figure C.2. While it is complicated, it may actually be simpler than current methods which may need over 750 steps to recover each lanthanide individually[38].

C.1 Methods

The flowcharts described above were carried out in the lab to test their effectiveness in separating the lanthanides. A total of 3 recoveries were performed: two recoveries on pre-protonated bacteria to recover the heavy lanthanides and middle lanthanides, and one recovery on liposomes to recover the heavy lanthanides. The procedural steps were the same as described for the filtration assay in Appendix A, however unnecessary pH washes were eliminated. For the bacterial recoveries only a pH 2.5 pre-protonation followed by a 1.5 wash were used to recover the heavy lanthanides and only a pH 5 pre-protonation followed by a pH 4 wash were used to recover the middle lanthanides. For the liposome recovery only two washes, a pH 2.5 wash followed by a pH 1.5 wash were used. In all tests, each wash was recovered and 100 µL was removed for ICP-MS sampling. After the first set of washes, each of the solutions that were enriched in the targeted lanthanides were brought to a pH of 5 with 0.2 M NaOH. These solutions where then passed through the filtration assay again, flowing over fresh batches of

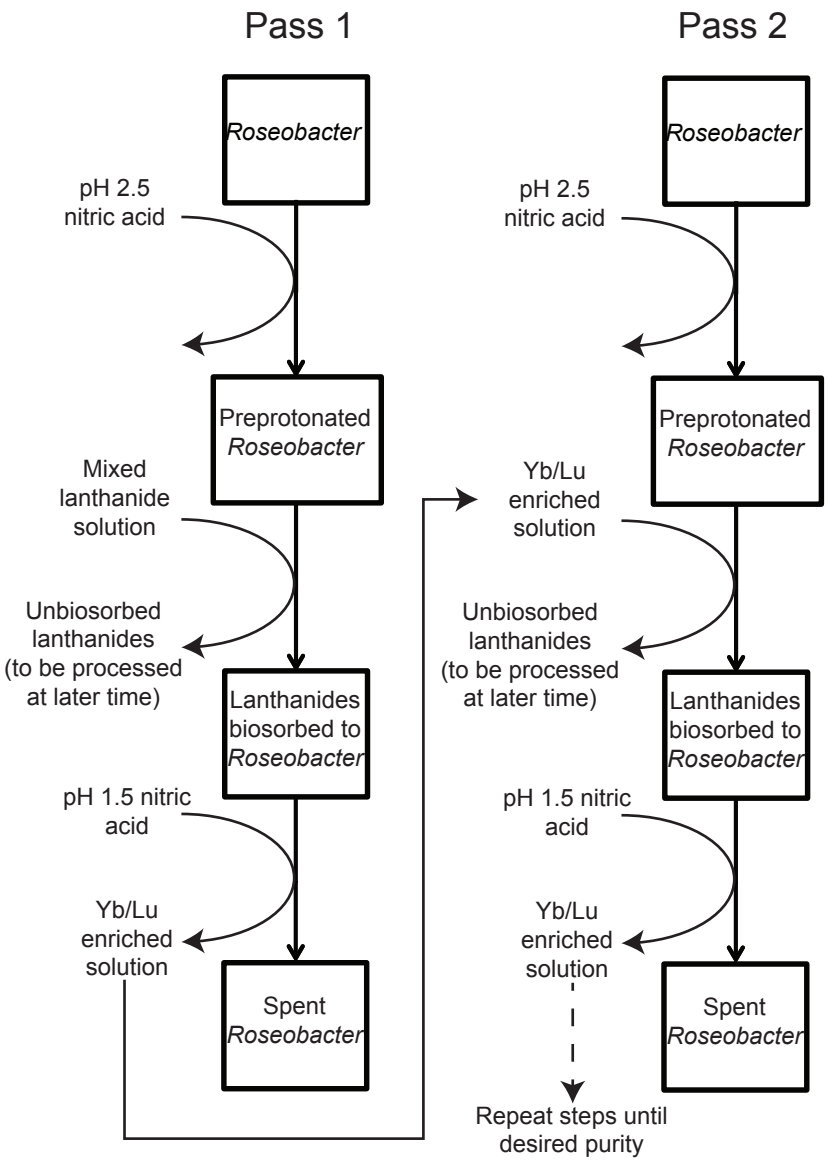

Figure C.1: Flowchart of heavy lanthanide recovery from a mixed lanthanide chloride solution using the filtration assay and *Roseobacter* sp. AzwK-3b. First, the *Roseobacter* sp. AzwK-3b cells are preprotonated by passing a pH 2.5 nitric acid wash past them. Then, the mixed lanthanide solution is passed over the cells to allow for biosorption. After, the cells are washed with a pH 1.5 nitric acid solution; the wash becomes enriched in Yb/Lu. This wash is exposed to new *Roseobacter* sp. cells and the process is repeated, each cycle enriching the solution in Yb/Lu. The unused material from each step is collected to recover the other lanthanides.

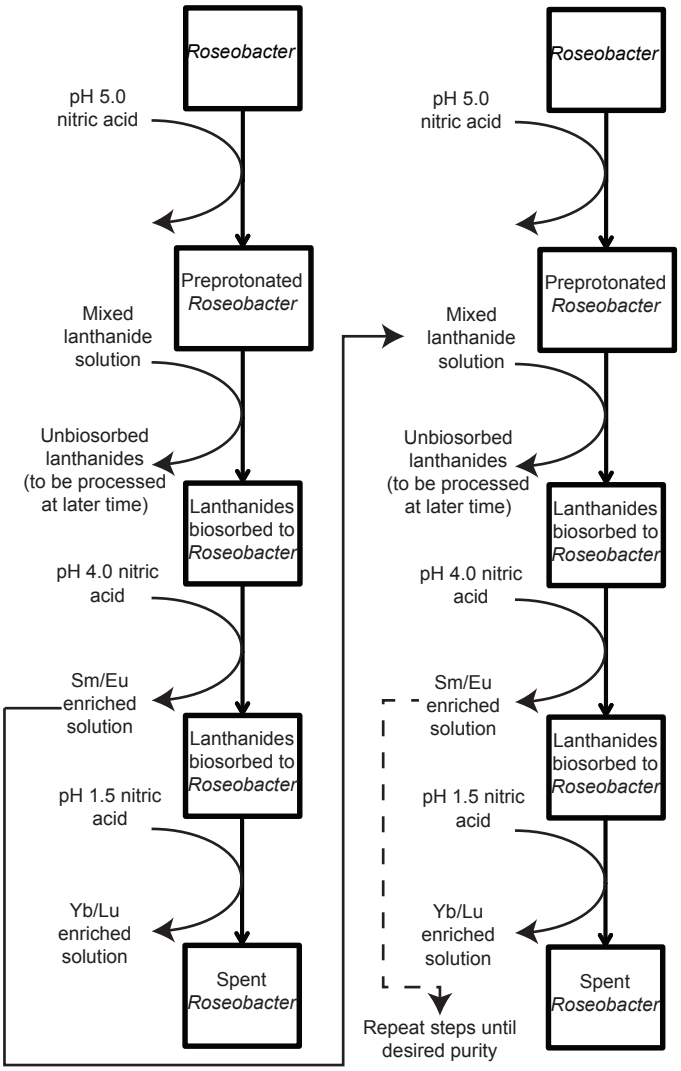

Figure C.2: Flowchart of middle lanthanide and heavy lanthanide recovery from a mixed lanthanide chloride solution using the filtration assay and *Roseobacter* sp. AzwK-3b. First, the *Roseobacter* sp. AzwK-3b cells are pre-protonated by passing a pH 5.0 nitric acid wash past them. Then, the mixed lanthanide solution is passed over the cells to allow for biosorption. After, the cells are washed with a pH 4.0 nitric acid solution; the wash becomes enriched in Sm/Eu. This wash is exposed to new *Roseobacter* sp. cells and the process is repeated, each cycle enriching the solution in Sm/Eu. After recovery of the middle lanthanides the bacteria are still binding the heaviest lanthanides, so they are washed with a pH 1.5 nitric acid wash. This wash solution contains a high amount of Yb/Lu and can be fed into its own recovery circuit. The unused material from each step is collected to recover all the other lanthanides.

pre-protonated bacteria or liposomes. The low pH washes were repeated, and 100 μL of each solution were removed for ICP-MS sampling.

D

Materials and methods for tellurium experiments

This appendix shows the experimental methods used for the tellurium experiments discussed in Chapter 8.

D.1 Media and reagents

The following tellurium sources were used in this study, metallic tellurium (Sigma-Aldrich, St. Louis, USA), potassium tellurite (Sigma-Aldrich, St. Louis, USA), tellurium dioxide (Spectrum Laboratory Products, Inc., New Brunswick, USA), bismuth telluride (Crescent Chemical Co., Inc., Islandia, USA), cadmium telluride (Strem Chemicals, Inc., Newburyport, USA), and copper autoclave slime (obtained from the Freeport-McMoRan Copper and Gold El Paso, TX refinery). The growth media for EPR3 was artificial seawater (ASW) which was sterilized by autoclaving at 121°C for 15 min.[50] For solid culture, ASW was solidified using 1.5% (wt/vol) agar and added to 10 cm diameter by 1.5 cm high plates. EPR3 was donated by C. Vetriani who isolated it from hydrothermal vent fluid in the East Pacific Rise[50]. (Figure D.1)

D.2 Approximation of tellurite's inhibitory concentration

The approximate minimum inhibitory concentration (MIC) of tellurite was determined by aerobically growing EPR3 in autoclaved ASW containing varying concentrations of tellurite and observing the maximum tellurite concentration at which cell growth occurred. A wide range of tellurite solutions (8 nM - 0.8mM) were tested initially to determine the approximate inhibitory concentration. A stock solution of ASW containing 0.8 mM tellurite was prepared by dissolving potassium tellurite in ASW. Five additional tellurite solutions were prepared from the 0.8 mM stock by performing 10-fold serial dilutions in ASW down to 8 nM. Each sample was inoculated with EPR3 (1:100 dilution of fully grown culture, OD 600nm = 0.7) and the liquid cultures were incubated at 37°C for 3 days with shaking at 160 rpm. Growth was evaluated based on UV-vis absorption at a wavelength of 600 nm. From this preliminary experiment, it was determined that the MIC of tellurite was between 80 μM and 0.8 mM. Additional tellurite-ASW solutions at concentrations within this range (0.8 mM, 0.5 mM, 0.3 mM, and 0.1 mM) were prepared by dissolving potassium tellurite in ASW. EPR3 was

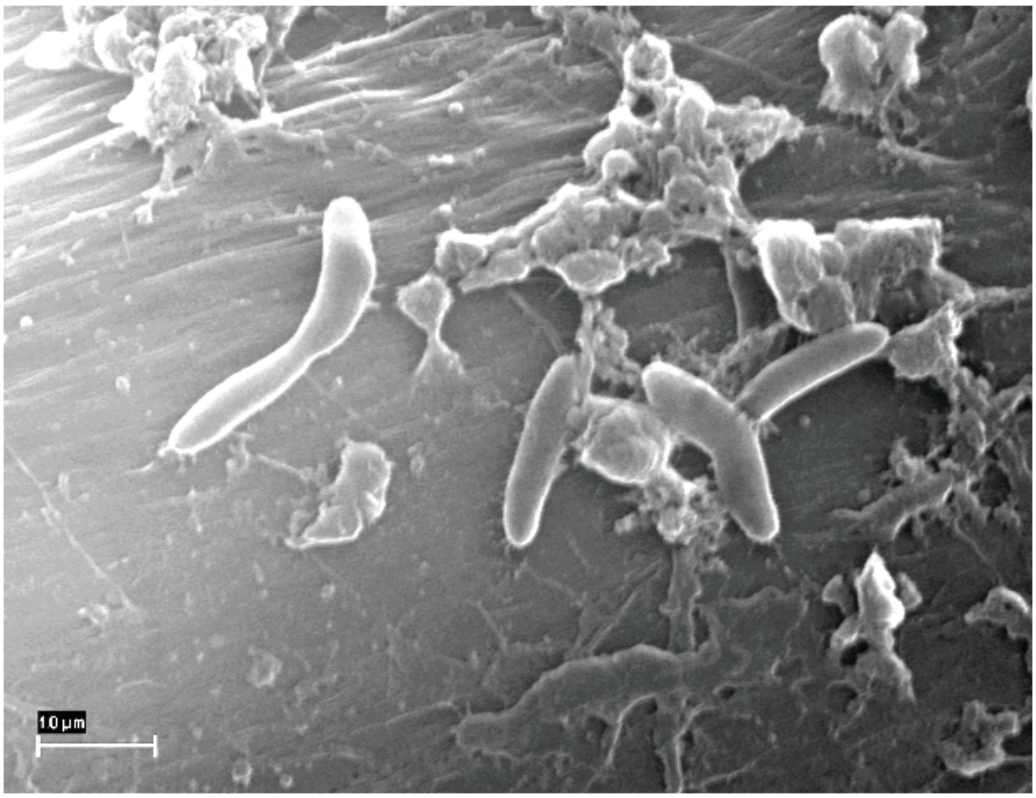

Figure D.1: SEM micrograph of *pseudoalteromonas* sp. EPR3

inoculated (1:100 dilution of fully grown culture, OD 600nm = 0.7) into each capped test tube liquid sample and incubated at 37°C for 72 h with continued shaking. Cell growth was observed visually by sample turbidity and a darkening of cells resulting from metallic tellurium precipitation. Sterile tellurite-ASW controls were also prepared at the same tellurite concentrations and did not show any turbidity throughout the length of the experiment. The MIC was determined to be 0.3 mM, and the chosen concentration of tellurite for subsequent experiments was 0.1 mM, which was slightly less than the MIC.

D.3 Growth curves with tellurite

Growth curves were produced for EPR3 incubated in a variety of tellurite concentrations. This experiment was performed in a 48-well plate in order to screen multiple concentrations. ASW containing 0.8 mM tellurite was added to the first row of the plate and then diluted in the remaining rows by performing 10-fold serial dilutions in sterile ASW. Each well was then inoculated with 10 μL of a fully grown culture of EPR3 (1:100 dilution of fully grown culture, OD 600nm = 0.7). Two additional control wells were filled with sterile ASW without tellurite. One was inoculated with EPR3 and the other was left sterile. The plate was incubated at 37 μC with continued shaking. Growth was monitored at 30 min intervals over the course of 1 day by measuring the absorbance of each sample at a wavelength of 600 nm. The entire process was automated using a pre-programmed robotic arm to manipulate the plates and measure absorbance.

D.4 Assay of dissolved tellurium concentration with time

EPR3's ability to transform tellurite was demonstrated by incubating EPR3 with a known concentration of tellurite in liquid ASW and measuring the decrease in the soluble tellurium concentration over time. Potassium tellurite was added to four 15 mL conical tubes each containing 5 g of sterile liquid

ASW to achieve a final concentration 0.09 mM tellurite. Three samples were inoculated with EPR3 (1:100 dilution) and the fourth was included as an untreated sterile control. All of the samples were capped and incubated aerobically at 37°C with continued shaking at 70 rpm. Approximately every 24 h for 4 days after inoculation, the samples were centrifuged (9000 g, 25°C) to separate any cells and solid tellurium from the supernatant ASW of the liquid culture. 50 µL of the supernatant from each sample was pipetted, weighed, and combined with 5 g of 2% trace metal free nitric acid in preparation for ICP-MS analysis.

D.5 Tellurium precipitation and volatilization assay on solid media

Precipitation and volatilization of tellurite, metallic tellurium, tellurium dioxide, autoclave slime, cadmium telluride, and bismuth telluride on solid ASW was determined by growing EPR3 on plates with powders of these compounds sprinkled near the center, then measuring gaseous tellurium and metallic tellurium production by ICP-MS and confocal Raman spectroscopy, respectively. A 0.1 mM tellurite agar plate was prepared by first dissolving potassium tellurite in sterile liquid ASW, and then solidifying the plate with agar and inoculating with EPR3. For the other, insoluble, tellurium compounds, 0.5 g of metallic tellurium, tellurium dioxide, and bismuth telluride, and 0.1 g of copper autoclave slime and cadmium telluride, were added to the center of ASW plates that had been inoculated with 100 µl of a fully grown culture of EPR3 (OD_{600nm} = 0.7). Identical plates, containing the tellurium compounds, but absent of EPR3, were made as controls. The control plates remained completely unchanged through the course of our experiments and no movement of the tellurium sources was noted. Photographs were taken of each plate before and after 48 h of incubation at 37 °C. The tellurite plate was aged an additional 120 h before a final photograph was taken. Adobe Photoshop CS3 software was used to match the brightness, contrast, and saturation of photos between aged and unaged plates. The matching was applied equally to all parts of the images. On the plates with cells, areas of cell growth

that blackened indicative of tellurium precipitation were cut with a razor blade from the agar and extracted for analysis. Confocal Raman spectroscopy (LabRAM Aramis Horiba Jobin YVON, 532 nm laser) was performed on these samples, the controls, and reference samples of the pure tellurium compounds. In this method, a region of interest was identified in the confocal optical image. Then, the microscope laser beam was focused onto a feature and the Raman spectrum recorded, typically using a micron diameter beam. Raman was chosen because of its ability to unambiguously distinguish the presence of metallic tellurium. Metallic tellurium exhibits very distinctive major Raman peaks at 120.4 $\pm$ 0.5 cm^{-1} and 140.7 $\pm$ 0.5 cm^{-1} [141], while tellurium dioxide is characterized by major Raman peaks at 121 cm^{-1}, 152 cm^{-1}, 174cm^{-1}, and 199 cm^{-1} [142]. None of the other controls, including the tellurite dissolved in ASW, exhibited any Raman signal between 100 cm^{-1} and 200 cm^{-1}. The Raman spectra of metallic tellurium, tellurium dioxide, and 0.1 mM tellurite in ASW agar are shown in Figure D.2.

The sensitivity of the Raman measurements was not quantified because it is a function of many variables which are difficult to control, especially those associated with light scattering, such as surface roughness and crystallographic orientation. Nevertheless, Raman spectra with good signal to noise were obtainable, and in each case the identification was unambiguous. A background on Raman spectroscopy and its function is discussed in the final section of this appendix.

The gaseous tellurium species was detected by loading the cut and extracted agar samples with bacterial tellurium precipitation into the gas sampling chamber of an ICP-MS (Agilent Technologies 7700x). In this configuration, the head space above the samples is carried to the ICP-MS and sampled for tellurium to determine the existence of gaseous tellurium, likely to include dimethyl telluride based on previous studies, along with other volatile tellurium compounds that are known to form.[127,143,128,124] A mass-to-charge ratio of 125 was used to detect tellurium (Te^{125}). The tellurium response from EPR3 with the various tellurium compounds was compared to controls of the tellurium sources on sterile ASW plates. The limit of detection for the ICP-MS system (10^{-12} g of tellurium) was approximately 100 to 1000 times smaller than the values in volatilized tellurium samples.

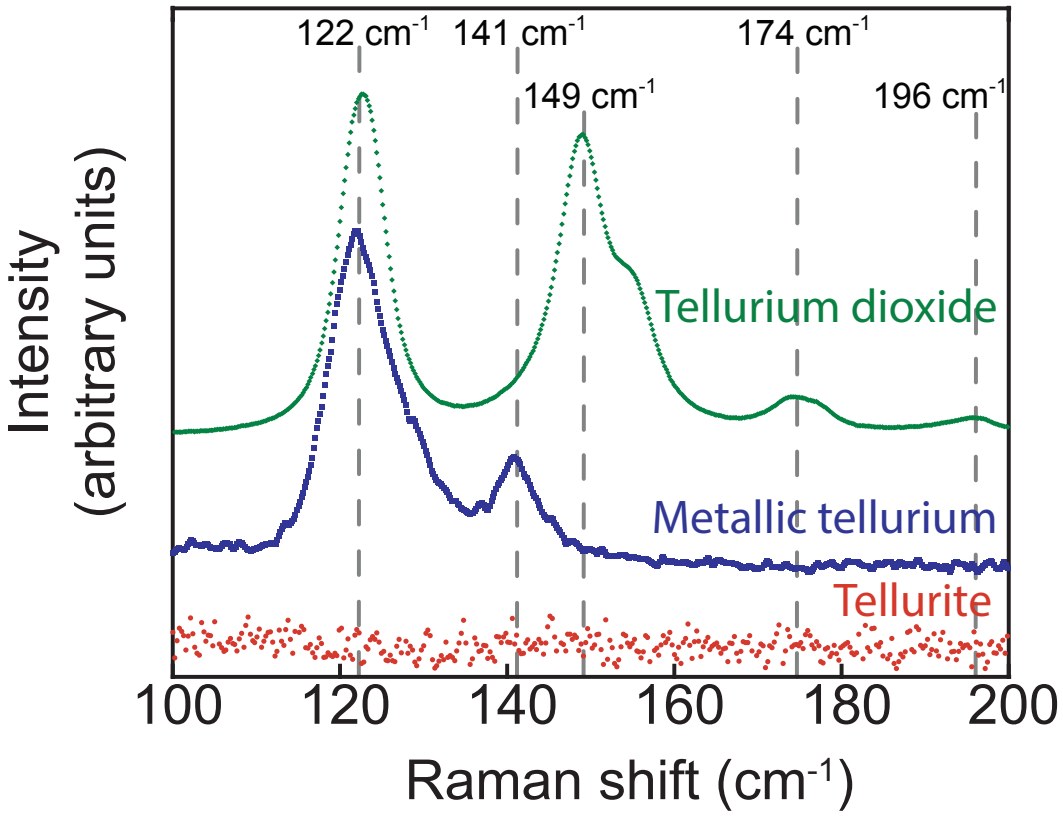

Figure D.2: Raman spectra of standards of metallic tellurium, tellurium dioxide, and tellurite. Used with permission [134].

D.6 Dissolved tellurium compound concentration assay

The solubility of each tellurium compound in ASW at 37°C was calculated by adding each compound to a known mass of sterile liquid ASW, and using ICP-MS to analyze the concentration of dissolved tellurium. Approximately 0.1 g of metallic tellurium, tellurium dioxide, autoclave slime, cadmium telluride, and bismuth telluride were added to 15 mL conical tubes containing 5 g of sterile liquid ASW. All samples, including a sterile ASW control, were capped and incubated at 37°C for 48 h with continued shaking. Next, the samples were centrifuged (9000 g, 25°C) to isolate the media with dissolved tellurium from the solid tellurium compounds. A known mass of the supernatant ASW was removed and diluted with a known mass of 2% trace metal free nitric acid to prepare for ICP-MS analysis. The ASW control contained no detectable concentration of tellurium.

D.7 Tellurium precipitation assay in liquid media

Precipitation of tellurium from tellurite, metallic tellurium, and tellurium dioxide in liquid ASW was observed by inoculating ASW containing these tellurium compounds with EPR3 and taking photographs and measuring visible light absorption. Approximately 0.1 g of metallic tellurium and tellurium dioxide, and 0.1 mM tellurite were added to capped tubes of sterile ASW, with 3 replicates of each. These samples, including a sample of tellurium-free ASW, were inoculated with EPR3 (1:100 dilution of fully grown culture). Then, along with a sterile ASW control, the samples were aerobically incubated at 37°C with continued shaking. At various time points, indicated in the results section, the samples were removed for photographic recording and UV-vis absorption spectrophotometry (Thermo Scientific Helios Omega) measurements. In preparation for the spectrophotometry, 500µL of each sample was removed and added to a plastic cuvette. After measuring the optical absorption, the solution was added back into the samples. Care was taken to avoid any biological contamination during these transfers. The sterile ASW control was taken as the baseline absorbance before each ab-

sorbance measurement. The absorbance was measured between 450 - 800 nm and integrated over this range for comparison between samples over time.

D.8 Liquid ICP-MS analysis assay

Liquid ICP-MS analysis was used to detect the concentration of nominal dissolved tellurium in liquid samples with high sensitivity (parts per trillion concentrations). A range of tellurium concentrations (blank - 1 ppm) were used as ICP-MS calibration standards, and indium and bismuth were used as ICP-MS internal standards. A mass-to-charge ratio of 125 was used to detect dissolved tellurium concentrations, which had a limit of detection of $\sim$20 nM (calculated based on blank samples that were included in each run compared to calculated tellurium concentrations in standards). The dissolved tellurium concentrations of ASW samples were calculated based on the concentration results from ICP-MS analysis and the known masses of ASW and 2% trace metal free nitric acid in each sample. When measuring the concentration of tellurium from incubated bismuth telluride, the internal standard consisted only of indium, and did not include bismuth.

D.9 Raman spectroscopy

The determination of material phases was performed using a Horiba Jobin Yvon Labram Aramis Raman spectrometer with a 532 nm laser was used throughout this dissertation. Raman functions by focusing a laser beam of known wavelength onto a material's surface. The surface reflects the majority of the beam at the same wavelength as the incident beam, but a small amount is slightly shifted to either higher or lower energies. The shift in energy is derived from the absorption of vibrational energy modes, and is known as the Raman shift. The Raman shift can be categorized into two types: Stokes scattering and anti-Stokes scattering. Stokes scattering occurs when electrons that are excited from the ground state energy level fall back to a vibrational energy level higher than that of the ground state.

The reflected light then has less energy than the incident light. Anti-Stokes scattering occurs when an electron is excited from a vibrational energy level, and then falls back into the ground energy level. In this case the reflected light is higher in energy than the incident light. These small Raman shifts in energy provide information about vibrational modes in the material, which can in turn provide knowledge of many properties, including crystal structure. There is no database that describes the Raman shift of materials, like exists for x-ray diffraction, so standards of known material and phases are often used to identify samples.

E

Recovery of lanthanides from devices

In Chapter 2 the importance of Nd magnets and Terfenol-d was discussed, along with the supply risk for the lanthanides used to produce these magnets. Unfortunately, minimal efforts have been made to recycle these devices, which could mitigate some of these risks. In Chapter 6 lanthanide biosorption and desorption were demonstrated to have utility in separating the lanthanides. In the following, NdFeB magnets and Terfenol-d ($Tb_{0.3}Dy_{0.7}Fe_{1.92}$) were put through the filtration assay in an attempt to recycle these lanthanides from their devices. Both magnets were first dissolved in 37% hydrochloric

acid, then neautralized to pH 5.0, and then put through the filtration assay, which used liposome adsorbants. Based on preliminary experimentation the following washes, pH 2 wash, pH 1.5 wash, 70% nitric acid wash, were sequentially passed over the liposomes across the filter, and the concentration of lanthanides and iron in each wash was measured.

E.1 Methods

1 mL of dissolved and pH neutralized magnetic material solution (approximately 2.0 μg/mL Tb and 4.6 μg/mL Dy for Terfenol-d, and 2 μg/mL Nd for the NdFeB magnet) was passed over 2 mg of liposomes (average of 700 μm diameter) in the filtration assay as previously described in Appendix A. Then, the following were passed over the liposomes: 5mL of water, 5mL of pH 2 nitric acid, 5 mL of water, 5 mL of pH 1.5 nitric acid, 5 mL of water, 1 mL of 70% nitric acid, 15 mL of water. Because the filter itself holds approximately 0.5 mL of water, much of the mass of lanthanides that desorbs from the 1 mL of 70% nitric acid will be removed with the following 15 mL water wash. Every wash was collected and sampled for metal concentration using ICP-MS. In each case we measured lanthanide content and iron content, but in the NdFeB no boron was measured.

E.2 Recycling of iron from NdFeB and Terfenol D

The results of these filtrations are shown in Figure E.1 and Figure E.2. The lanthanides predominantly desorbed during the pH 2 wash with 36% of the praseodymium, 37% of neodymium, 66% of the terbium, and 65% of the dysprosium separating from the liposomes during that wash. The iron is almost completely desorbed during the 70% nitric acid wash and its ensuing water wash, with 96% of the iron from the neodymium magnet and nearly 100% of the iron from the Terfenol-d being removed. The 70% nitric acid wash is very harsh, and so it likely breaking down the liposomes. It isn't clear then, if the iron was bound to the liposome surfaces before the nitric acid wash, or if the iron had actually

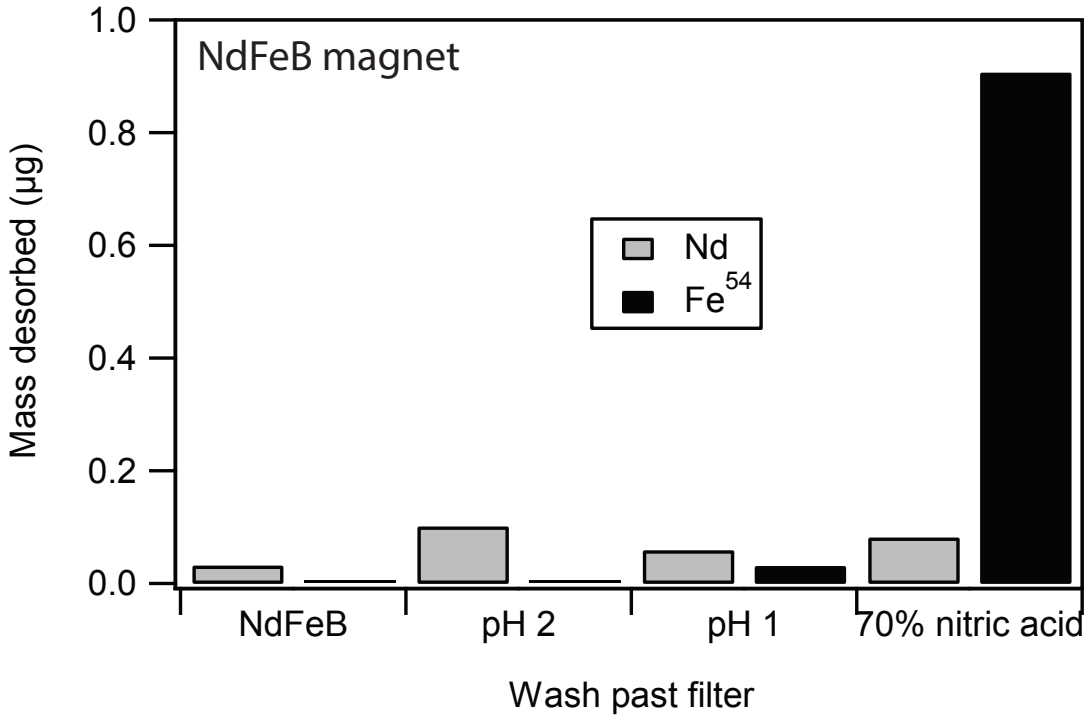

Figure E.1: Iron separation from an Nd magnet. First the magnet was put into solution and then passed through the filtration assay with liposomes. The bar graphs show the desorption of Nd and Fe^{54} as a function of pH washes. Each chart shows the mass desorbed as a function of pH wash for the different relevant elements. The Nd is primarily desorbed by the pH 2 wash, while the Fe^{54} is almost entirely removed by the 70% nitric acid wash.

made its way into the liposomes and was only released after the liposomes were broken down by the nitric acid. It is apparent, visually, that the liposomes do change their structure in the presence of 70% nitric acid (Figure E.3), so either of these scenarios is plausible. Investigating this will be the subject of future work.

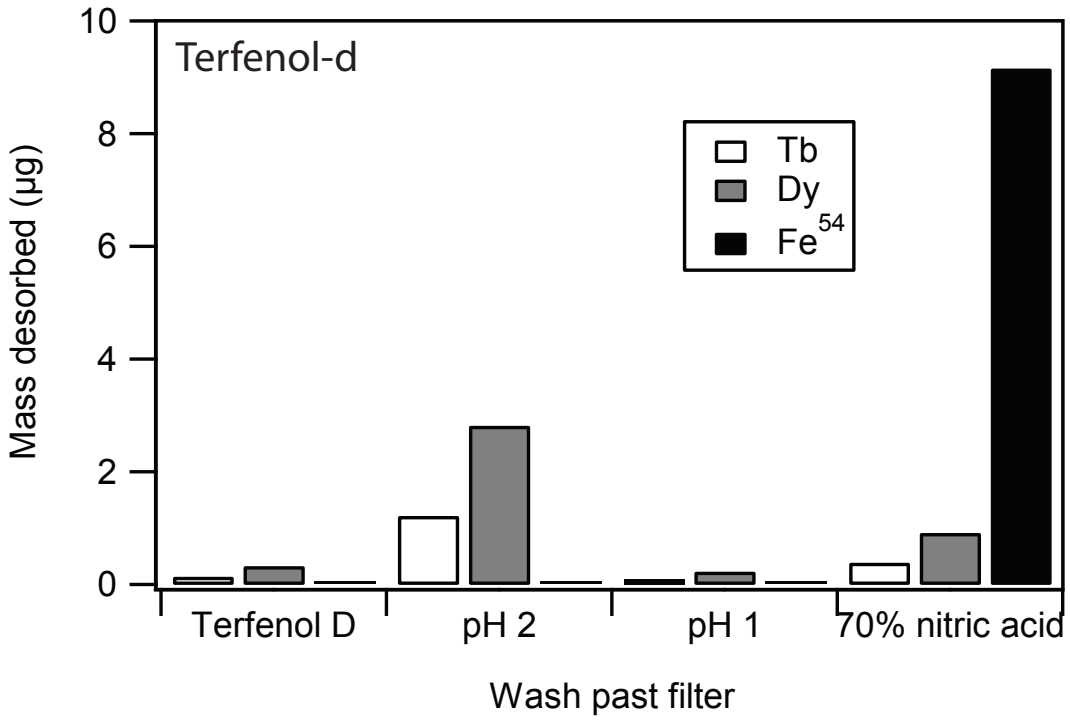

Figure E.2: Separation of Fe^{54} from Tb and Dy using the filtration assay and liposomes. Terfenol D was solubilized and passed through the filtration assay along with pH 2, pH 1, and 70% nitric acid washes. The Tb and Dy are primarily eluted with the pH 2 wash while almost no Fe^{54} is removed until the 70% nitric acid wash. The assay may be helpful in the recycling of Tb, Dy, and Fe from Terfenol-d.

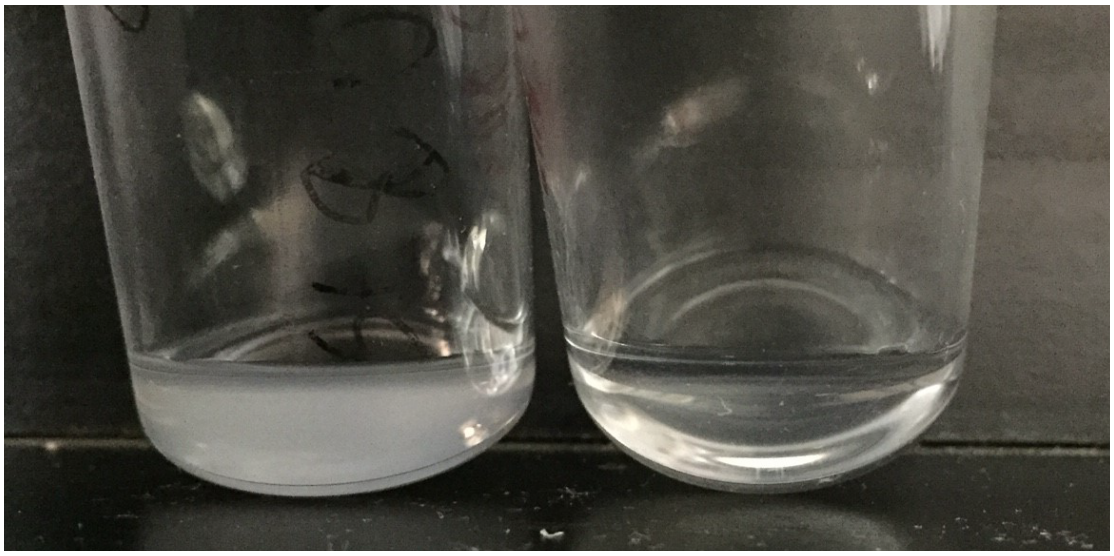

Figure E.3: Photographs of liposomes at pH neutral water (right side) and in 70% nitric acid (left side). After exposure to 70% nitric acid the liposomes precipitated out of the solution and made it appeared cloudy.

F

Tellurium and lanthanide supply risk case studies

In this appendix two case studies are described that illustrate the real-world consequences of tellurium and lanthanide supply risk. The first shows how tellurium availability may limit CdTe photovoltaic production. The second shows how Nd based magnet scarcity may influence wind turbine production, and how Nd production in the United States could make a meaningful impact on its availability.

F.1 Tellurium demand case study

As discussed in Chapter 2, tellurium is a critical material for future energy technologies that is also scarce. This scarcity could hinder the bourgeoning PV industry if it continues to be produced at current levels. In 2011, the world's largest CdTe PV manufacturer, First Solar, used ~115 tonnes of tellurium to produce PV modules capable of prodocing 2 GW of power[144,145], consuming half of tellurium's 300 tonnes produced world-wide, although estimates vary[30,146,34,31]. According to data from 2012, First Solar planned to have a production capacity of 2.9 GW per year by the end of that year, and planned to produce at full capacity[144]. If we assume an average solar irradiance of 1000 W/m^2 and 17% efficiency we determine a power density of 170 W/m^2. This results in an estimate of 17 km^2 of solar cells being produced that year. If CdTe is laid down at 3 μm thick then 50 m^3 of CdTe is needed. With a density of 5.85 g/cm^3, and a little more than half of that being tellurium, 150 metric tonnes of tellurium were needed to produce this quantity of solar cells, however global estimates of tellurium production were around 300 tonnes[30,146,34,31]. It seems impossible for First Solar to satisfy their demand unless new tellurium recovery methods are developed to recover it from wasted sources, such as the 70% lost during copper refining[36,37], or recycle it from devices, such as used solar cells.

As a result, many reports have been published regarding tellurium's scarcity and its impact on the CdTe PV market[30,147,145,148,149]. Given that the raw material cost of tellurium accounts for nearly 10% of the total cost of a CdTe module, low tellurium production and increasing price will consequently hinder solar cell implementation. Projections show that recycling tellurium could largely eliminate issues with scarcity[150], but there is a lack of research in CdTe recycling and the suggested methods are expensive and rely on the use of harsh chemicals such as concentrated sulfuric acid[151,152,153].

F.2 Neodymium demand case study

As discussed in Chapter 2, the rapidly changing energy landscape is creating a greater-than-ever demand for the neodymium in permanent magnets to power wind turbines and hybrid/electric cars. The U.S. Department of Energy reports that the production of this element is critical to the United States' energy goals and that current production may be inadequate in matching future device needs[19]. The following analysis shows that shifting neodymium production to the mine where it is extracted in the United States could improve energy security.

About 1 kg of neodymium is used in each electric car, and about 500kg of neodymium is needed per MW in a wind turbine[154]. In 2012 13,000MW of wind turbines were installed in the United States, amounting to 6,500 metric tonnes of neodymium[155]. In the same year 400,000 hybrid electric vehicles were sold in the Unites States, amounting to 400 metric tonnes of neodymium used[156]. In that year there were exportation quotas placed on the lanthanides by China limiting the rest of the world's usage to 31,000 metric tonnes of all the rare earths[157]. The United States' use of neodymium alone accounts for more than 20% of this quota, and this does not account for other countries or other lanthanides. Fortunately, the exportation quotas on rare earths were just recently halted in January 2015. Otherwise current installation rates of wind turbines and production of electric vehicles may have needed to be slowed.

This supply risk could have been potentially relieved by the Mountain Pass lanthanide mine in the United States. This mine produced 4,000 metric tonnes of rare earths in 2013 (primarily lanthanum and cerium), however due to uneconomical separations only lanthanum and cerium are individually recovered, as well as a praseodymium/neodymium compound, and the rest of sent to be separated elsewhere. According to an elemental analysis of the mountain pass ore (Figure F.1) neodymium makes up around 11% of the ore. If this neodymium could be easily separated that would be an additional 440 metric tonnes produced, enough to produce a significant portion of the electric vehicles purchased in

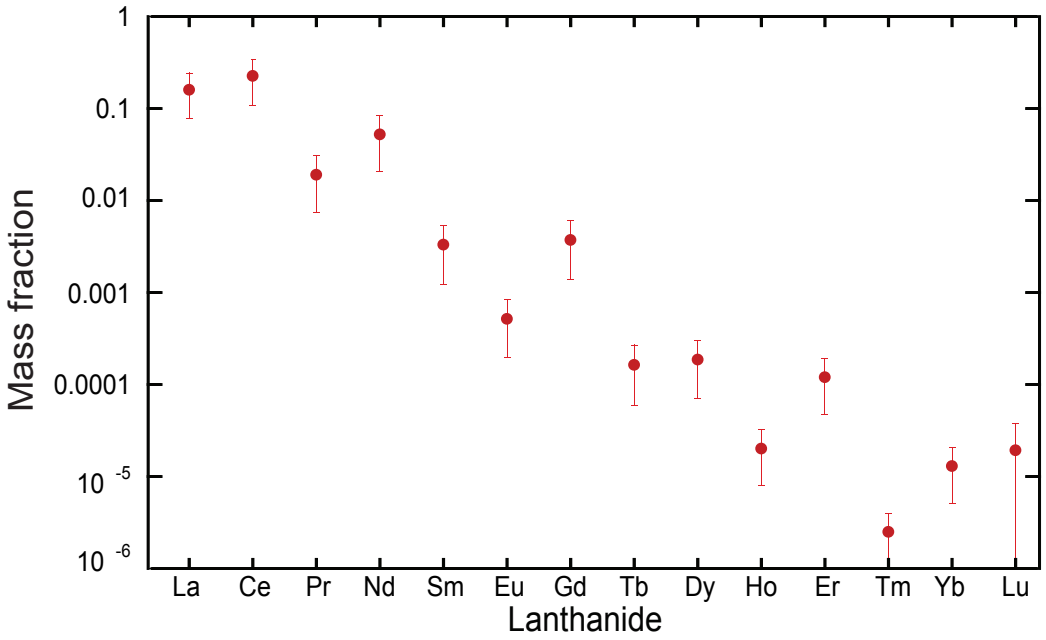

Figure F.1: Mass fraction of lanthanides in Bastnaesite concentrate from the Mountain Pass lanthanide mine as determined by ICP-MS.

the United States in 2013.

References

[1] Michael D. Gerst and T. E. Graedel. In-Use Stocks of Metals: Status and Implications. *Environmental Science & Technology*, 42(19):7038–7045, October 2008.

[2] Robert R. Crichton and Mireille Charloteaux-Wauters. Iron transport and storage. *European Journal of Biochemistry*, 164(3):485–506, May 1987.

[3] Domy C. Adriano. *Trace Elements in Terrestrial Environments: Biogeochemistry, Bioavailability, and Risks of Metals*. Springer, New York, 2001.

[4] F M M Morel and N M Price. The biogeochemical cycles of trace metals in the oceans. *Science*, 300(5621):944–7, May 2003.

[5] R.P. Mason, W.F. Fitzgerald, and F.M.M. Morel. The biogeochemical cycling of elemental mercury: Anthropogenic influences. *Geochimica et Cosmochimica Acta*, 58(15):3191–3198, August 1994.

[6] G J Olson, J A Brierley, and C L Brierley. Bioleaching review part B: progress in bioleaching: applications of microbial processes by the minerals industries. *Applied microbiology and biotechnology*, 63(3):249–257, December 2003.

[7] Bohumil Volesky. Removal and recovery of heavy metals by biosorption. In Bohumil Volesky, editor, *Biosorption of heavy metals*, chapter 1.2, pages 7–43. CRC Press, Boca Raton, 1990.

[8] T Rohwerder, T Gehrke, K Kinzler, and W Sand. Bioleaching review part A: progress in bioleaching: fundamentals and mechanisms of bacterial metal sulfide oxidation. *Applied microbiology and biotechnology*, 63(3):239–248, December 2003.

[9] Klaus Bosecker. Bioleaching: metal solubilization by microorganisms. *FEMS Microbiology Reviews*, 20(3-4):591–604, January 2006.

[10] Mark Brininstool. Copper commodities summary. Technical report, United State Geological Survey, 2014.

[11] Derek R. Lovley and John D. Coates. Bioremediation of metal contamination. *Current Opinion in Biotechnology*, 8(3):285–289, 1997.

[12] Bohumil Volesky. Detoxification of metal-bearing effluents: biosorption for the next century. *Hydrometallurgy*, 59(2-3):203–216, February 2001.

[13] Christopher White, Simon C. Wilkinson, and Geoffrey M. Gadd. The role of microorganisms in biosorption of toxic metals and radionuclides. *International Biodeterioration & Biodegradation*, 35(1-3):17–40, January 1995.

[14] I Wagner-Döbler. Pilot plant for bioremediation of mercury-containing industrial wastewater. *Applied microbiology and biotechnology*, 62(2-3):124–33, August 2003.

[15] Gordon B. Haxel, James B. Hedrick, and Greta J. Orris. Rare earth elements - critical resources for high technology. Technical report, U.S. Geological Survey, Washington, D.C., 2002.

[16] U.S. Department of Justice and Federal Trade Commission. Horizontal merger guidelines, 2010.

[17] T.E. Graedel. On the future availability of the energy metals. *Annual Review of Materials Research*, 41(1):323–335, August 2011.

[18] Michael W. Gaultois, Taylor D. Sparks, Christopher K. H. Borg, Ram Seshadri, William D. Bonificio, and David R. Clarke. Data-Driven Review of Thermoelectric Materials: Performance and Resource Considerations. *Chemistry of Materials*, 25(15):2911–2920, 2013.

[19] Diana Bauer, David Diamond, Jennifer Li, Michael McKittrick, David Sandalow, and Paul Telleen. *U.S. Department of Energy critical materials strategy*. U.S. Department of Energy, December 2011.

[20] Mary Elvira Weeks. The discovery of the elements. VI. Tellurium and selenium. *Journal of Chemical Education*, 9(3):474, March 1932.

[21] Robert D Brown. Tellurium. In Patricia A Plunkert and Thomas S Jones, editors, *Metal prices in the United States through 1998*, pages 147–149. United States Government Printing Office, Washington, D.C., 1999.

[22] Bolko von Roedern and Harin S. Ullal. The role of polycrystalline thin-film PV technologies in competitive PV module markets. In *2008 33rd IEEE Photovolatic Specialists Conference*, pages 1–4, San Diego, CA, May 2008. National Renewable Energy Laboratory, IEEE.

[23] G. Homm and P. J. Klar. Thermoelectric materials-compromising between high efficiency and materials abundance. *physica status solidi (RRL) - Rapid Research Letters*, 5(9):324–331, September 2011.

[24] Michael Woodhouse, Alan Goodrich, Robert Margolis, Ted James, Ramesh Dhere, Tim Gessert, Teresa Barnes, Roderick Eggert, and David Albin. Perspectives on the pathways for cadmium telluride photovoltaic module manufacturers to address expected increases in the price for tellurium. *Solar Energy Materials and Solar Cells*, 115:199–212, August 2013.

[25] Martin A. Green, Keith Emery, Yoshihiro Hishikawa, Wilhelm Warta, and Ewan D. Dunlop. Solar cell efficiency tables (version 42). *Progress in Photovoltaics: Research and Applications*, 21(5):827–837, August 2013.

[26] Martin A. Green. Thin-film solar cells: review of materials, technologies and commercial status. *Journal of Materials Science: Materials in Electronics*, 18(S1):15–19, April 2007.

[27] Harin S. Ullal and Bolko von Roedern. Thin film CIGS and CdTe photovoltaic technologies: commercialization, critical issues, and applications. In *22nd European Photovoltaic Solar Energy Conference and Exhibition*, pages 1–4, Milan, IT, 2007. National Renewable Energy Laboratory, IEEE.

[28] R. Amatya and R. J. Ram. Trend for thermoelectric materials and their earth abundance. *Journal of Electronic Materials*, 41(6):1011–1019, December 2011.

[29] Andreas Patyk. Thermoelectrics: Impacts on the environment and sustainability. *Journal of Electronic Materials*, 39(9):2023–2028, December 2009.

[30] Björn A. Andersson. Materials availability for large-scale thin-film photovoltaics. *Progress in Photovoltaics: Research and Applications*, 8(May 1999):61–76, February 2000.

[31] Martin A. Green. Estimates of Te and In prices from direct mining of known ores. *Progress in Photovoltaics: Research and Applications*, 17(5):347–359, August 2009.

[32] Weldon Read. Personal Interview, 2011.

[33] Shijie Wang, Brad Wesstrom, and Jean Fernandez. A novel process for recovery of Te and Se from copper slimes autoclave leach solution. *Journal of Minerals and Materials Characterization and Engineering*, 2(1):53–64, 2003.

[34] Martin A. Green. Improved estimates for Te and Se availability from Cu anode slimes and recent price trends. *Progress in Photovoltaics: Research and Applications*, 14:743–751, December 2006.

[35] P. H. Jennings. Extractive metallurgy of tellurium. In W. Charles Cooper, editor, *Tellurium*, chapter 2, pages 14–53. Von Nostrand Reinhold Company, New York, 1971.

[36] Pierre L Claessens and Carl W White. Method of tellurium separation from copper electrorefining slime, 1993.

[37] Jack S Stafiej, Pierre Claessens, and Carl W White. Tellurium extraction from copper electrorefining slimes, 1999.

[38] C.K. Gupta and N. Krishnamurthy. *Extractive Metallurgy of Rare Earths*. CRC Press, Boca Raton, 2005.

[39] Peter C. Dent. Rare earth elements and permanent magnets. *Journal of Applied Physics*, 111(7):07A721(1) – 07A721(6), March 2012.

[40] E. A. Nesbitt and J. H. Wernick. *Rare earth permanent magnets*. Academic Press, New York, 1973.

[41] Man-Seung Lee, Gwang-Seop Lee, Jin-Young Lee, Sung-Don Kim, Jae-Woo Ahn, and Joon-Soo Kim. Solvent extraction of Gd from chloride solution with PC88A. *Materials Transactions*, 46(2):259–262, 2005.

[42] Kang Ding, William E. Seyfried, Zhong Zhang, Margaret K. Tivey, Karen L. Von Damm, and Albert M. Bradley. The in situ pH of hydrothermal fluids at mid-ocean ridges. *Earth and Planetary Science Letters*, 237(1-2):167–174, August 2005.

[43] E Douville, J L Charlou, E H Oelkers, P Bienvenu, and C F Jove Colon. The rainbow vent fluids (36 ° 14 V N , MAR): the inf luence of ultramafic rocks and phase separation on trace metal content in Mid-Atlantic Ridge hydrothermal f luids. *Chemical Geology*, 184:37–48, 2002.

[44] Eric Douville, Philippe Bienvenu, Jean Luc Charlou, Jean Pierre Donval, Yves Fouquet, Pierre Appriou, and Toshitaka Gamo. Yttrium and rare earth elements in fluids from various deep-sea hydrothermal systems. *Geochimica et Cosmochimica Acta*, 63(5):627–643, March 1999.

[45] Byung Mok Yoon, Sang Chul Shim, Hyung Chik Pyun, and Dong Soo Lee. Hydride generation atomic absorption determination of tellurium species in environmental samples with in situ concentration in a graphite furnace. *Analytical sciences*, 6(4):561–566, 1990.

[46] I B Ł Butler, R W Nesbitt, Butler I.B., and Nesbitt R.W. Trace element distributions in the chalcopyrite wall of a black smoker chimney: insights from laser ablation inductively coupled plasma mass spectrometry (LA-ICP-MS). *Earth and Planetary Science Letters*, 167(3):335–345, 1999.

[47] C A Mancuso Nichols, J Guezennec, and J P Bowman. Bacterial exopolysaccharides from extreme marine environments with special consideration of the southern ocean, sea ice, and deep-sea hydrothermal vents: a review. *Marine biotechnology*, 7(4):253–71, 2005.

[48] James F Holden and Michael W. W. Adams. Microbe–metal interactions in marine hydrothermal environments. *Current Opinion in Chemical Biology*, 7(2):160–165, April 2003.

[49] Julius T Csotonyi, Erko Stackebrandt, and Vladimir Yurkov. Anaerobic respiration on tellurate and other metalloids in bacteria from hydrothermal vent fields in the eastern Pacific Ocean. *Applied and environmental microbiology*, 72(7):4950–4956, July 2006.

[50] Costantino Vetriani, Yein S Chew, Susan M Miller, Jane Yagi, Jonna Coombs, Richard A Lutz, and Tamar Barkay. Mercury adaptation among bacteria from a deep-sea hydrothermal vent. *Applied and environmental microbiology*, 71(1):220–226, January 2005.

[51] Christopher Rathgeber, Natalia Yurkova, Erko Stackebrandt, J Thomas Beatty, Vladimir Yurkov, and Thomas J. Beatty. Isolation of tellurite- and selenite-resistant bacteria from hydrothermal vents of the Juan de Fuca Ridge in the Pacific Ocean. *Applied and Environmental Microbiology*, 68(9):4613–4622, September 2002.

[52] Christopher Rathgeber, Natalia Yurkova, Erko Stackebrandt, Peter Schumann, Elaine Humphrey, J Thomas Beatty, and Vladimir Yurkov. Metalloid reducing bacteria isolated from deep ocean hydrothermal vents of the Juan de Fuca Ridge, *Pseudoalteromonas telluritireducens* sp. nov. and *Pseudoalteromonas spiralis* sp. nov. *Current microbiology*, 53(5):449–456, November 2006.

[53] Vladimir Yurkov and Julius Csotonyi. Aerobic anoxygenic phototrophs and heavy metalloid reducers from extreme environments. *Recent Research Developments in Bacteriology*, 1:247–300, 2003.

[54] M. M. Yakimov, P. N. Golyshin, S. Lang, E. R. B. Moore, W.-R. Abraham, H. Lunsdorf, and K. N. Timmis. Alcanivorax borkumensis gen. nov., sp. nov., a new, hydrocarbon-degrading and surfactant-producing marine bacterium. *International Journal of Systematic Bacteriology*, 48(2):339–348, April 1998.

[55] I. Finnegan, S. Toerien, L. Abbot, F. Smit, and H. G. Raubenheimer. Identification and characterisation of an Acinetobacter sp. capable of assimilation of a range of cyano-metal complexes, free cyanide ions and simple organic nitriles. *Applied Microbiology and Biotechnology*, 36(1):142–144, October 1991.

[56] J J Nieto, R Fernandez-Castillo, M C Marquez, A Ventosa, E Quesada, and F Ruiz-Berraquero. Survey of metal tolerance in moderately halophilic eubacteria. *Appl. Envir. Microbiol.*, 55(9):2385–2390, September 1989.

[57] Colleen M Hansel and Chris A Francis. Coupled photochemical and enzymatic Mn(II) oxidation pathways of a planktonic *Roseobacter*-Like bacterium. *Applied and environmental microbiology*, 72(5):3543–3549, May 2006.

[58] D. R. Learman, B. M. Voelker, A. I. Vazquez-Rodriguez, and C. M. Hansel. Formation of manganese oxides by bacterially generated superoxide. *Nature Geoscience*, 4(2):95–98, January 2011.

[59] Alison Buchan, José M González, and Mary Ann Moran. Overview of the marine roseobacter lineage. *Applied and environmental microbiology*, 71(10):5665–77, October 2005.

[60] Catherine Vogel and Nicholas S. Fisher. Metal accumulation by heterotrophic marine bacterioplankton. *Limnology and Oceanography*, 55(2):519–528, 2010.

[61] Orianna Bretschger, Anna Obraztsova, Carter A Sturm, In Seop Chang, Yuri A Gorby, Samantha B Reed, David E Culley, Catherine L Reardon, Soumitra Barua, Margaret F Romine, Jizhong Zhou, Alexander S Beliaev, Rachida Bouhenni, Daad Saffarini, Florian Mansfeld, Byung-Hong Kim, James K Fredrickson, and Kenneth H Nealson. Current production and metal oxide reduction by Shewanella oneidensis MR-1 wild type and mutants. *Applied and environmental microbiology*, 73(21):7003–12, November 2007.

[62] Yuri A Gorby, Svetlana Yanina, Jeffrey S McLean, Kevin M Rosso, Dianne Moyles, Alice Dohnalkova, Terry J Beveridge, In Seop Chang, Byung Hong Kim, Kyung Shik Kim, David E Culley, Samantha B Reed, Margaret F Romine, Daad A Saffarini, Eric A Hill, Liang Shi, Dwayne A Elias, David W Kennedy, Grigoriy Pinchuk, Kazuya Watanabe, Shun'ichi Ishii, Bruce Logan, Kenneth H Nealson, and Jim K Fredrickson. Electrically conductive bacterial nanowires produced by Shewanella oneidensis strain MR-1 and other microorganisms. *Proceedings of the National Academy of Sciences of the United States of America*, 103(30):11358–63, July 2006.

[63] Hua Fang, Wei Zhou, Zhengya Cao, Feifan Tang, Dandan Wang, Kailin Liu, Xiangwei Wu, Xiao'e Yang, Yongge Sun, and Yunlong Yu. Combined remediation of DDT congeners and cadmium in soil by Sphingobacterium sp. D-6 and Sedum alfredii Hance. *Journal of Environmental Sciences*, 24(6):1036–1046, June 2012.

[64] Varenyam Achal, Xiangliang Pan, and Daoyong Zhang. Bioremediation of strontium (Sr) contaminated aquifer quartz sand based on carbonate precipitation induced by Sr resistant Halomonas sp. *Chemosphere*, 89(6):764–8, October 2012.

[65] Soledad Arias, Ana del Moral, Maria Rita Ferrer, Richard Tallon, Emilia Quesada, and Victoria Béjar. Mauran, an exopolysaccharide produced by the halophilic bacterium Halomonas maura, with a novel composition and interesting properties for biotechnology. *Extremophiles : life under extreme conditions*, 7(4):319–26, August 2003.

[66] S Hirano and K T Suzuki. Exposure, metabolism, and toxicity of rare earths and related compounds. *Environmental health perspectives*, 104 Suppl(Suppl 1):85–95, March 1996.

[67] Simon P Fricker. The therapeutic application of lanthanides. *Chemical Society reviews*, 35(6):524–33, June 2006.

[68] Jean-Claude G Bünzli. Lanthanide luminescence for biomedical analyses and imaging. *Chemical reviews*, 110(5):2729–55, May 2010.

[69] Claudio Turro, Patty K.-L. Fu, and Patricia M. Bradley. Lanthanide ions as luminescent probes of proteins and nucleic acid. In Astrid Sigel and Helmut Sigel, editors, *Metal ions in biological systems. Vol. 40. The lanthanides and their interrelations with biosystems*, chapter 9, pages 324–347. Marcel Dekker, Inc., New York, 2003.

[70] Yves Andrès, H.John MacCordick, and Jean-Claude Hubert. Adsorption of several actinide (Th, U) and lanthanide (La, Eu, Yb) ions by Mycobacterium smegmatis. *Applied Microbiology and Biotechnology*, 39(3), June 1993.

[71] Bryne T. Ngwenya, J. Fred W. Mosselmans, Marisa Magennis, Kirk D. Atkinson, Janette Tourney, Valerie Olive, and Robert M. Ellam. Macroscopic and spectroscopic analysis of lanthanide adsorption to bacterial cells. *Geochimica et Cosmochimica Acta*, 73(11):3134–3147, 2009.

[72] Y. Andrès, G. Thouand, M. Boualam, and M. Mergeay. Factors influencing the biosorption of gadolinium by micro-organisms and its mobilisation from sand. *Applied Microbiology and Biotechnology*, 54(2):262–267, August 2000.

[73] M.L. Merroun, K. Ben Chekroun, J.M. Arias, and M.T. González-Muñoz. Lanthanum fixation by *Myxococcus xanthus*: cellular location and extracellular polysaccharide observation. *Chemosphere*, 52(1):113–120, 2003.

[74] A. C. Texier, Y. Andrès, and P. L. Cloirec. Selective biosorption of lanthanide (La, Eu) ions by *Mycobacterium smegmatis*. *Environmental Technology*, 18(8):835–841, August 1997.

[75] Anne-Claire Texier, Yves Andrès, Myriam Illemassene, and Pierre Le Cloirec. Characterization of lanthanide ions binding sites in the cell wall of Pseudomonas aeruginosa. *Environmental Science & Technology*, 34(4):610–615, February 2000.

[76] Anne-Claire Texier, Yves Andrès, and Pierre Le Cloirec. Selective biosorption of lanthanide (La, Eu, Yb) ions by *Pseudomonas aeruginosa*. *Environmental Science & Technology*, 33(3):489–495, February 1999.

[77] V. A. Anagnostopoulos and B. D. Symeopoulos. Sorption of europium by malt spent rootlets, a low cost biosorbent: effect of pH, kinetics and equilibrium studies. *Journal of Radioanalytical and Nuclear Chemistry*, 295(1):7–13, July 2012.

[78] Sufia K Kazy, Susanta K Das, and Pinaki Sar. Lanthanum biosorption by a *Pseudomonas* sp.: equilibrium studies and chemical characterization. *Journal of industrial microbiology & biotechnology*, 33(9):773–783, September 2006.

[79] Robson C. Oliveira, Claire Jouannin, Eric Guibal, and Oswaldo Garcia Jr. Samarium(III) and praseodymium(III) biosorption on *Sargassum* sp.: batch study. *Process Biochemistry*, 46(3):736–744, 2011.

[80] L Philip, L Iyengar, and C Venkobachar. Biosorption of U, La, Pr, Nd, Eu and Dy by Pseudomonas aeruginosa. *Journal of Industrial Microbiology and Biotechnology*, 25(1):1–7, July 2000.

[81] Yoshio Takahashi, Xavier Châtellier, Keiko H. Hattori, Kenji Kato, and Danielle Fortin. Adsorption of rare earth elements onto bacterial cell walls and its implication for REE sorption onto natural microbial mats. *Chemical Geology*, 219(1-4):53–67, June 2005.

[82] Yukiho Hosomomi, Yuzo Baba, Fukiko Kubota, Noriho Kamiya, and Masahiro Goto. Biosorption of rare earth elements by Escherichia coli. *Journal of Chemical Engineering of Japan*, 46(7):450–454, 2013.

[83] Yoshio Takahashi, Mika Yamamoto, Yuhei Yamamoto, and Kazuya Tanaka. EXAFS study on the cause of enrichment of heavy REEs on bacterial cell surfaces. *Geochimica et Cosmochimica Acta*, 74(19):5443–5462, 2010.

[84] George K. Schweitzer and Lester L. Pesterfield. *The aqueous chemistry of the elements*. Oxford University Press, New York, 2010.

[85] Nilanjana Das and Devlina Das. Recovery of rare earth methals through biosorption: an overview. *Journal of Rare Earths*, 31(10):933–943, 2013.

[86] S. Markai, Y. Andrès, G. Montavon, and B. Grambow. Study of the interaction between europium (III) and *Bacillus subtilis*: fixation sites, biosorption modeling and reversibility. *Journal of Colloid and Interface Science*, 262(2):351–361, 2003.

[87] Şenol Sert, Ceren Kütahyali, Süleyman İnan, Zeynep Talip, Berkan Çetinkaya, and Meral Eral. Biosorption of lanthanum and cerium from aqueous solutions by *Platanus orientalis* leaf powder. *Hydrometallurgy*, 90(1):13–18, 2008.

[88] M.C. Palmieri, O. Jr. Garcia, and P. Melnikov. neodymium biosorption from acidic solutions in batch system. *Process Biochemistry*, 36:441–444, 2000.

[89] David Borrok, Jeremy B Fein, and Charles F Kulpa. Proton and Cd adsorption onto natural bacterial consortia: testing universal adsorption behavior. *Geochimica et Cosmochimica Acta*, 68(15):3231–3238, 2004.

[90] Nathan Yee and Jeremy Fein. Cd adsorption onto bacterial surfaces: A universal adsorption edge? *Geochimica et Cosmochimica Acta*, 65(13):2037–2042, July 2001.

[91] Yoshio Takahashi, Kazuhiro Kondo, Asami Miyaji, Yusuke Watanabe, Qiaohui Fan, Tetsuo Honma, and Kazuya Tanaka. Recovery and separation of rare Earth elements using salmon milt. *PloS one*, 9(12):e114858, January 2014.

[92] Jenny S. Cox, D. Scott Smith, Lesley A. Warren, and F. Grant Ferris. Characterizing heterogeneous bacterial surface functional groups using discrete affinity spectra for proton binding. *Environmental Science & Technology*, 33(24):4514–4521, December 1999.

[93] Jean Remacle. The cell wall and metal binding. In Bohumil Volesky, editor, *Biosorption of heavy metals*, chapter 2.1, pages 83–92. CRC Press, Boca Raton, 1990.

[94] Bryne T Ngwenya, Ian W Sutherland, and Lynn Kennedy. Comparison of the acid-base behaviour and metal adsorption characteristics of a gram-negative bacterium with other strains. *Applied Geochemistry*, 18(4):527–538, April 2003.

[95] Gilles Guibaud, Sophie Comte, François Bordas, Sèverine Dupuy, and Michel Baudu. Comparison of the complexation potential of extracellular polymeric substances (EPS), extracted from activated sludges and produced by pure bacteria strains, for cadmium, lead and nickel. *Chemosphere*, 59(5):629–38, April 2005.

[96] V. Guiné, L. Spadini, G. Sarret, M. Muris, C. Delolme, J.-P. Gaudet, and J. M. F. Martins. Zinc Sorption to Three Gram-Negative Bacteria: Combined Titration, Modeling, and EXAFS Study. *Environmental Science & Technology*, 40(6):1806–1813, March 2006.

[97] Masato Ueshima, Brian R. Ginn, Elizabeth A. Haack, Jennifer E.S. Szymanowski, and Jeremy B. Fein. Cd adsorption onto Pseudomonas putida in the presence and absence of extracellular polymeric substances. *Geochimica et Cosmochimica Acta*, 72(24):5885–5895, December 2008.

[98] Masanori Matsukawa and E P Greenberg. Putative exopolysaccharide synthesis genes influence Pseudomonas aeruginosa biofilm development. *Journal of bacteriology*, 186(14):4449–56, July 2004.

[99] D Mengin-Lecreulx and J van Heijenoort. Effect of growth conditions on peptidoglycan content and cytoplasmic steps of its biosynthesis in Escherichia coli. *Journal of bacteriology*, 163(1):208–12, July 1985.

[100] David A. Fowle and Jeremy B. Fein. Experimental measurements of the reversibility of metal–bacteria adsorption reactions. *Chemical Geology*, 168(1-2):27–36, July 2000.

[101] Dawei Wang, Rikkert J Nap, István Lagzi, Bartlomiej Kowalczyk, Shuangbing Han, Bartosz A Grzybowski, and Igal Szleifer. How and why nanoparticle's curvature regulates the apparent pKa of the coating ligands. *Journal of the American Chemical Society*, 133(7):2192–7, February 2011.

[102] Simon Cotton. *Lanthanide and actinide chemistry*. Wiley, West Sussex, 2006.

[103] Peter Atkins, Tina Overton, Jonathan Rourke, Mark Weller, and Fraser Armstrong. *Inorganic chemistry*. Oxford University Press, New York, 5th edition, 2010.

[104] Derek Marsh. *CRC handbook of lipid bilayers*. CRC Press, Boca Raton, 1990.

[105] Katsumi Matsuzaki, Ken-ichi Sugishita, and Koichiro Miyajima. Interactions of an antimicrobial peptide, magainin 2, with lipopolysaccharide-containing liposomes as a model for outer membranes of Gram-negative bacteria. *FEBS Letters*, 449(2-3):221–224, April 1999.

[106] Juan Sabín, Gerardo Prieto, Paula V Messina, Juan M Ruso, Roque Hidalgo-Alvarez, and Félix Sarmiento. On the effect of Ca^{2+} and La^{3+} on the colloidal stability of liposomes. *Langmuir : the ACS journal of surfaces and colloids*, 21(24):10968–75, November 2005.

[107] Juan Sabín, Gerardo Prieto, Simona Sennato, Juan Ruso, Roberta Angelini, Federico Bordi, and Félix Sarmiento. Effect of Gd^{3+} on the colloidal stability of liposomes. *Physical Review E*, 74(3):031913, September 2006.

[108] Tomoki Tanaka and Yamazaki Masahito. Membrane fusion of giant unilamellar vesicles of neutral phospholipid membranes induced by La3+. *Langmuir*, 20:5160–5164, May 2004.

[109] Tomoki Tanaka, Yukihiro Tamba, Shah Md Masum, Yuko Yamashita, and Masahito Yamazaki. La^{3+} and Gd^{3+} induce shape change of giant unilamellar vesicles of phosphatidylcholine. *Biochimica et Biophysica Acta (BBA) - Biomembranes*, 1564(1):173–182, August 2002.

[110] Neil F. Ashton, Colin McDermott, and A. Brench. Chemistry of extraction of nonreacting solutes. In Teh C. Lo, Malcolm H. I. Baird, and Carl Hanson, editors, *Handbook of solvent extraction*, chapter 1, pages 4–35. John Wiley & Sons, New York, 1983.

[111] Thomas Girard Chasteen, Derie Esteban Fuentes, Juan Carlos Tantaleán, and Claudio Christian Vásquez. Tellurite: history, oxidative stress, and molecular mechanisms of resistance. *FEMS microbiology reviews*, 33(4):820–832, July 2009.

[112] W Reisert. The so-called bismuth breath. *American Journal of Pharmacology*, 56:177–180, 1884.

[113] Alexander Fleming. On the specific antibacterial properties of penicillin and potassium tellurite. Incorporating a method of demonstrating some bacterial antagonisms. *The Journal of Pathology and Bacteriology*, 35(6):831–842, 1932.

[114] Fayne L. Tucker, John F. Walper, Milo Don Appleman, and Jerry Donohue. Complete reduction of tellurite to pure tellurium metal by microorganisms. *J. Bacteriol.*, 83(6):1313–1314, June 1962.

[115] Amnon Albeck, Hana Weitman, Benjamin Sredni, and Michael Albeck. Tellurium compounds: Selective inhibition of cysteine proteases and model reaction with thiols. *Inorganic Chemistry*, 37(8):1704–1712, April 1998.

[116] B Deuticke, P Lütkemeier, and B Poser. Tellurite-induced damage of the erythrocyte membrane. Manifestations and mechanisms. *Biochimica et biophysica acta*, 1109(1):97–107, August 1992.

[117] Francesca Borsetti, Valentina Tremaroli, Francesca Michelacci, Roberto Borghese, Christine Winterstein, Fevzi Daldal, and Davide Zannoni. Tellurite effects on *Rhodobacter capsulatus* cell viability and superoxide dismutase activity under oxidative stress conditions. *Research in microbiology*, 156(7):807–813, August 2005.

[118] José M Pérez, Iván L Calderón, Felipe A Arenas, Derie E Fuentes, Gonzalo A Pradenas, Eugenia L Fuentes, Juan M Sandoval, Miguel E Castro, Alex O Elías, and Claudio C Vásquez.

Bacterial toxicity of potassium tellurite: unveiling an ancient enigma. *PLoS ONE*, 2(2):e211, January 2007.

[119] Raymond J Turner, Yair Aharonowitz, Joel H Weiner, and Diane E Taylor. Glutathione is a target in tellurite toxicity and is protected by tellurite resistance determinants in *Escherichia coli*. *Canadian Journal of Microbiology*, 47(1):33–40, January 2001.

[120] Raymond J. Turner. Tellurite toxicity and resistance in Gram-negative bacteria. *Recent research developments in microbiology*, 5:69–77, 2001.

[121] Janine Kessi and Kurt W Hanselmann. Similarities between the abiotic reduction of selenite with glutathione and the dissimilatory reaction mediated by *Rhodospirillum rubrum* and *Escherichia coli*. *The Journal of biological chemistry*, 279(49):50662–50669, December 2004.

[122] Valentina Tremaroli, Stefano Fedi, and Davide Zannoni. Evidence for a tellurite-dependent generation of reactive oxygen species and absence of a tellurite-mediated adaptive response to oxidative stress in cells of Pseudomonas pseudoalcaligenes KF707. *Archives of Microbiology*, 187(2):127–135, 2007.

[123] Iván L Calderón, Alex O Elías, Eugenia L Fuentes, Gonzalo A Pradenas, Miguel E Castro, Felipe A Arenas, José M Pérez, and Claudio C Vásquez. Tellurite-mediated disabling of [4Fe-4S] clusters of *Escherichia coli* dehydratases. *Microbiology*, 155(Pt 6):1840–1846, June 2009.

[124] Jerry W Swearingen, Manuel A. Araya, Mary F. Plishker, Claudia P Saavedra, Claudio C Vásquez, and Thomas G Chasteen. Identification of biogenic organotellurides in *Escherichia coli* K-12 headspace gases using solid-phase microextraction and gas chromatography. *Analytical biochemistry*, 331(1):106–114, August 2004.

[125] Marjorie L. Bird and Frederick Challenger. The Formation of organo-metalloidal Compounds by micro-organisms. Part VII. Dimethyl telluride. *Journal of the Chemical Society*, pages 163–168, 1939.

[126] Frederick Challenger. Biological methylation. *Chemical Reviews*, 36(3):315–361, June 1945.

[127] Manuel A Araya, Jerry W Swearingen, Mary F Plishker, Claudia P Saavedra, Thomas G Chasteen, and Claudio C Vásquez. *Geobacillus stearothermophilus* V *ubiE* gene product is involved in the evolution of dimethyl telluride in *Escherichia coli K-12* cultures amended with potassium tellurate but not with potassium tellurite. *Journal of biological inorganic chemistry*, 9(5):609–615, July 2004.

[128] Patrick R L Ollivier, Andrew S Bahrou, Thomas M Church, and Thomas E Hanson. Aeration controls the reduction and methylation of tellurium by the aerobic, tellurite-resistant marine yeast *Rhodotorula mucilaginosa*. *Applied and environmental microbiology*, 77(13):4610–4617, July 2011.

[129] Monique Sabaty, Cécile Avazéri, David Pignol, and André Vermeglio. Characterization of the reduction of selenate and tellurite by nitrate reductases. *Applied and environmental microbiology*, 67(11):5122–5126, November 2001.

[130] V Yurkov, J Jappe, and a Vermeglio. Tellurite resistance and reduction by obligately aerobic photosynthetic bacteria. *Applied and environmental microbiology*, 62(11):4195–8, November 1996.

[131] Cécile Avazéri, Raymond J Turner, Jeannine Pommier, Joël H Weiner, Gérard Giordano, and André Verméglio. Tellurite reductase activity of nitrate reductase is responsible for the basal resistance of Escherichia coli to tellurite. *Microbiology*, 143(4):1181–1189, April 1997.

[132] Iván L Calderón, Felipe A Arenas, José Manuel Pérez, Derie E Fuentes, Manuel A Araya, Claudia P Saavedra, Juan C Tantaleán, Sergio E Pichuantes, Philip A Youderian, and Claudio C Vásquez. Catalases are NAD(P)H-dependent tellurite reductases. *PLoS ONE*, 1(1):e70, January 2006.

[133] Shaun M Baesman, Thomas D Bullen, James Dewald, Donghui Zhang, Seamus Curran, Farhana S Islam, Terry J Beveridge, and Ronald S Oremland. Formation of tellurium nanocrystals during anaerobic growth of bacteria that use Te oxyanions as respiratory electron acceptors. *Applied and environmental microbiology*, 73(7):2135–2143, April 2007.

[134] William D. Bonificio and David R. Clarke. Bacterial recovery and recycling of tellurium from tellurium-containing compounds by *Pseudoalteromonas* sp. EPR3. *Journal of Applied Microbiology*, 117(5):1293–1304, 2014.

[135] Thomas G Chasteen and Ronald Bentley. Biomethylation of selenium and tellurium: microorganisms and plants. *Chemical reviews*, 103(1):1–25, January 2003.

[136] Christopher J Daughney, David A Fowle, and Danielle Fortin. The effect of growth phase on proton and metal adsorption by Bacillus subtilis. *Geochimica et Cosmochimica Acta*, 65(7):1025–1035, 2001.

[137] Strem Chemicals Inc. Dimethyl cadmium material safety data sheet, 2011.

[138] John S. Thayer. Biological methylation of less-studied elements. *Applied Organometallic Chemistry*, 16(12):677–691, 2002.

[139] Benjamin E. Wolfe, Julie E. Button, Marcela Santarelli, and Rachel J. Dutton. Cheese Rind Communities Provide Tractable Systems for In Situ and In Vitro Studies of Microbial Diversity. *Cell*, 158(2):422–433, July 2014.

[140] Avanti Polar Lipids. Preparations of liposomes, 2014.

[141] A. Pine and G. Dresselhaus. Raman Spectra and Lattice Dynamics of Tellurium. *Physical Review B*, 4(2):356–371, July 1971.

[142] A.P. Mirgorodsky, T. Merle-Méjean, J.-C Champarnaud, P. Thomas, and B. Frit. Dynamics and structure of TeO2 polymorphs: model treatment of paratellurite and tellurite; Raman scattering evidence for new γ- and δ-phases. *Journal of Physics and Chemistry of Solids*, 61:501–509, 2000.

[143] Patrick R L Ollivier, Andrew S Bahrou, Sarah Marcus, Talisha Cox, Thomas M Church, and Thomas E Hanson. Volatilization and precipitation of tellurium by aerobic, tellurite-resistant marine microbes. *Applied and environmental microbiology*, 74(23):7163–7173, December 2008.

[144] First Solar Inc. Form 10-K annual report for the period ending 12/31/11, 2012.

[145] Martin A. Green. Learning experience for thin-film solar modules: First Solar, Inc. case study. *Progress in Photovoltaics: Research and Applications*, 19(4):498–500, June 2011.

[146] Vasilis M Fthenakis. Sustainability of photovoltaics: The case for thin-film solar cells. *Renewable and Sustainable Energy Reviews*, 13(9):2746–2750, 2009.

[147] Chiara Candelise, Mark Winskel, and Robert Gross. Implications for CdTe and CIGS technologies production costs of indium and tellurium scarcity. *Progress in Photovoltaics: Research and Applications*, 20(6):816–831, September 2012.

[148] Rodrigues Carlos Reiser, F.K.M. and Rosa Diogo. High-technology elements for thin-film photovoltaic applications: a demand-supply outlook on the basis of current energy and PV market growths scenarios. In *5th User Forum Thin-Film Photovoltaics*, pages 120–125, Würzburg, DE, 2009.

[149] Ken Zweibel. The impact of tellurium supply on cadmium telluride photovoltaics. *Science*, 328(5979):699–701, May 2010.

[150] Max Marwede and Armin Reller. Future recycling flows of tellurium from cadmium telluride photovoltaic waste. *Resources, Conservation and Recycling*, 69:35–49, 2012.

[151] V. M. Fthenakis and W. Wang. Extraction and separation of Cd and Te from cadmium telluride photovoltaic manufacturing scrap. *Progress in Photovoltaics: Research and Applications*, 14:363–371, June 2006.

[152] Vasilis M. Fthenakis and W. Wang. *Leaching of cadmium, tellurium and copper from cadmium telluride photovoltaic modules progress report*. Brookhaven National Laboratory, Upton, NY, 2004.

[153] Gudny Okkenhaug. *Environmental risks regarding the use and final disposal of CdTe PV modules. Document No. 20092155-00-5-R.* Oslo, Norway, 2010.

[154] Doris Schüler, Matthias Buchert, Ran Liu, Stefanie Dittrich, and Cornelia Merz. Study on rare earths and their recycling. Technical report, Institute for Applied Ecology and The Greens European Free Alliance in the European Parliament, Darmstadt, 2011.

[155] Ryan Wiser and Mark Bolinger. 2012 Wind Technologies Market Report. Technical report, Department of Energy, Oak Ridge, 2013.

[156] U.S. Department of Energy. Use of hybrid electric vehicle sales by model, 2012.

[157] Joseph Gambogi. The rare earths minerals commodities summary. Technical report, United States Geological Survey, 2014.